Numerical calculation of coastal trapped wave modes

[This manuscript is a non-peer reviewed preprint submitted to EarthArXiv.]

Ryo Furue*[1] and Yuki Tanaka[2]

[1] *JAMSTEC, Yokohama, Japan*

[2] *Tokyo University of Marine Science and Technology, Tokyo, Japan*

Abstract

A numerical method is developed to calculate coastal trapped wave (CTW) modes in the low-frequency limit ($\omega \ll f$). The modes are solutions to a 2-dimensional eigenvalue problem. Useful properties like orthogonality are derived from the bilinear form associated with the operator of the eigenvalue problem. Our formulation uses the z coordinates and the CTW equation is discretized with a finite-difference method. We transform the set of the finite-difference equations in such a way that it has an analogous bilinear form and hence has an exact orthogonality condition and a few exact properties that the original differential equation has. By casting the set into a matrix form, we further prove that there are exactly as many modes as there are gridpoints in the vertical. We also prove another property that makes it trivial to filter out unphysical solutions. With our code, which have been made publicly available, all the numerical CTW modes are obtained at once for a given $N(z)$ and bottom topography $z = -h(x)$. By no means does our code supersedes Brink and Chapman's (1987), however, the latter being much more versatile.

*Corresponding author: Ryo Furue, ryofurue@gmail.com, https://orcid.org/0000-0003-0563-1189

1 Introduction

1.1 Coastal trapped wave modes

Coastal trapped waves (CTWs) are subinertial waves that propagate with the coastline on their right-hand (left-hand) side in the northern (southern) hemisphere. See, for example, the review papers Brink (1991) and Hughes et al. (2019), and references therein. When the stratification is negligible, as for shallow continental shelf, and for $\omega \ll f$, CTWs reduce to "shelf waves" (e.g., Robinson 1964; Buchwald and Adams 1997); and when the bottom slope is a vertical wall followed by a flat bottom and for $\omega \ll f$, they reduce to coastal Kelvin waves (Hughes et al. 2019).

When f is assumed to be constant, the background stratification is assumed to be uniform in the horizontal directions, i.e., $N = N(z)$, and the bottom topography is uniform in the longshore direction, i.e., $z = -h(x)$, the wave takes a separable form $p = F(x,z)\,\phi(y,t)$, where x and y are the cross-shore and long-shore coordinates, and F is a solution to a 2-dimensional (2-d) eigenvalue problem, where the frequency is the eigenvalue (Wang and Mooers 1976; Clarke 1977). Further, when $\omega \ll f$, the longshore wavenumber can be factored out of the equations, and the eigenvalue problem can be cast into a form where the longshore propagation speed, c, plays the role of the eigenvalue. The longshore propagation becomes non-dispersive, with $\phi(y,t)$ being a solution to the monodirectional wave equation $\phi_t + \phi_y/c = 0$. Once the eigenpairs have been obtained for the 2-d eigenvalue problem, the 4-d solutions can be constructed as a superposition $p(x,y,z,t) = \sum_n F^{(n)}(x,z)\phi^{(n)}(y,t)$.

These modes have been used to interpret observed variability (e.g., Clarke 1977; Church et al. 1986) and also to construct theoretical coastal response to a given forcing (e.g., Furue 2022; Tanaka & Kida 2025, manuscript in preparation ??????????????).

The so-called "vertical modes" have also been widely used. When the "slope" is purely vertical and intersects a flat bottom, the CTW eigenvalue problem is separable between x and z (section 2 below) and the z structure function $\psi(z)$ is a solution to the well-known vertical-mode eigenvalue problem (e.g., McCreary 1981). In this case, not only do the CTW modes reduce to the product of a vertical mode and an associated offshore decay as $\exp[-|x/(c/f)|]$, but also the linearized, inviscid primitive equations are separable between z and (x,y,t) and the (x,y,t) functions obey the reduced-gravity equations, which the vertical-mode eigenvalue $c^{(n)}$ enters as the characteristic speed of gravity waves (e.g., McCreary 1981). Therefore the 4-d solutions of the linearized primitive equations can be expressed as a superposition of the form $p = \sum_n \psi^{(n)}(z)p^{(n)}(x,y,t)$, where $\psi^{(n)}$ is the n-th vertical mode and $p^{(n)}$ is the solution to the corresponding reduced-gravity equations. Even when there are no analytic solutions for $\psi^{(n)}(z)$ or $p^{(n)}(x,y,t)$, it is relatively easy to calculate each numerically. This framework is so useful that it has been used in a number of studies to construct theoretical 4-d flow field (e.g., Miyama et al. 2006; Song et al. 2023; Furue et al. 2024).

To numerically calculate the $F(x,z)$ modes for general CTWs, the Fortran program by Brink and Chapman (1987) has been widely used. Although versatile, this program is not quite convenient when one wants to calculate a set of modes. That may have been a reason why the superposition $p = \sum_n F^{(n)}(x,z)\phi^{(n)}(y,t)$ has not been often carried out.

Moreover, orthogonality of the modes is desired in expanding variability in terms of the modes. For the numerical vertical modes, it is relatively easy to ensure that the numerical

vertical modes are exactly orthogonal (see section 3 below), but it is not clear how to produce numerical CTW modes that are orthogonal.

1.2 Present study

The main goal of this paper is develop a computer program to calculate all the CTW modes at once under the low-frequency approximation ($\omega \ll f$) which satisfy useful properties including orthogonality. To achieve this goal, we carry out mathematical analysis on the set of finite-difference equations, which by itself may be useful for other similar numerical problems. We explain this analysis in detail for this reason.

The code originates from Tanaka's (2023) using the sigma coordinates but the present one uses the z coordinates and allows for variable grid spacing. These properties allow for the mixture of gentle slopes and very steep (even purely vertical) slopes in the bottom topography, making our code suitable for deep Kelvin-wave-like CTWs along the continental slope.

Section 2 briefly summarizes the eigenvalue problem of CTW modes and derives orthogonality and other properties of the solutions using the bilinear form associated with the problem. Section 3 develops a finite-difference scheme, derives an associated bilinear form, and proves that the solutions have exactly the same properties as the solutions to the original differential equation. In particular, it derives an exact orthogonality condition for the finite-difference solutions. This analysis also derives a few useful exact properties of the numerical solutions. Finally, section 5 summarizes the paper.

Sections S1 and S2 provide details omitted in sections 2 and 3, respectively. These supplementary sections are designed to be as much self-contained as possible to enable the interested reader to skip sections 2 and 3 of the main text and read the supplementary text instead.

2 Coastal trapped wave modes

We consider slow ($\omega \ll f$) coastal trapped waves on an f plane along a western boundary ($x > 0$). The bottom topography is $z = -h(x)$ and uniform in y. We assume that $h_x \geq 0$. The background stratification, $N(z)$, is assume to be uniform in the horizontal directions. In this case, coastal wave solutions can be written as $p = \sum_{n=0}^{\infty} \phi^{(n)}(y,t) F^{(n)}(x,z)$.

The CTW modes, $F^{(n)}$, are the solutions to the eigenvalue problem

$$F_{xx} + \left(\frac{F_z}{\tilde{N}^2}\right)_z = 0 \qquad \text{in the interior } (0 < x \text{ and } -h(x) < z < 0), \tag{1a}$$

$$\frac{F_z}{\tilde{N}^2} = -\frac{f^2}{g} F \qquad \text{on } z = 0, \tag{1b}$$

$$F_x \to 0 \qquad \text{as } x \to \infty, \tag{1c}$$

$$F_x + \frac{1}{h_x}\frac{F_z}{\tilde{N}^2} = \frac{f}{c} F \qquad \text{on } z = -h(x), \tag{1d}$$

where $\tilde{N} \equiv N(z)/f$; the eigenvalue is f/c. The "slope boundary condition" (1d) can be used even when part of the slope is purely vertical ($h_x = \infty$) or purely horizontal ($h_x = 0$); in which case, (1d) reduces to either

$$F_x = \frac{f}{c} F \qquad \text{(along a vertical wall: } h_x \to \infty\text{)} \quad \text{or}$$

$$\frac{F_z}{\tilde{N}^2} = 0 \qquad \text{(along a flat part of the bottom: } h_x = 0\text{)}.$$

We often invoke the rigid-lid condition $g \to \infty$, but we retain the free-surface term in this derivation, not because the solutions change much but for *mathematical convenience* (see below).

Note that the CTW equations become separable when the "slope" is a purely-vertical wall followed by a flat bottom and then the n-th eigenfunction takes the form of $F^{(n)}(x,z) = \exp(-x/|c^{(n)}/f|)\,\psi^{(n)}(z)$, a Kelvin-wave mode, where $\psi^{(n)}(z)$ is the n-th vertical mode and $c^{(n)}$ is the associated eigenvalue (section S1.3). Otherwise, the CTW problem remains a two-dimensional eigenvalue problem.

When deriving orthogonality and other properties of the solutions, it is convenient to use these "inner products":

$$\begin{aligned} \langle q, r \rangle &\equiv \iint_{\Omega} \mathrm{d}x\, \mathrm{d}z\, q\, r \\ \langle q, r \rangle_{\mathrm{b}} &\equiv \int_0^{\infty} \mathrm{d}x\, h_x\, q\, r|_{z=-h(x)}\,, \end{aligned} \tag{2}$$

where Ω is the entire ocean domain in the x-z plane. The second inner product is a line integral along the slope or bottom $z = -h(x)$. Flat regions, if any, of the slope do not contribute to the integral as $h_x = 0$ there. If the slope includes purely vertical regions, the integral still works because $\mathrm{d}x\, h_x = -\mathrm{d}z$, and the slope integral becomes a vertical integral there (see eq. (S1.16)). The integral $\langle q, r \rangle_{\mathrm{b}}$ is therefore expressed as a sum of vertical integrals over vertical portions and slope integrals of the above form. Both these integrals are bilinear and symmetric.

Denoting the interior operator in (1a) by

$$\mathcal{L}r \equiv r_{xx} + \left(\frac{r_z}{\tilde{N}^2}\right)_z$$

and assuming that (F, c) is an eigenpair, we find

$$\begin{aligned}\langle r, \mathcal{L}F\rangle = &-\iint_\Omega \mathrm{d}x\,\mathrm{d}z\left(r_x F_x + \frac{r_z F_z}{\tilde{N}^2}\right) - \frac{f^2}{g}\int_0^\infty \mathrm{d}x\ rF|_{z=0} \\ &- \frac{f}{c}\int_0^\infty \mathrm{d}x\, h_x\ rF|_{z=-h(x)}\end{aligned} \tag{3a}$$

after integration by parts and substitution of the boundary conditions, or equivalently

$$\langle r, \mathcal{L}F\rangle = A(r, F) - \frac{f}{c}\langle r, F\rangle_\mathrm{b}, \tag{3b}$$

where A is another bilinear symmetric form,

$$A(q, r) \equiv -\iint_\Omega \mathrm{d}x\,\mathrm{d}z\left(r_x F_x + \frac{r_z F_z}{\tilde{N}^2}\right) - \frac{f^2}{g}\int_0^\infty \mathrm{d}x\ rF|_{z=0}\,. \tag{4}$$

See eq. (S1.10) and the discussion that leads to it.

Since $\mathcal{L}F = 0$ when F is an eigenfunction (eq. (1a))

$$\langle r, \mathcal{L}F\rangle = A(r, F) - \frac{f}{c}\langle r, F\rangle_\mathrm{b} = 0. \tag{5}$$

First, suppose that there are two eigenfunctions, $F^{(l)}$ and $F^{(n)}$, the latter with an eigenvalue $c^{(n)}$. Plugging $F = F^{(n)}$, $c = c^{(n)}$, and $r = F^{(l)}$ into (5) gives

$$\langle F^{(l)}, \mathcal{L}F^{(n)}\rangle = A(F^{(l)}, F^{(n)}) - \frac{f}{c^{(n)}}\langle F^{(l)}, F^{(n)}\rangle_\mathrm{b} = 0, \tag{6a}$$

and swapping l and n gives

$$\langle F^{(n)}, \mathcal{L}F^{(l)}\rangle = A(F^{(n)}, F^{(l)}) - \frac{f}{c^{(l)}}\langle F^{(n)}, F^{(l)}\rangle_\mathrm{b} = 0. \tag{6b}$$

Subtracting the second equality from the first gives

$$\left(\frac{f}{c^{(l)}} - \frac{f}{c^{(n)}}\right)\langle F^{(l)}, F^{(n)}\rangle_\mathrm{b} = 0$$

because $A(,)$ and $\langle,\rangle_\mathrm{b}$ are both symmetric. This proves the orthogonality that

$$\langle F^{(l)}, F^{(n)}\rangle_\mathrm{b} = 0 \quad \text{if } c^{(l)} \neq c^{(n)}.$$

Next, if (F, c) is an eigenpair, (F^*, c^*) is also an eigenpair since (1) includes only real coefficients. Plugging $(F^{(l)}, c^{(l)}) = (F, c)$ and $(F^{(n)}, c^{(n)}) = (F^*, c^*)$ into the above derivation gives

$$\left(\frac{f}{c} - \frac{f}{c^*}\right)\langle F, F^*\rangle_\mathrm{b} = 0.$$

But, this time,

$$\frac{f}{c} - \frac{f}{c^*} = 0$$

is the result because $\langle F, F^* \rangle_\mathrm{b} = \int \mathrm{d}x\, h_x\, |F|^2\big|_{z=-h(x)} > 0$. [$\langle F, F^* \rangle_\mathrm{b} = 0$ would imply that $F|_{z=-h(x)} = 0$ where $h_x \neq 0$. We do not know how we can exclude that possibility, but we are able to exclude that possibility for our numerical solutions. See section 3.3.] This proves that the eigenvalues are real. We can also ignore complex eigenfunctions without loss of generality (section S1.2.3).

Finally, plugging $l = n$ into (6a) gives

$$A(F, F) - (f/c)\langle F, F \rangle_\mathrm{b} = 0.$$

Since $A(,)$ is negative definite (eq. (4)) and $\langle , \rangle_\mathrm{b}$ is positive definite,

$$f/c < 0.$$

That is, CTWs propagate southward ($c < 0$) along the western boundary in the northern hemisphere ($f > 0$).

In the next section, we develop a finite-difference scheme and its matrix representation that have all these properties by constructing finite-difference analogues of $\langle q, \mathcal{L}r \rangle$, $A(q, r)$, and $\langle q, r \rangle_\mathrm{b}$.

3 Discretized system

To solve (1) numerically, we use a standard finite-difference method. But, how do we choose a method among various possible ways to discretize the equations? Here, we aim at constructing a finite-difference scheme that has the same integral properties as derived above.

The key is the following observation. Each of the two terms on the left-hand side of (1a) takes the form of a "flux" divergence, which enabled the integration by parts that led to (4). We hence choose a discretization scheme that allows for "integrations by parts".

To present how this idea is applied to a finite-difference equations in the simplest possible terms, we take the second term of (1a), $(r_z/N^2)_z$, as an example (section 3.1). We then present our finite-difference scheme for the full CTW problem and derive its properties (section 3.2). We cast the finite-difference equations into a matrix form to solve the eigenvalue problem using matrix solvers in common linear algebra libraries and to further derive a few important properties of the solutions (section 3.3).

3.1 1-d analogue

The differential operator of the second term of (1a) is the same as that of the well-known eigenvalue problem (S1.20) for "vertical modes". With the definition

$$\mathcal{L}'r \equiv (r_z/N^2)_z, \tag{7a}$$

the 1-d eigenvalue problem is

$$\mathcal{L}'F + c^{-2}F = 0, \tag{7b}$$
$$F_z/N^2 = -F/g \quad \text{at } z = 0, \tag{7c}$$
$$F_z/N^2 = 0 \quad \text{at } z = -D. \tag{7d}$$

The operator is "conservative" in that there is no "source" or "sink" in the interior and the only potential source/sink comes from the boundaries:

$$\int_{-D}^{0} \mathrm{d}z\, \mathcal{L}'r = [r_z/N^2]_{z=-D}^{0}. \tag{7e}$$

From this property, we can further show that the "bilinear form" $\langle q, \mathcal{L}'r\rangle$ is a symmetric and negative-definite integral plus boundary terms:

$$\begin{aligned}\langle q, \mathcal{L}'r\rangle \equiv \int_{-D}^{0} \mathrm{d}z\, q\mathcal{L}'r &= \int_{-D}^{0} \mathrm{d}z\, [(qr_z/N^2) - q_z r_z/N^2] \\ &= [qr_z/N^2]_{-D}^{0} - \int_{-D}^{0} \mathrm{d}z\, q_z r_z/N^2.\end{aligned} \tag{7f}$$

If $r = F$ is an eigenfunction,

$$\langle q, \mathcal{L}'F\rangle = -\,qF/g|_{z=0} - \int_{-D}^{0} \mathrm{d}z\, q_z F_z/N^2 \equiv A(q, F), \tag{7g}$$

using the boundary conditions (7c) and (7d). Further, since $\mathcal{L}'F + c^{-2}F = 0$,

$$0 = \langle q, \mathcal{L}'F + c^{-2}F\rangle = A(r,F) + c^{-2}\langle q, F\rangle. \tag{7h}$$

This problem has the same structure as the CTW problem discussed in the preceding subsection. The symmetry of $A(,)$ and $\langle,\rangle$ proves that the vertical modes are orthogonal to each other and that the eigenvalues c^2 are all real. The negative definiteness of $A(,)$ further proves that $c^2 > 0$.

Under a standard finite difference scheme, the operator of the vertical-mode equation (7b) can be

$$\mathcal{L}'r\big|_k = \frac{1}{\Delta z_k}\left(\frac{r_{k-1}-r_k}{N^2_{k-1}\Delta\bar{z}_{k-1}} - \frac{r_k - r_{k+1}}{N^2_k\Delta\bar{z}_k}\right), \tag{8a}$$

for $k = 1,\ldots,M$, where the r_k value is defined at the center of grid cell k, N_k defined at the lower edge of cell k, Δz_k is the height of cell k, and $\Delta\bar{z}_k \equiv (\Delta z_k + \Delta z_{k+1})$ is the distance between the cell centers. With this definition, the eigenvalue problem is

$$\mathcal{L}'F\big|_k + c^{-2}F_k = 0, \quad k = 1,\ldots,M \tag{8b}$$

$$\frac{F_0 - F_1}{N^2_0\Delta\bar{z}_0} = -\frac{1}{g}\overline{F}_0, \tag{8c}$$

$$\frac{F_M - F_{M+1}}{N^2_0\Delta\bar{z}_M} = 0, \tag{8d}$$

where $\overline{F}_0 \equiv (F_0 + F_1)/2$ is the surface value. This finite-difference scheme is identical to that results from the CTW finite-difference scheme below when the "slope" is a vertical wall followed by a flat bottom (section S2.6).

The operator is conservative in that

$$\int \mathrm{d}z\, \mathcal{L}'r \sim \sum_{k=1}^{M}\Delta z_k \mathcal{L}'\psi|_k = \frac{r_0 - r_1}{N^2_0\Delta\bar{z}_0} - \frac{r_M - r_{M+1}}{N^2_M\Delta\bar{z}_M} \tag{8e}$$

(eq. (S2.3)); only the contributions from boundary fluxes remain. This is the analogue of (7e). This is because the finite difference is designed so that exactly the same flux r_z/N^2 that exits one cell across an edge enters the adjacent cell. This is how OGCMs ensure, say, the conservation of salinity (???? REFERENCES ???????????).

Since $\langle,\rangle$ is a vertical integration, its natural definition for the present discrete system is

$$\langle q, r\rangle \equiv \sum_{k=1}^{M}\Delta z_k\, q_k\, r_k.$$

With this definition,

$$\begin{aligned}\langle q, \mathcal{L}'r\rangle &= \sum_{k=1}^{M}\Delta z_k q_k \frac{1}{\Delta z_k}\left(\frac{r_{k-1}-r_k}{N^2_{k-1}\Delta\bar{z}_{k-1}} - \frac{r_k - r_{k+1}}{N^2_k\Delta\bar{z}_k}\right)\\ &= q_1\frac{r_0 - r_1}{N^2_0\Delta\bar{z}_0} - q_M\frac{r_M - r_{M+1}}{N^2_M\Delta\bar{z}_M}\\ &\quad - \sum_{k=1}^{M-1}\Delta\bar{z}_k\frac{q_k - q_{k+1}}{\Delta\bar{z}_k}\frac{1}{N^2_k}\frac{r_k - r_{k+1}}{\Delta\bar{z}_k}\end{aligned} \tag{8f}$$

(eq. (S2.4b)). This is the analogue of (7f). The derivation above uses an analogue of "integration by parts", which is possible only because the finite difference is written in a "conservative" form.

When $r = F$ is an eigenvector, we plug in the boundary conditions. From the bottom boundary condition, the bottom flux term in (8f) vanishes. To bring the surface-flux term to a symmetric form, we add a new term that is identically zero and split the original term into two halves:

$$\begin{aligned} & q_1 \frac{F_0 - F_1}{N_0^2 \Delta\bar{z}_0} && + 0 \\ = & \, q_1 \left(\frac{1}{2} \frac{F_0 - F_1}{N_0^2 \Delta\bar{z}_0} + \frac{1}{2} \frac{F_0 - F_1}{N_0^2 \Delta\bar{z}_0} \right) && + \frac{q_0}{2} \left(-\frac{1}{g} \overline{F}_0 + \frac{1}{g} \overline{F}_0 \right) \\ = & -\frac{\overline{q}_0 \overline{F}_0}{g} - \frac{\Delta\bar{z}_0}{2} \frac{q_0 - q_1}{\Delta\bar{z}_0} \frac{1}{N_0^2} \frac{F_0 - F_1}{\Delta\bar{z}_0}. \end{aligned} \tag{8g}$$

Several intermediate steps have been omitted. See the derivation of eq. (S2.5). Plugging this expression into (8f) yields

$$\begin{aligned} \langle q, \mathcal{L}' F \rangle = & -\frac{\overline{q}_0 \overline{F}_0}{g} \\ & - \frac{\Delta\bar{z}_0}{2} \frac{q_0 - q_1}{\Delta\bar{z}_0} \frac{1}{N_0^2} \frac{F_0 - F_1}{\Delta\bar{z}_0} - \sum_{k=1}^{M-1} \Delta\bar{z}_k \frac{q_k - q_{k+1}}{\Delta\bar{z}_k} \frac{1}{N_k^2} \frac{F_k - F_{k+1}}{\Delta\bar{z}_k} \\ \equiv & \, A(q, F). \end{aligned} \tag{8h}$$

This is the analogue of (7g). The second line can be interpreted as the vertical integral $\int_{-D}^{0} \mathrm{d}z \, q_z \psi_z / N^2$ evaluated with the trapezoidal rule, where the integrand is defined at the edges of the cells. The contribution from the bottom edge, e.g., $k = M$ of the summation, has vanished because of the bottom boundary condition.

Finally, since the discrete version of the eigenvalue problem is $\mathcal{L}' F|_k + c^{-2} F_k = 0$ for $k = 1, \ldots, M$, we obtain the same expression as (7h). From their definition, it is clear that $A(,)$ and $\langle , \rangle$ are symmetric and that $A(F, F)$ is negative. Even though we assumed that F satisfies the boundary conditions to arrive at the above expression, $A(q, r)$ as defined above is generally negative definite: Assume that $A(r, r) = 0$ for an $r \neq 0$; since all the terms in A are squares of real numbers, each must vanish; for the second line of $A(r, r)$ above to vanish, $r_0 = r_1 = \cdots = r_M \neq 0$, but then $\overline{r}_0 = (r_0 + r_1)/2 = r_0 \neq 0$, implying that $A(r, r) < 0$ because of the first line. Contradiction.

To summarize, a "conservative" (flux) formalism enables "integration by parts" of the bilinear form $\langle q, \mathcal{L}' F \rangle$ and the resultant interior integral becomes symmetric and negative. The boundary terms can be converted to a negative and symmetric form by adding and subtracting terms that obey the boundary conditions.

3.2 Finite-differencing CTW equations

In this section, we show that a standard finite-difference version of (1a) has the same properties as developed above.

We use the z coordinates, first, for simplicity; we have not tried to construct a finite-difference scheme for the sigma coordinates that has the same integral properties. The z coordinates also have a distinct advantage that they can handle slopes that include

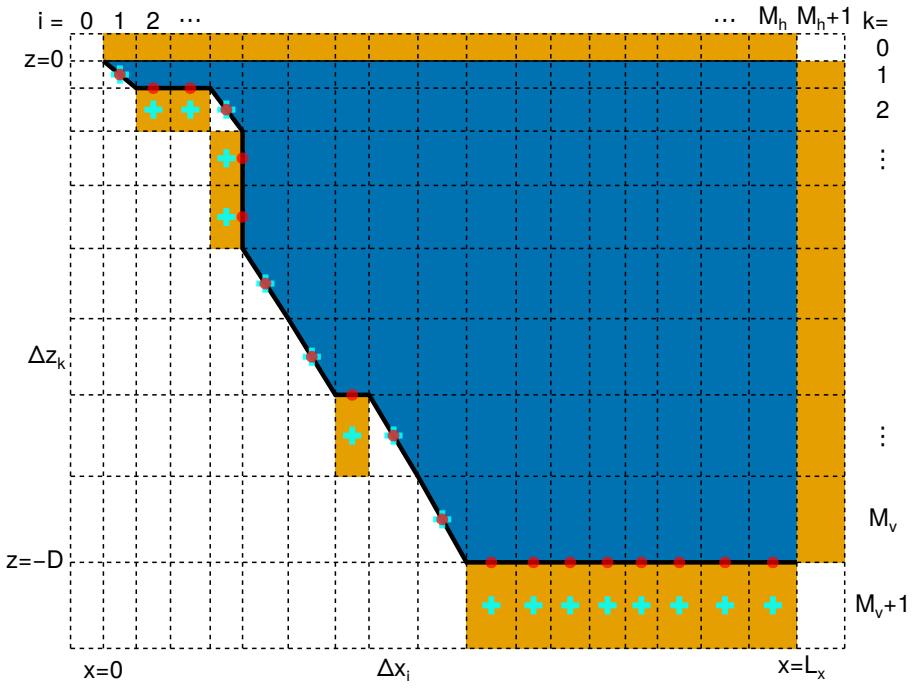

Figure 1: Schematic diagram of the grid, indexing scheme, and gridpoint arragement. The thick solid line indicates the continental slope and bottom at $z = h(x)$, and the thin solid line, the sea surface at $z = 0$. The offshore edge of the computational domain is at $x = L_\mathrm{x}$. The dashed lines indicate the grid and F values are defined at the center of each gridbox. The indices run over $i = 0, \ldots, M_\mathrm{h} + 1$ and $k = 0, \ldots, M_\mathrm{v} + 1$, where $i = 1, \ldots, M_\mathrm{h}$ and $k = 1, \ldots, M_\mathrm{v}$ cover the physical domain. "Lobe" regions are set above the sea surface $k = 0$ and to the right of the physical domain $i = M_\mathrm{h} + 1$; the values in these lobes are used in order to define F_x, F_z, and $\bar{F} = [F(i = M_\mathrm{h}) + F(i = M_\mathrm{h} + 1)]/2$ on the right boundary and $\bar{F} = [F(k = 0) + F(k = 1)]/2$ on the surface. Along the slope-bottom boundary (thick black line), the boundary values are defined on the boundary (red circles); those values are, however, "stored" in the F array at the adjacent cell-center positions (cyan crosses) where the boundary is horizontal or vertical. Where the boundary is diagonal, however, the boundary point coincides with the cell center and the F value is naturally stored there. Our code ensures that $\Delta z_0 = \Delta z_1$ and $\Delta x_{M_\mathrm{h}+1} = \Delta z_{M_\mathrm{h}}$.

purely-vertical sections. Indeed, when the entire slope is a vertical wall followed by a flat bottom, our finite-difference scheme below becomes separable in x and z and yields a finite-difference version of the vertical-mode eigenvalue problem and a finite-difference analogue of $X_{xx} + (c/f)^2 X = 0$, which gives the offshore exponential decay of the Kelvin mode (section S2.6).

Figure 1 shows the grid configuration for a continental slope followed by a flat bottom. The slope depicted in Fig. 1 is artificial in order to indicate that our scheme allows for flat portions and purely-vertical ones within the slope. The right boundary condition that $\lim_{x\to\infty} F_x = 0$ (eq. (1c)) is replaced by $F_x|_{x=L_\mathrm{x}} = 0$. As long as $x = L_\mathrm{x}$ is far enough as compared with the offshore decay scale of the baroclinic modes (See examples of solutions in section 4), the value L_x should not matter. BC87 recommend, as a rule of thumb, that L_x be twice the width of the slope.

The F values are defined at the center of each grid cell in the interior. We use the notation $F(i, k)$ or $F_{i,k}$ for the value at cell (i, k), whichever is convenient or clearer in the context. We sometimes omit one of the indices like "F_{k+1}" to mean $F_{i,k+1}$ if the context allows.

Above the sea surface and to the right of the right boundary are "ghost cells". The surface ghost cells constitute the surface "lobe" and the right ghost cells the right "lobe". They also have F values at their centers and participate in the equations through the relation $\overline{F}_0 = (F_0 + F_1)/2$, where F_0 is the value in a surface ghost cell, F_1 is the value just below the surface, and $\overline{F}_0$ is the value right at the surface. The right lobe is used similarly.

For the surface and right-edge boundary conditions, we use the symbol $\overline{F}$ as a short hand for the simple average like $\overline{F}_0 = (F_0 + F_1)/2$. The variables that participate in each equation are still the interior variable and the neighboring ghost-cell variable. The average like $(F_0 + F_1)/2$ is the right one because our code ensures that $\Delta z_0 = \Delta z_1$ and $\Delta x_{M_\mathrm{h}+1} = \Delta x_{M_\mathrm{h}}$. Along the slope-bottom boundary, however, the width or height of the neighboring ghost cell is different from the interior one and the average like $\overline{F}_0 = (F_0 + F_1)/2$ is not the right one. This makes it hard (impossible?) to construct the symmetric form (see below).

To avoid this problem, the boundary values of $\overline{F}$ are "defined" on the slope/bottom boundary (circles on the thick black line in Fig. 1), *not as an average between the interior value and the ghost-cell value.* The ghost cells to the left of vertical walls or those below flat bottoms (cyan crosses in Fig. 1) do *not* have their own F values; they are just used to "store" $\overline{F}$ values in our computer program. We still use the notation $F_{i,k}$ to represent the value stored in cell (i, k). The "corner cell", a cell split by a diagonal segment (thick black line) of the slope, is a special case: the boundary value $\overline{F}$ is defined at its cell center.

With this preparation, the operator of the interior equation (1a) is

$$\begin{aligned}\mathcal{L}F|_{i,k} = \frac{1}{\Delta x_i}\left(\frac{F_{i+1,k} - F_{i,k}}{\Delta \bar{x}_i} - \frac{F_{i,k} - F_{i-1,k}}{\Delta \bar{x}_{i-1}}\right) \\ + \frac{1}{\Delta z_k}\left(\frac{F_{i,k-1} - F_{i,k}}{\tilde{N}^2_{k-1}\Delta \bar{z}_{k-1}} - \frac{F_{i,k} - F_{i,k+1}}{\tilde{N}^2_k \Delta \bar{z}_k}\right) \quad \text{for } (i,k) \in \Omega. \end{aligned} \tag{9}$$

This form is a straightforward extension of (8a) and obviously "conservative". The ocean domain Ω represents the set of the "interior" gridpoints, excluding the boundary points (circles in Fig. 1) and the ghost points (orange cells).

If there were no "corner cells" (Fig. 1), that is, if the "slope" consisted entirely of vertical and horizontal steps, the slope boundary condition (1d) would reduce either to $F_x = (f/c)F$ (where $h_x \to \infty$) or to $F_z = 0$ (where $h_x = 0$) at each segment of the steps. In this case, the following derivation would not be much more complicated than in the above 1-d case. Initially, we did use this scheme and obtained numerical solutions. It turned out, however, the accuracy of the solutions was not adequate as compared with that of solutions from BC87's program (not shown). For this reason, we have introduced the corner cells, which have brought our solutions much closer to those from BC87's program (section 4) at the cost of the significantly more complicated derivation below.

With the definition (9), our finite-difference version of (1) is

$$\mathcal{L}F|_{i,k} = 0, \qquad (i,k) \in \Omega \tag{10a}$$

$$\frac{F_{i,0} - F_{i,1}}{\tilde{N}_0^2 \Delta\bar{z}_0} + \frac{f^2}{g}\frac{F_{i,0} + F_{i,1}}{2} = 0, \qquad i = 1, \ldots, M_\mathrm{h}, \tag{10b}$$

$$\frac{F_{M_\mathrm{h}+1,k} - F_{M_\mathrm{h},k}}{\Delta\bar{x}_{M_\mathrm{h}}} = 0, \qquad k = 1, \ldots, M_\mathrm{v}, \tag{10c}$$

$$\frac{F_{i+1,k} - F_{i,k}}{\Delta\bar{x}_i} + \frac{\Delta x_i}{\Delta z_k}\frac{F_{i,k-1} - F_{i,k}}{\Delta\bar{z}_{k-1}\tilde{N}_{k-1}} = \frac{f}{c}F_{i,k}, \qquad (i,k) \in \text{Corner Cells}. \tag{10d}$$

$$\frac{F(i_\mathrm{s}[k],k) - \overline{F}(i_\mathrm{s}[k]-1,k)}{\Delta x_{i_\mathrm{s}[k]}/2} = \frac{f}{c}\overline{F}(i_\mathrm{s}[k]-1,k), \quad k \in [k|\text{vertical wall}]. \tag{10e}$$

$$\frac{F(i,k_\mathrm{s}[i]) - \overline{F}(i,k_\mathrm{s}[i]+1)}{\Delta z_{k_\mathrm{s}[i]}/2} = 0, \qquad i \in [i|\text{flat bottom}]. \tag{10f}$$

The last three equations come from the slope boundary condition (1d). The first of the three boundary conditions is a straightforward rendition of (1d) because $h_x = \Delta z_k/\Delta x_i$ for the corner cell (i,k). To derive this, we have used Gauss's theorem on the area integral of $\mathcal{L}F$ over the triangle within the corner cell (blue area, Fig. 1). This is a standard "finite-volume method", that is, to construct a conservative discretized form from a multi-dimensional divergence (??????? REFERENCES ??????????). The other two versions of the slope boundary condition are also straightforward renditions of $F_x = (f/c)F$ and $F_z/\tilde{N}^2 = 0$. Recall, however, that the values denoted by $\overline{F}$ are defined on the boundary (circles in Fig. 1), not as an average between the neighboring interior and ghost-cell values.

We now calculate

$$\langle q, \mathcal{L}F\rangle \equiv \sum_{(i,k)\in\Omega} \Delta x_i \Delta z_k \, q_{i,k} (\mathcal{L}F)_{i,k}$$

for an eigenvector F. The techniques are the same as for the 1-d case above: integration by parts and the addition and subtraction of boundary terms. The calculation is shown in section S2.3, which is tedious without being difficult. The result is (S2.25). Without reproducing it here, we summarize it in the familiar form:

$$A(q,F) - \frac{f}{c}\langle q, F\rangle_\mathrm{b} = 0,$$

where A takes an analogous form to (4). The boundary "integral" is

$$\langle q, r\rangle_\mathrm{b} \equiv \sum_{k=1}^{M_\mathrm{v}} \Delta z_k \, \overline{q}_k \, \overline{r}_k, \tag{11}$$

where $\overline{q}_k$'s and $\overline{r}_k$'s denote the slope-boundary values (circles on the slope in Fig. 1 except for those on the flat-bottom segments). The orthogonality of the modes

$$\langle F^{(l)}, F^{(n)}\rangle_\mathrm{b} = 0 \quad \text{if } c^{(l)} \neq c^{(n)}$$

and the reality of the eigenvalues follow from the symmetry of $A(,)$ and $\langle,\rangle_\mathrm{b}$ and additionally, the negative definiteness of A proves that $f/c < 0$ except for the barotropic mode under the rigid-lid approximation (section S2.2).

As discussed in section 2, the continuous version of this boundary integral is

$$\langle q, r\rangle_{\rm b} = \int_0^\infty {\rm d}x\, h_x\; q\, r|_{z=-h(x)}\,, \tag{12}$$

which potentially includes purely-vertical regions within the slope. The relation of this continuous form with the discrete version (11) is the observation that ${\rm d}x\, h_x = -{\rm d}z$. To obtain a clearer correspondence, we first remove the flat parts of the slope/bottom: the range of integration is $\partial\Omega' \equiv \{x \mid 0 < x < \infty \;\&\; h_x(x) > 0\}$, the removal not affecting the value of the integral because $h_x = 0$ there. We next change variables from x to z by $z = -h(x)$. Then the "bottom" is $x = s(z)$, which is the inverse of $z = -h(x)$. The inverse does not exist on the flat parts of the slope/bottom (Which value should x take along a flat bottom $z = z_1$?), but the flat parts have already been removed from the integral and are expressed as harmless jumps in $s(z)$. The new range of integration, therefore, is from $z = 0$ to $z = -D$ without any gaps, and

$$\langle q, r\rangle_{\rm b} = \int_{\partial\Omega'} {\rm d}x\, h_x\; q\, r|_{z=-h(x)} = \int_0^{-D} (-{\rm d}z)\; q\, r|_{x=s(z)} = \int_{-D}^0 {\rm d}z\;\; q\, r|_{x=s(z)}\,.$$

This is a natural counterpart of the discrete form (11). When the "slope" is a purely vertical wall followed by a flat bottom, the CTW modes are reduced to vertical modes and the inner product $\langle q, r\rangle_{\rm b}$ reduces to the regular vertical integral and the orthogonality of CTW modes reduces to that of the vertical modes (section S1.3). Exactly the same story holds for the discrete form (11) (section S2.6).

Orthogonality in terms of (11) implies that there should be at most $M_{\rm v}$ independent modes even though there are much more gridpoints. This is what we prove in the next section among other things.

3.3 Matrix formalism

While most mathematical properties of the finite-difference scheme have been derived from the raw finite-difference forms in the previous section, we translate the set of the finite-difference equations into a matrix equation for three reasons: 1) With the matrix formalism, we can fairly easily prove that there are exactly $M_{\rm v}$ physical solutions to the finite-difference eigenvalue problem even though the eigenvalue problem itself has as many solutions as there are active gridpoints and that the remaining solutions are all unphysical with $c = 0$; 2) Our computer program to solve the equations uses solvers of matrix eigenvalue problems and so the user would need to understand the matrix formalism to understand the code; 3) We will show how to make the matrices symmetric below, which will enable our code to utilize a much faster and easier-to-use eigenvalue solver than general solvers. As to the last point, if the matrices are symmetric, the bilinear forms (section S2.3) are also symmetric, but not necessarily the other way around. Section S2.4 provides all the details and this subsection shows an outline and summarizes the results.

3.3.1 Constructing the matrices

First, we have viewed the discrete F values as arranged in the 2-d plane: $F_{i,k}$, as in Fig. 1. For the matrix form, we line up all these "active" variables in a column vector $\vec{F} = [\ldots, F_{1,1}, \ldots, F_{1,2}, \ldots]^T$. "Active" variables are those that are used in one of the finite-difference equations (10) (Fig. 1). In doing so, we give the gridpoint (i, k) of

each active $F_{i,k}$ a serial number $\nu(i,k)$ and write $F[\nu(i,k)] \equiv F_{i,k}$. With this notation, $\vec{F} = [F[1], F[2], \ldots, F[M]]^T$, where M is the total number of the active gridpoints.

In this view, each equation in the set (10) takes the form of either

$$\sum_\nu A[\lambda,\nu]\, F[\nu] = 0 \quad \text{or} \quad \sum_\nu A[\lambda,\nu]\, F[\nu] = \frac{f}{c} \sum_\nu B[\lambda,\nu]\, F[\nu],$$

where λ is a serial number of the particular equation. A and B are the matrices we are constructing. Since only 2–4 F variables are involved in each equation, A and B are very "sparse"—all their components being zero except for those 2–4 nonzero components per row.

Next, we multiply (10a) by $\Delta x_i \Delta z_k$, (10b) by Δz_k, (10c) by Δx_i, (10d) and (10e) by Δz_k, and (10f) by Δx_i. These factors are necessary to achieve symmetry and have been inspired by the calculation of $\langle F, \mathcal{L}F\rangle$ in section 3: we will see that with our definition of the matrices, we find that (almost) $\vec{q}^T A \vec{r} = A(\vec{q},\vec{r})$ and that $\vec{q}^T B \vec{r} = \langle \vec{q},\vec{r}\rangle_\mathrm{b}$.

We also have to add and subtract boundary terms to some of the left-hand sides of the equations. This corresponds to the technique we explained in section 3.2 to bring $\langle q, \mathcal{L}r\rangle$ to a symmetric form. Section S2.4 defines A and B to be symmetric from the beginning, but, to reduce the information density here, we first explain the method of arranging the equations to determine the matrices. At this point B is already symmetric, but A is not. We then explain how to modify A to bring it to a symmetric form.

We determine the numbering (order) of the equations and the numbering of the active gridpoints so that A and B become symmetric. Only the relation between these two sets of numbers matters and the exact ordering of the equations does not, except that we put the equations involving (f/c) to the last for convenience (see below).

For each interior cell (i,k), there is one interior equation (10a) which is centered at that gridpoint. We number the equations and the gridpoints in such a way that $\lambda = \nu(i,k)$, the serial number of the equation being equal to the serial number of that central gridpoint. In this way, $A[\nu,\nu]$, the diagonal of A, becomes the coefficient of that central $F[\nu]$ value, where $\nu = \nu(i,k)$. We have now defined the first M_int rows of A, where M_int is the number of the interior points and the number of the interior equations. We consider the interior gridpoints as "used" now.

We next line up the surface boundary conditions (10b). Each of the M_h equations includes one interior point $F_{i,1}$ and one ghost point $F_{i,0}$, the latter having not been "used" yet. We now order these equations and the ghost points in such a way that $\lambda = \nu(i,0)$. The diagonal $A[\nu,\nu]$ is now the coefficient of $F[\nu]$, where $\nu = \nu(i,0)$. We have now defined rows $\lambda = M_\mathrm{int} + 1$ to $M_\mathrm{int} + M_\mathrm{h}$ of A and "used" the surface ghost cells. In the same manner, we define the next M_v rows of A for the right-edge boundary conditions (10c).

We next line up the flat-bottom boundary conditions (10f), which apply not only to the flat-bottom region but also to flat regions, if any, within the slope (Fig. 1). Let the number of the flat-bottom gridpoints be M_flat and the number of corner points be M_corner; then $M_\mathrm{flat} + M_\mathrm{corner} = M_\mathrm{h}$ (Fig. 1). The "unused" F values are $\overline{F}(i, k_\mathrm{s}[i]+1)$, which are "stored" in the ghost cell $(i, k_\mathrm{s}[i]+1)$. As for the preceding equations, then, we set $\lambda = \nu(i, k_\mathrm{s}[i]+1)$, which defines the M_flat new rows of A.

So far, B has not appeared in the equations and therefore its first $M_{\rm int}+M_{\rm h}+M_{\rm v}+M_{\rm flat}$ rows are all zero. Next, we line up (10d) and (10e) together in the order of $k=1,\ldots,M_{\rm v}$; that is, vertical-wall gridpoints and corner gridpoints are arranged vertically in their natural order (Fig.1). Accordingly, each "unused" point is either a corner point $F(i,j)$, in which case $\lambda=\nu(i,j)$, or a vertical-wall point $\overline{F}(i_{\rm s}[k]-1,k)$, in which case $\lambda=\nu(i_{\rm s}[k]-1,k)$. This determines the remaining $M_{\rm v}$ rows of A and B. Importantly, B has only $M_{\rm v}$ non-zero components and they are all along the diagonal: $B(\nu,\nu)=\Delta z_k$ for the last $M_{\rm v}$ rows.

We can use these matrices to numerically solve the eigenvalue problem, but A is not symmetric. The central point $\nu_1=\nu(i,1)$ of the interior equation (10a) is just below the sea surface, and the equation includes the ghost cell $\nu_0=\nu(i,0)$ above the surface. For symmetry, the coefficient $A(\nu_1,\nu_0)$ of $F(i,0)$ in that interior equation must be equal to the corresponding coefficient $A(\nu_0,\nu_1)$ in the boundary equation (10b) whose "central" point is $(i,0)$. Specifically, the derivative

$$\frac{F_{i,0}-F_{i,1}}{\tilde{N}_0^2\Delta\bar{z}_0}$$

appears both in the interior equation (10a) at $(i,1)$ and in the $z=0$ boundary equation (10b) at $(i,0)$. The off-diagonal component

$$A[\nu(i,1),\nu(i,0)]=\Delta x_i\frac{1}{\tilde{N}_0^2\Delta\bar{z}_0}$$

of the interior equation is not equal to the off-diagonal component

$$A[\nu(i,0),\nu(i,1)]=-\Delta x_i\frac{1}{\tilde{N}_0^2\Delta\bar{z}_0}+\Delta x_i\frac{f^2}{g}\frac{1}{2}$$

of the boundary equation. In other words, the problem of the surface boundary condition is that the boundary term $(f^2/g)(F_0+F_1)$ enters A.

To remedy this, we use essentially the same technique as used in transforming the bilinear by modifying the surface-boundary term in (8g). Specifically, we "split" the derivative in the interior equation into two halves and replace one of them with the boundary value using the boundary condition (10b):

$$\begin{aligned}&\frac{F_{i,0}-F_{i,1}}{\tilde{N}_0^2\Delta\bar{z}_0}\\ =&\frac{1}{2}\frac{F_{i,0}-F_{i,1}}{\tilde{N}_0^2\Delta\bar{z}_0}+\frac{1}{2}\frac{F_{i,0}-F_{i,1}}{\tilde{N}_0^2\Delta\bar{z}_0}\\ =&\frac{1}{2}\frac{F_{i,0}-F_{i,1}}{\tilde{N}_0^2\Delta\bar{z}_0}-\frac{1}{2}\frac{f^2}{g}\frac{F_{i,0}+F_{i,1}}{2}.\end{aligned}\tag{13}$$

After this transformation,

$$A[\nu(i,1),\nu(i,0)]=\frac{\Delta x_i}{2}\frac{1}{\tilde{N}_0^2\Delta\bar{z}_0}-\frac{\Delta x_i}{2}\frac{f^2}{g}\frac{1}{2}.$$

On the other hand, we multiply the boundary equation (10b) by $-1/2$ and then its off-diagonal component becomes

$$A[\nu(i,0),\nu(i,1)]=\frac{\Delta x_i}{2}\frac{1}{\tilde{N}_0^2\Delta\bar{z}_0}-\frac{\Delta x_i}{2}\frac{f^2}{g}\frac{1}{2},$$

which is equal to the off-diagonal component of the interior equation, $A[\nu(i,1),\nu(i,0)]$.

Likewise, the left-hand side of the corner-cell equation (10d) has to be modified in the same way where its center is just below the sea surface (Fig. 1). Otherwise, the slope boundary equation needs no modification because the boundary term $(f/c)\overline{F}$ occurs on the right-hand side, entering B without affecting A. The other boundary conditions need no modifications except that the flat-bottom equation needs a sign flip.

3.3.2 Properties of the matrix eigenvalue problem

In this way, we now have a generalized matrix eigenvalue problem with symmetric matrices A and B:

$$A\vec{F} = \frac{f}{c}B\vec{F}, \tag{14}$$

which is called "generalized" because of B. Multiplying $\vec{q}^{\,T}$ on both sides, we can follow the same argument as in the preceding sections to prove that f/c is real and that the eigenvectors are orthogonal in the sense that

$$\vec{F}^{(l)T}B\vec{F}^{(n)} = 0 \quad \text{if } c^{(l)} \neq c^{(l)}.$$

As explained above, the components of B are all zero except on the diagonal of the last M_v rows from the vertical-wall or corner-point boundary equations, where $B[\nu,\nu] = \Delta z_k$. Therefore,

$$\vec{q}^{\,T}B\vec{r} = \sum_{k=1}^{M_\mathrm{v}} \Delta z_k \overline{q}_k \overline{r}_k,$$

where $\overline{q}_k$ and $\overline{r}_k$ refers either to the vertical-wall boundary point or to the corner point, whichever it is at depth k. That is, $\vec{q}^{\,T}B\vec{r} = \langle \vec{q},\vec{r}\rangle_\mathrm{b}$ as defined in the previous subsection (eq. (11)).

The calculation of $\vec{q}^{\,T}A\vec{r}$ (section S2.5) is similarly to, and as tedious as, that of $A(q,r)$ (section S2.3). It turns out that $\vec{q}^{\,T}A\vec{r}$ is almost equal to $A(\vec{q},\vec{r})$ and that $\vec{q}^{\,T}A\vec{F} = A(\vec{q},\vec{F})$ if $\vec{F}$ is an eigenvector. This is because we used the bottom boundary condition $F_z/\tilde{N}^2 = 0$ to eliminate the bottom flux term from $A(\vec{q},\vec{F})$ whereas the matrix A just uses the left-hand sides of the boundary equations and the calculation of $\vec{q}^{\,T}A\vec{r}$ does not use equalities like $F_z/\tilde{N}^2\Big|_{z=-D} = 0$.

Near the end of the preceding subsection, we deduced that $A(\vec{q},\vec{r})$ is negative definite under the free-surface condition. The same argument applies to $\vec{q}^{\,T}A\vec{r}$ (section S2.5), proving that the matrix A is negative definite. That not only proves that $f/c < 0$ but also leads to an important property as follows.

Consider a column vector of the form

$$\vec{F}' = [a[1], a[2], \ldots, a[M'], 0, \ldots, 0]^T, \tag{15}$$

where $M' \equiv M - M_\mathrm{v}$. This vector gives $B\vec{F}' = 0$ because all the first M' rows of B are zero. This $\vec{F}'$ with $c = 0$ is therefore a solution, whatever the values $a[\nu]$ are, to the eigenvalue problem

$$B\vec{F}' = \frac{c}{f}A\vec{F}',$$

which is equivalent to (14). This solution is clearly unphysical, with a random distribution of values off the slope-bottom boundary. Since there are M' linearly independent vectors of the form (15), there are M' independent unphysical eigenvectors with $c = 0$.

Conversely, if $c = 0$, the associated eigenvector must satisfy $B\vec{F} = 0$, that is, $\Delta z_k \overline{F}_k = 0$ for all k. Such a vector must hence be of the form (15).

Is it, then, possible that $B\vec{F} = A\vec{F} = 0$ and $c \neq 0$? The answer is no. If $A\vec{F} = 0$, then $\vec{F}^T A\vec{F} = 0$; but this is possible only when $\vec{F} =$ uniform $\neq 0$ under the rigid-lid condition. In this case, $B\vec{F} \neq 0$.

This proves that there are exactly M' eigenvectors associated with $c = 0$ and the remaining solutions have $c \neq 0$. This fact makes it easy to filter out these unphysical solutions.

Moreover, from the negative definiteness of A, we can prove that there are exactly M eigenvectors (section S2.4.7). This proves (under the free-surface condition) that there are exactly $M_{\mathrm{v}} = M - M'$ physical eigenvectors with $c \neq 0$. (We do not know how to prove this under the rigid-lid condition, but from our experience with numerical solutions, we always find exactly M_{v} physical solutions even under the rigid-lid condition. There may be a way to prove this.)

4 Numerical solutions

This matrix eigenvalue problem is solved numerically using the LAPACK library (Anderson et al. 1999). For the free-surface case, the matrix equation is $(-B)\vec{F} = (c/f)(-A)\vec{F}$ (sections 3.3 and S2.4). It is solved with the DSYGD subroutine, which is specialized in cases where both matrices are symmetric and the matrix on the right-hand side is positive definite. [The algorithmic description of this subroutine is found in the "Generalized Symmetric Eigenproblems (GSEP)" section of Anderson et al. (1999).] Unphysical solutions are distinguished because $c/f = 0$ for them (section 3.3).

For the rigid-lid case, the matrix equation is $A\vec{F} = (f/c)B\vec{F}$; it is solved with the DGGEV subroutine, which is a general general-eigenvalue problem solver. This subroutine returns two values, denoted α and β in the manual, for each solution such that α/β is the eigenvalue. If the eigenvalue is $\pm\infty$, the routine returns $\beta = 0$. [The algorithmic description of this subroutine is found in the "Generalized Nonsymmetric Eigenproblems (GNEP)" section of Anderson et al. (1999).] This situation indicates that $c = 0$, enabling us to distinguish the unphysical solutions. For the barotropic mode, whose eigenvalue should be $c = \pm\infty$, the subroutine returns a very small α/β value.

As of this writing, we use LAPACK 3.12.0, which comes with macOS 16 (https://developer.apple.com/documentation/accelerate/blas-library).

In what follows, we show examples of solutions from our code. The test cases are listed in table 1. Solution CS0 uses a linear continental, a constant stratification, and a uniform grid to show basic features of the solutions. To demonstrate that the solutions from our code are very similar to those from BC87's, we obtain a set of solutions with as similar a configuration as possible from BC87's code and compare the two sets of solutions. Since our purpose is not a systematic comparison, however, this is the only example for such comparison.

Solution CS1 then uses the same configuration except with a little more realistic stratification. This solution points to a problem of a uniform grid. Solution CS hence modifies the grid spacing to make it suite the variable stratification better. This demonstrates the usefulness of variable grid spacing.

Solution ShCS next explores changes when a gentle continental shelf is attached to the steep continental slope. This test again demonstrates the usefulness of having a vastly different grid spacing between the shelf and continental slope. Solution ShVW then replaces the continental slope with a vertical wall, exploiting an advantage of the z coordinates. These two solutions also suggest a scientifically interesting issue of the coupling between shelf waves and Kelvin waves. Finally, VW removes the continental shelf, demonstrating

Table 1: Test solutions.

Solution	Slope	$N(z)$	Δz
CS0	linear	const	uniform
CS1	linear	exponential	uniform
CS	linear	exponential	$\propto 1/N(z)$
ShCS	shelf+slope	exponential	$\propto 1/N(z)$
ShVW	shelf+wall	exponential	$\propto 1/N(z)$
VW	wall	exponential	$\propto 1/N(z)$

the similarity between the structure on along the continental slope in ShVW and the vertical structure of the vertical-wall modes (Kelvin wave modes). As such, the final three test solutions are designed to demonstrate advantages of our code as well as to inspire a future study.

4.1 Linear continental slope and uniform N

In the first test (CS0), we use a simple configuration, where there is a linear continental slope for $0 < x < 100\,\mathrm{km}$ followed by a flat bottom at 5000 m. The right edge of the computational domain is at $x = 300\,\mathrm{km}$. Even though our code, since it uses the z coordinates, can handle a vanishing depth at $x = 0$, we set $h(0) = 50\,\mathrm{m}$ before the linear slope starts. This is in order to compare our solutions with corresponding solutions from BC87's code, which uses the sigma coordinates. The Coriolis parameter is set to $10^{-4}\,\mathrm{rad/s}$, a value at 43°N. This configuration is inspired by the continental slope off southeastern Australia around 142°E, 40°S (Han et al 2025, revision under review). The Brunt-Väisälä frequency is set to $N = 0.003\,\mathrm{rad/s} = \mathrm{const.}$ for this first test and will be set to a somewhat more realistic profile in the next test. The free-surface boundary condition is used.

For our code, $\Delta z_1 = 50\,\mathrm{m}$ so that the initial "vertical wall" $h(0) = 50\,\mathrm{m}$ is expressed by a single grid cell. Subsequently, there are 50 cells in the vertical such that $\Delta z_k = 99\,\mathrm{m}$ for $k = 2, \ldots, 51$ and $\Delta x_i = \Delta z / h_x = 2\,\mathrm{km}$ for $i = 1, \ldots, 50$. In this way the slope from $z = -50\,\mathrm{m}$ to $z = -5000\,\mathrm{m}$ and from $x = 0$ to $x = 100\,\mathrm{km}$ is all expressed by a series of "diagonals" (Fig. 1) since one vertical step Δz_k is always followed by one horizontal step $\Delta x_i = \Delta x_{k-1} = \Delta z_{k-1}/h_x$. After the continental slope in the flat-bottom region, Δx_i is gradually increased like $\Delta x_{i+1} = r \Delta x_i$ with $r \approx 1.1$ until $x = L_\mathrm{x}$ is reached. The grid spacing Δx_i of the flat-bottom region is slightly adjusted so that the right edge exactly coincides with $x = L_\mathrm{x}$. As a result, there are $M_\mathrm{h} = 75$ grid cells in the x direction. As indicated above, $M_\mathrm{v} = 51$.

We use the version of BC87's code called `bigload4.for` (see the addendum https://www.whoi.edu/cms/files/Fortran_30425.htm to Brink and Chapman (1987)). This version uses an offshore boundary condition that $u_x = 0$ at $x = L_\mathrm{x}$, which is equivalent to $p_x = 0$ in the long-wave approximation because $fu = -p_y/\rho_\mathrm{o}$ and both u and p are separated between (x, z) and (y, t).

For BC87's code, we set $\Delta x = 2\,\mathrm{km}$ to get a comparable horizontal resolution on the slope, which gives 151 gridpoints over $0 \le x \le 300\,\mathrm{km}$. (Note that the gridpoints are located at vertices of the cells in BC87's code.) The sigma grid spacing is set to 1/50 (non-dimensional) and therefore there are 51 gridpoints in the vertical. The vertical resolution is then comparable at the bottom of the continental slope ($x = 100\,\mathrm{km}$, $h = 5000\,\mathrm{km}$) with that of our code while the vertical resolution becomes higher toward the coast as $h(x)$ decreases in the sigma coordinates.

To obtain solutions that are equivalent to those from our code, the free-surface boundary condition (with the same g value of course) and the long-wave approximation are used. The code searches for such a value of ω as to satisfy the eigenvalue problem starting from initial guesses. But, because of the long-wave approximation, $\omega = c\ell$, which enables us to specify initial guesses of ω on the basis of c values by fixing ℓ to an arbitrary value. The initial guesses of ω we provide are centered around $c^{(n)}\ell$ for each mode n, where the value of $c^{(n)}$ is the solution from our code. The relative accuracy ($\Delta\omega/\omega$) is set to 0.0005, 1/10 of the value quoted in BC87 as typical. To check whether the solution is the right

one, we count the number of zero-crossings along the wall-slope boundary (first along the vertical wall at $x = 0$ and then along the slope $z = -h(x)$). The number should agree with the mode number. [We are not aware of mathematical proof for the present eigenvalue problem, although this is common empirical knowledge and there are other eigenvalue problems for which this property is proven; e.g., the vertical-mode eigenvalue problem (7) (e.g., Courant and Hilbert 1989) and shallow-water modes in a channel (Iga 1995).] Each search converged to the right mode for $n = 1$–10 and to the wrong mode for the given $c^{(11)}$. Since our purpose is not to discuss the accuracy of higher modes, which would be difficult as we do not know true solutions, we stop at $n = 10$.

We ignore the barotropic mode, which, from our program, has an eigenvalue of $c^{(0)} \simeq 1640\,\mathrm{m/s}$ and an almost uniform $F^{(0)}(x, z)$ field (not shown). This eigenvalue is too large for the true offshore barotropic mode, whose eigenvalue should be $c^{(0)} \approx \sqrt{gH} \approx 220\,\mathrm{m/s}$. The reason for the large value is not clear. It may be resulting from the artificial boundary at $x = L_\mathrm{x}$.

In comparing solutions from the two programs, we normalize the solutions using a common norm based on the boundary inner product (2) in such a way that $\langle F^{(n)}, F^{(n)}\rangle_\mathrm{b}/D = 1$ for each n, where D is the total depth, that is, the depth of the flat-bottom region. Because the boundary inner product is a form of vertical integral (eq. (S1.16)), this normalization makes $F^{(n)}$ dimensionless and of $\mathcal{O}(1)$. For our finite-difference scheme, this inner product takes the form of (11).

For BC87's discretization scheme, we do not know whether there exists a documentation that discusses discretized versions of the inner product. Considering that the data are defined at vertices of grid cells, we tentatively use the most natural trapezoidal rule for the boundary integral:

$$\langle q, r\rangle_\mathrm{b} = \sum_{k=1}^{M_\sigma} \frac{h(0)}{M_\sigma - 1} \frac{q(0,k-1) + q(0,k)}{2} \frac{r(0,k-1) + r(0,k)}{2} + \sum_{i=1}^{M_x} \Delta z_i \frac{q(i-1,K) + q(i,K)}{2} \frac{r(i-1,K) + r(i,K)}{2}, \tag{16}$$

where $i = 0$ and $i = M_x$ are the left and right edges of the grid and $k = 0$ and $k = M_\sigma$ are the sigma levels at the sea surface and bottom. The first summation is a discretized version of the vertical integral along the vertical wall at $x = 0$; the second summation represents the along-bottom integral $\int \mathrm{d}x\, h_x q\, r$ (eq. (2)) because

$$\mathrm{d}x\, h_x \sim \Delta x \frac{h_i - h_{i-1}}{\Delta x} = \Delta z_i,$$

where $\Delta z_i \equiv h_i - h_{i-1}$ and therefore $\Delta z_i = 0$ off the continental slope. In the addendum (https://www.whoi.edu/cms/files/Fortran_30425.htm) to the original documentation, BC87 promised that $\langle F, F\rangle_\mathrm{b} = f$ in the output from their program. [See Brink (1989) for the reason for this normalization.] Using the tentative formula (16), then, we have confirmed that $\langle F, F\rangle_\mathrm{b} = f$ (precisely speaking, $|1 - \langle F, F\rangle_\mathrm{b}/f| < 10^{-15}$) for all the 10 modes, which strongly suggests that the above inner product is what BC87 use in their code. Using this norm, we re-normalize the solutions from BC87's code so that $\langle F^{(n)}, F^{(n)}\rangle_\mathrm{b}/D = 1$ for each mode. We also flip signs, if necessary, to ensure that the spatial pattern agrees between the two sets of solutions.

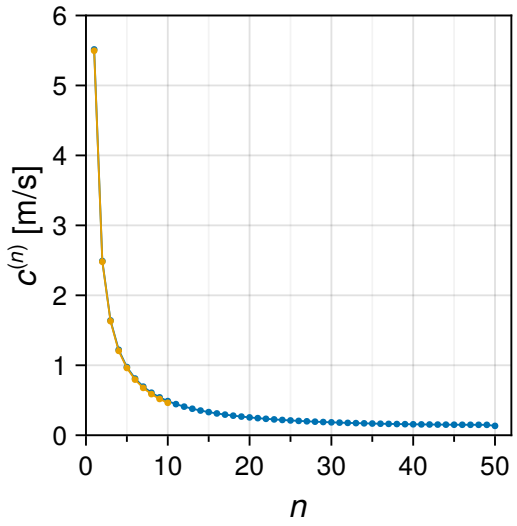

Figure 2: Solution CS0: Eigenvalue vs mode number for our code (blue) and BC87's (orange). Mode 0 (barotropic) is omitted. Only modes 1–10 are obtained with BC87's code. See text for details.

Figure 2 compares $c^{(n)}$ from the two methods. The $c^{(n)}$ values from our code are slightly larger than those from the other code, with the relative error larger for higher modes. Figure 3 shows the $F^{(n)}(x, z)$ fields as well as the $c^{(n)}$ values for the lowest 4 modes from the two programs. The only visual difference is that sometimes the locations and shapes of some of the zero contour lines differ. The difference in $c^{(n)}$ is about 0.01 m/s for them.

For more quantitative comparison, we plot $F^{(n)}$ along the bottom in Fig. 4. The solutions from our code (circles) slightly deviate from those from BC87's code (curves) at the peaks and troughs of the curves in the bottom half of the slope ($50\,\mathrm{km} < x < 100\,\mathrm{km}$) for modes 3 and 4. As Fig. 3 indicates, both the vertical and horizontal scales of variability decrease for higher modes, and therefore it is expected that difference between different finite-difference schemes will be larger for higher modes. It is, however, hard to pinpoint the reason for the difference.

4.1.1 Orthogonality

The most natural measure of orthogonality is the standard correlation coefficient:

$$r(\lambda, n) \equiv \frac{\langle F^{(\lambda)}, F^{(n)} \rangle_\mathrm{b}}{\langle F^{(\lambda)}, F^{(\lambda)} \rangle_\mathrm{b}^{1/2} \langle F^{(n)}, F^{(n)} \rangle_\mathrm{b}^{1/2}}.$$

Perfect orthogonality means that $r(\lambda, n) = 0$ when $\lambda \neq n$. For our discretization scheme, we have proven this property for the finite-difference equations (section 3.2); we have also confirmed that $|r(\lambda, n)| < 10^{-7}$ for all combinations of the 51 numerically-obtained modes. Our code carries out all calculations in double precision and (for this test) saves the result in single precision; the accuracy of 10^{-7} is consistent with single precision.

For BC87's code, we use the discrete inner product (16). The correlation is below 0.05 between mode 1 and the other 9 modes (Fig. 5). The correlation becomes larger for higher modes; for mode $\lambda > 2$, correlation with mode $\lambda + 1$ tends to be most prominent. In a

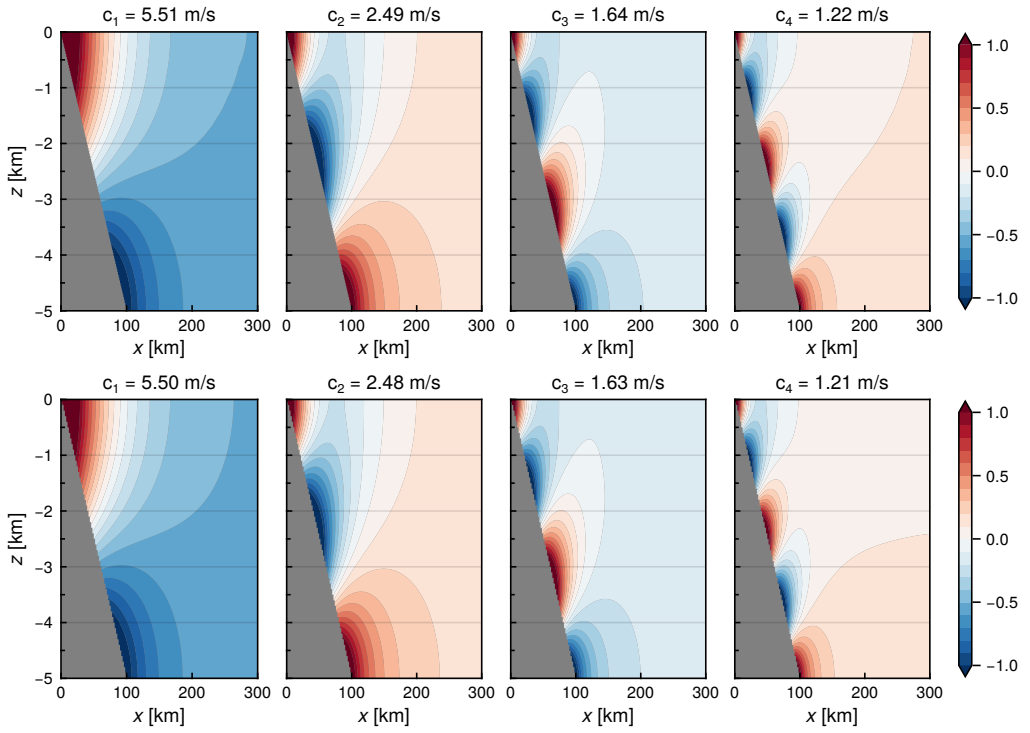

Figure 3: Solution CS0: $F^{(n)}(x, z)$ for $n = 1$–4 from our code (upper panels) and BC87's (lower panels). The eigenvalues are shown at the top of each panel.

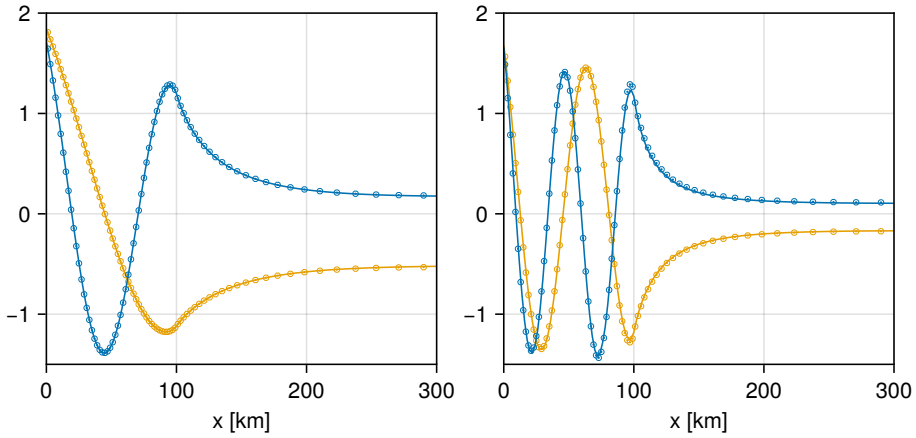

Figure 4: Solution CS0: Bottom trace, $F^{(n)}(x, z = -h(x))$, of the mode functions for $n = 1, 2$ (left panel) and $n = 3, 4$ (right panel) from our code (circles) and BC87's (lines). Each circle has a dot at its center.

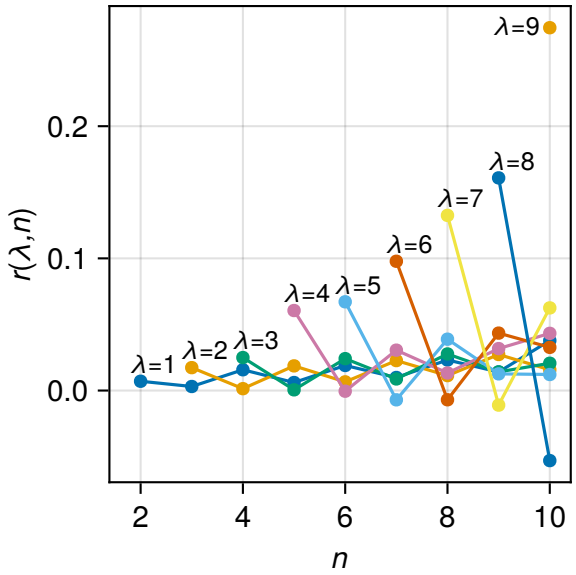

Figure 5: Solution CS0: Plot of the correlation coefficient $r(\lambda, n)$ for each $\lambda = 1, \ldots, 9$ from BC87's code. Only the off-diagonal components, $\lambda < n \leq 10$, are plotted. See text for details.

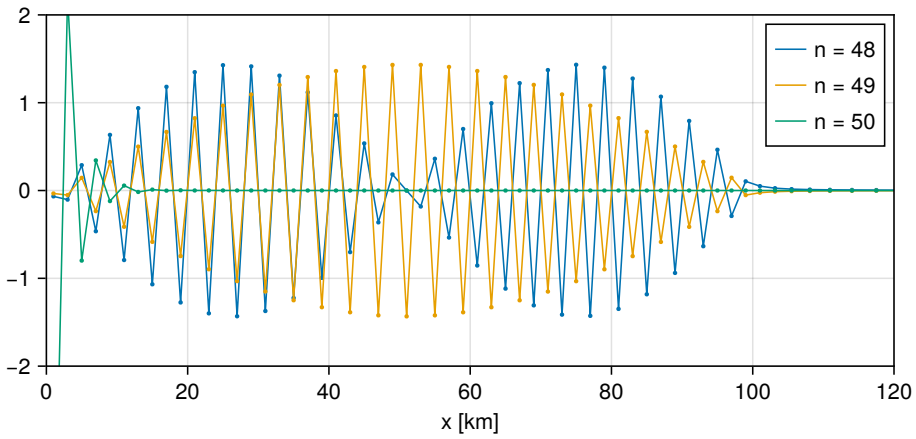

Figure 6: Solution CS0: Bottom trace, $F^{(n)}(x, z = -h(x))$, of the mode function for the last 3 modes from our code.

sense, this result indicates that the inner product (16) is "wrong" for BC87's code but we do not know how to discover the "correct" discrete version of the inner product.

4.1.2 Higher modes

Even though all eigenmodes are exact solutions to the matrix eigenvalue problem (up to the precision of the floating-point number representation on the computer), and even though they all have not-unrealistic eigenvalues and exactly satisfy the orthogonality condition, they can still be *unphysical in a different way.* Figure 6 shows the bottom traces of $F^{(n)}$ for the last 3 modes. For $n = 48$ and 49, most loops (peaks and troughs) are captured only by single gridpoints, suggesting that these modes are only marginally resolved. Indeed, mode 50 "collapses" to a totally unphysical profile; the reason must be that the actual wavelength of the mode is too small for the grid to represent. This sudden jump from $n = 49$ to $n = 50$ may be the reason for the slight deviation from the general trend in the $c^{(n)}$ curve (Fig. 2), where $c^{(50)}$ drops a little more than is expected from the smooth curve.

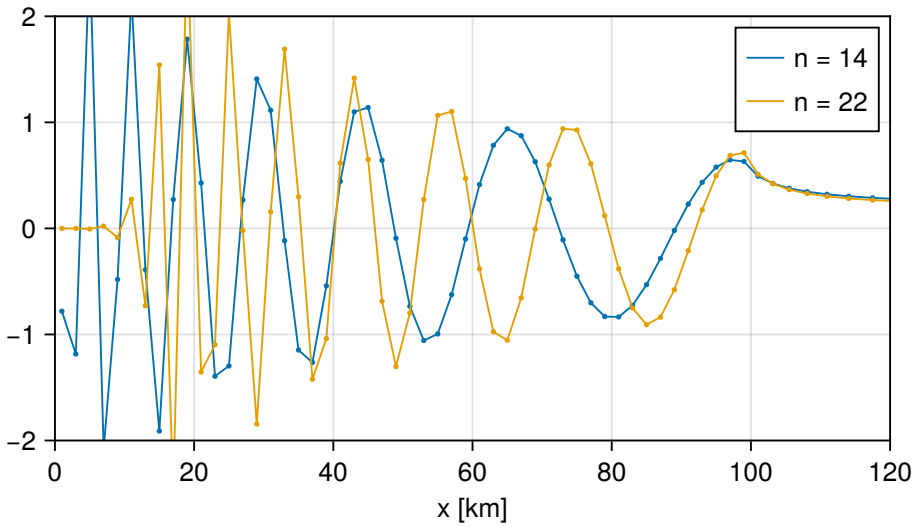

Figure 7: Solution CS1: Bottom trace, $F^{(n)}(x, z = -h(x))$, of the mode function for $n = 14$ and 22.

In reality, higher modes will be damped more strongly by bottom friction and other mixing and would contribute much less to real variability. The present analysis of the behavior of higher modes is, however, helpful when we use the modes to expand variability or forcing (e.g., see Tanaka & Kida 2025, manuscript in preparation ??????????????????).

We do not expect that further analysis of the realism of such high modes would be necessary; in the present paper, we present this result mainly as an aid for the user to determine necessary horizontal and vertical resolution depending on the problem they intends to solve. The next test solution illustrates the point.

4.2 Linear continental slope and exponential $N(z)$

In the next test, CS1, we switch to an exponential $N(z)$ profile; $N(0) = N_1 = 4.5\times10^{-3}\,\mathrm{rad/s}$ at the sea surface, $N(-D) = N_2 = 0.5 \times 10^{-3}\,\mathrm{rad/s}$ at the bottom, $z = -D = -5000\,\mathrm{m}$, and an exponential profile inbetween:

$$N(z) = N_2 + (N_1 - N_2)\frac{\exp\,(D + z)/s - 1}{\exp\,D/s - 1},$$

where $s = 1700\,\mathrm{m}$ is the vertical scale of the exponential. This stratification is a subjective ("by eye") fitting of the annual-mean stratification around 142°E, 40°S from the $1° \times 1°$ version of the World Ocean Atlas 2018 (Garcia et al. 2019). The background stratification is the only difference from the previous solution, CS0.

Figure 7 shows the bottom traces of a relatively low mode and a medium mode. The most prominent difference from the uniform-N case is that the local wavenumber tends to be large where N is large in each mode. As a result, the mode function "collapses" near the surface when the local wavelength has become shorter than the grid spacing. The curve for $n = 22$ in Fig. 7 is an example of this: it is nearly zero over $0 < x < 7\,\mathrm{km}$. Naturally, the "collapsed" region near the surface advances to depth for higher modes (not shown). For the unifrom-N case, CS0, this collapse did not happen until the very end of resolution ($n = 50$) because the local wavelengths were almost uniform along the slope.

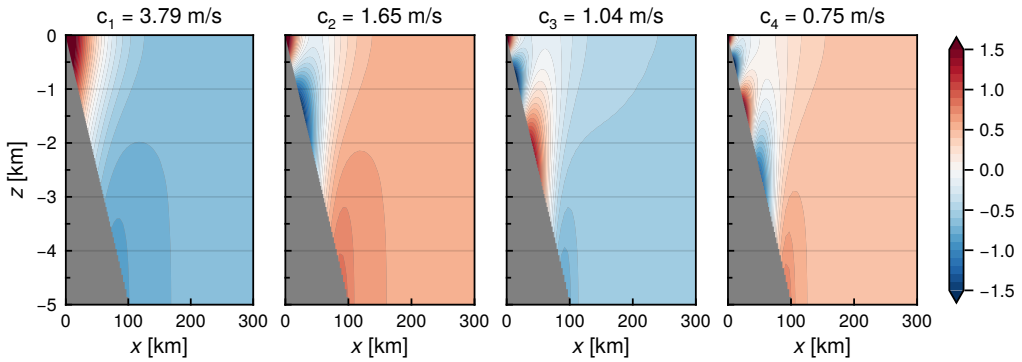

Figure 8: Solution CS: $F^{(n)}(x, z)$ for $n = 1$–4 from our code. Note that the contouring range is wider here than for Fig. 3.

This WKB-like relation between local wavenumbers and stratification is likely behind the recommendation of using the stretched coordinates $\mathrm{d}\zeta = \mathrm{d}z/N$ for the calculation of vertical modes (Early et al. 2020). Inspired by this discussion, we next determine Δz_k in such a way that Δz_k is approximately proportional to the local value of $1/N$. As a result, for the new test (Solution CS), the vertical grid spacing is about 38 m near the surface and 290 m near the bottom. The height of the initial vertical wall at $x = 0$ is also $\Delta z_1 \approx 38$ m. With this arrangement, there are 51 cells in the vertical. The horizontal resolution is determined by $\Delta x_i = \Delta z_{i+1}/h_x$ for $i = 1, \ldots$ until the flat bottom region is reached at $x = 100$ km. The Δx in the flat-bottom region is determined by $\Delta x_{i+1} = \alpha \Delta x_i$ with $\alpha \approx 1.1$ until the right edge of the computational domain is reached at $x = L_\mathrm{x}$. Since Δx is much larger near the bottom of the slope, there are only 65 grid cells in the x direction for this solution as compared with 75 in the previous solutions.

Figure 8 shows modes 1–4 from this solution. Unlike the uniform-N case, CS0, the amplitude of oscillation along the slope is largest near the surface, decreasing downslope. Because of the normalization $\langle F, F\rangle_\mathrm{b}/D = 1$, the amplitude is much larger than 1 at the surface and is much smaller than 1 near the bottom. Fig. 9 shows the bottom traces of the first four modes and selected high modes. This time, the mode function remains "healthy" up until $n \sim 40$ and the "collapse" starts only around $n \sim 45$. The curve (orange) for $n = 44$ starts to lose amplitude near the bottom ($x = 100$ km), the one (green) for $n = 46$ is nearly zero over 80 km $< x <$ 100 km, and the highest mode ($n = 50$) has nearly zero amplitude over 30 km $< x <$ 100 km. This result indicates that the upper ocean is somewhat oversampled and the lower ocean is somewhat undersampled; even though the scaling $\Delta z \propto 1/N$ delays the collapse but is not an ideal scaling.

4.3 Solutions with a continental shelf

Since our code uses the z coordinates, it can handle purely-vertical walls, which would help theoretically compare CTWs with Kelvin waves or interpret coastal waves in coarse-resolution OGCMs where the continental slopes are very poorly resolved. As a demonstration, solutions for three bottom profiles are compared. Those profiles are shown in Figs. 10 and 11 below.

4.3.1 Shelf with continental slope

For the first bottom topography of the set, ShCS, we use the same continental slope as previous solutions but attach a wide continental shelf: Specifically, the shelf is a linear

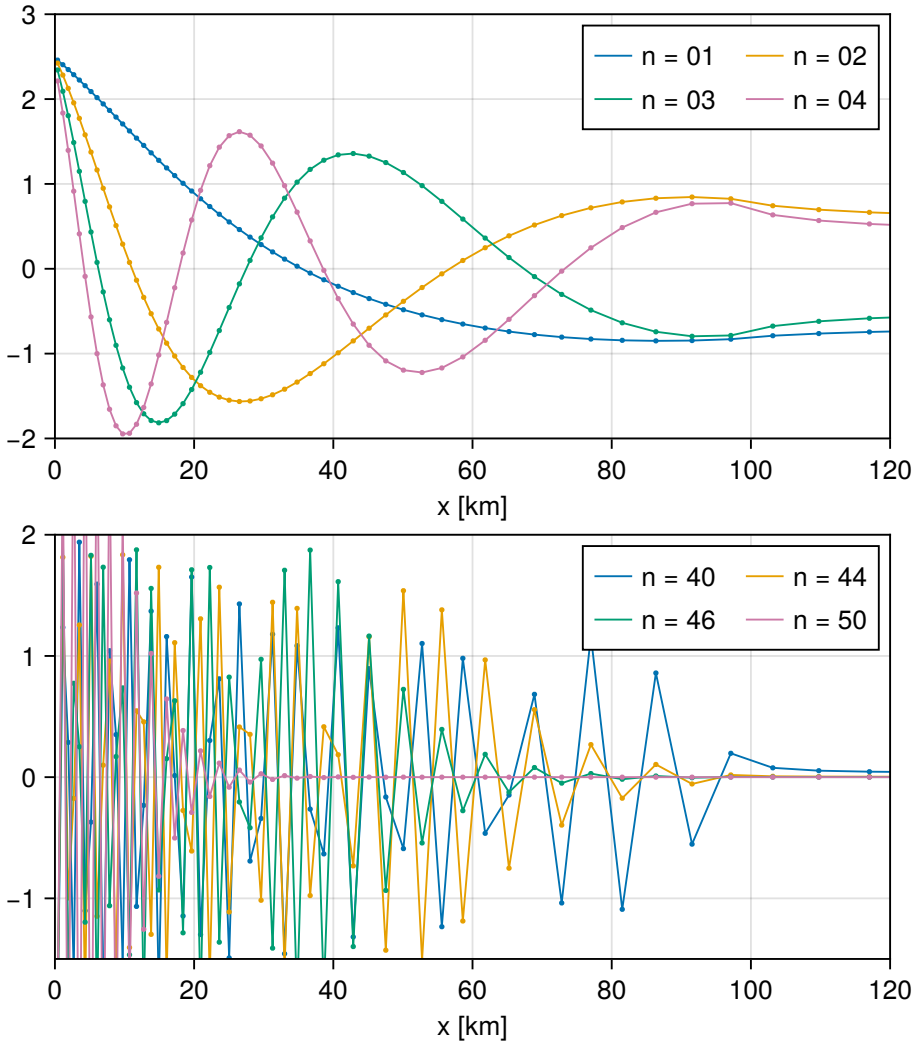

Figure 9: Solution CS: Bottom trace, $F^{(n)}(x, z = -h(x))$, of the mode function for $n = 1$–4 (upper panel) and for selected high modes.

slope from $(x, z) = (0, 0)$ to $(150\,\mathrm{km}, -100\,\mathrm{m})$ and the continental slope is a linear slope from the latter point (which is the shelf break) to $(x, z) = (250\,\mathrm{km}, -5000\,\mathrm{m})$. The extent of the flat-bottom region, 200 km, is the same as for Solution CS.

Preliminary numerical solutions (not shown) indicated that the bottom trace $F^{(n)}(x, z = -h(x))$ is oscillatory in x on the shelf and requires smaller Δx near the coast as the apparent wavelength is shorter there. For this reason, we use an empirical grid spacing that increases from $\Delta x_1 \simeq 2\,\mathrm{km}$ to $\Delta x_{15} \simeq 15\,\mathrm{km}$ just before the shelf break. The vertical grid spacing is determined by $\Delta z_k = \Delta x_i h_x$ for each $k = i = 1 \ldots, 15$. The horizontal and vertical grid spacing below the shelf break is very similar to that of Solution CS and the horizontal resolution along the flat bottom is also very similar to that of Solution CS. There are 63 gridpoints in the vertical with 15 for the shelf and 48 for the continental slope. There are 78 gridpoints in the x direction with 15 in the flat-bottom region.

Figure 10 compares modes 1–8 of ShCSwith "corresponding" modes of CS. This "correspondence" requires i) that the number of nodes on the continental slope must be the same and ii) that the $F(x, z)$ structure must look similar and the characteristic speed c must be similar. Criterion (i) is objective and criterion (ii) is subjective. When we discuss the structure of the solution on the continental shelf below, we look at the bottom trace (not shown) as it is not visible in Fig. 10. We also note that the amplitude on the shelf is ∼3–15 (not shown) for the first 12 modes of Solution ShCS. The contribution of this large amplitude to the total energy can still be small as it is weighted by Δz not by Δx (see eq. (11)).

Mode 1 of ShCS appears to be a mode-0 shelf wave[1]; its $c^{(1)}$ is too large for a baroclinic CTW and the amplitude is almost entirely confined to the shelf with a very weak tail on the continental slope. There is no node on the shelf and there is one somewhat down the continental slope. Solution CS does not have a counterpart.

Mode 2 of ShCS has one node on the shelf and another along the continental slope. Mode 1 of CS] also has one node along the slope and the $F(x, z)$ structure is similar between the two solutions. The characteristic speed is also similar. This result suggests that mode 2 of ShCS can be interpreted basically as a mode-1 CTW on the continental slope with a "tail" that takes the form of a shelf wave.

Mode 3 of ShCS has still one node on the shelf and two along the continental slope, where even though the structure is not very different from that of mode 2 of CS, the amplitude is much smaller than on the shelf, where the amplitude reaches ∼15 (not shown). For this reason, mode 3 of ShCS may be interpreted as a "mode-1" shelf wave with a baroclinic CTW-like tail on the continental slope.

Like mode-2, mode 4 of ShCS has a very similar structure and amplitude along the continental slope to that of mode 2 of CS.

The subsequent modes do not necessarily follow this pattern: Mode 5 of ShCS is very similar to mode 3 of CS, with two nodes on the shelf; Mode 7 has 3 and 4 nodes on the shelf and slope, respectively, and mode 8 has 3 and 5 nodes on the shelf and slope, respectively, Mode 6 of ShCS falls between modes 5 and 7 in that it has 2 and 3 nodes on the shelf and slope, respectively, and one node very close to the shelf break. Even though

[1]Robinson (1964) considered a shallow-water equation on a linear shelf followed by a cliff down to a deep flat bottom at low frequencies and found wave-like modes ($J_0(x/\mu)$). See also Mysak (1980).

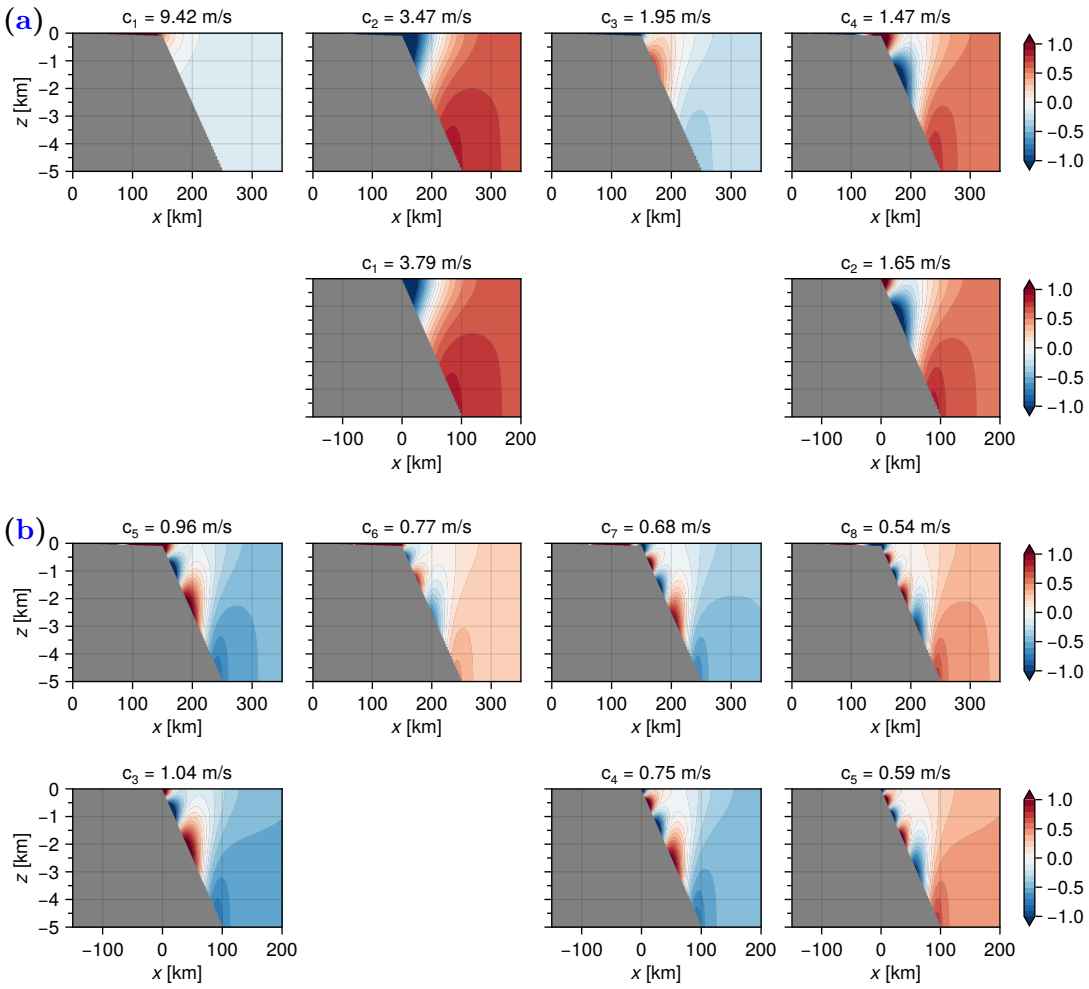

Figure 10: $F^{(n)}(x, z)$: (a) $n = 1$–4 for ShCS (upper) and $n = 1, 2$ for CS (lower), and (b) $n = 5$–8 for ShCS (upper) and $n = 3$–5 for CS (lower).

it has a very similar structure to mode 3 of CS if signs are flipped, its amplitude is smaller and the wave speed is too different. For this solution the coupling between the shelf and slope modes does not quite follow the patterns for the other modes.

4.3.2 Shelf with vertical wall

The next solution, ShVW, replaces the continental slope with a vertical wall. The horizontal and vertical grid spacing on the shelf and the vertical grid spacing below the shelf break are exactly the same as for ShCS. The horizontal grid spacing along the flat bottom is much smaller to resolve smaller horizontal scales of the modes (Fig. 11): next to the vertical wall, $\Delta x_{15} \simeq 0.8\,\mathrm{km}$, extending according to $\Delta x_{i+1} \approx 1.1\Delta x_i$ up to the right edge. The extent of the flat-bottom region is the same as for ShCS. The number of the gridpoints is the same in the vertical as for ShCS; there are only 49 gridpoints in the horizontal as there is no continental slope.

The last test, VW, just removes the continental shelf; the boundary is a vertical wall followed by a flat-bottom. The only exception is the corner grid cell where the bottom of the vertical wall meets the flat bottom; this cell is automatically tapered and the right-angled bottom-left corner is replaced by a diagonal slope by our code as in Fig. 1. The vertical grid spacing is very similar to those of CS, ShCS, and ShVW with $\Delta z \propto 1/N$ and there are 51 grid cells in the vertical, same as CS. The horizontal grid spacing is exactly the same as that of the flat-bottom region of ShVW.

Figure 11 shows these two solutions in the same manner as Fig. 10. The sequence from $n = 1$ to $n = 8$ of ShVW (Fig. 11, upper rows of (a) and (b)) is qualitatively similar to that of ShVW (Fig. 10). Mode 1 of ShVW is basically a mode-0 shelf wave with a weak tail on the vertical wall, where the node is. The characteristic speed is similar to that of ShCS. Mode 2 of ShVW is very similar to mode 1 of VW with one node on the slope (wall). Mode 3 of ShVW has a large amplitude on the shelf (not shown) with a weak tail, which has a similar structure as mode 1 of VW; it has one node each on the shelf and on the slope and one node very close to the shelf break. Mode 4 of ShVW is very similar to mode 2 of VW with two nodes on slope (wall). The descriptions of modes 5, 7, and 8 are the same as for the corresponding modes in Fig. 10.

Mode 6 of ShVW is again similar to that of ShCS, with 2 and 3 nodes on the shelf and slope, respectively, and one node very close to the shelf break. This time, however, the amplitude on the wall is not much smaller than that of mode 5, and $c^{(6)}$ of ShVW is not too different from $c^{(c)}$ of VW.

Coupling between the shelf and slope modes thus seems to be subtle. While this is an interesting subject, we leave it for future studies as our present purpose is to demonstrate the usefulness of the z coordinates when dealing with steep slopes or even vertical walls.

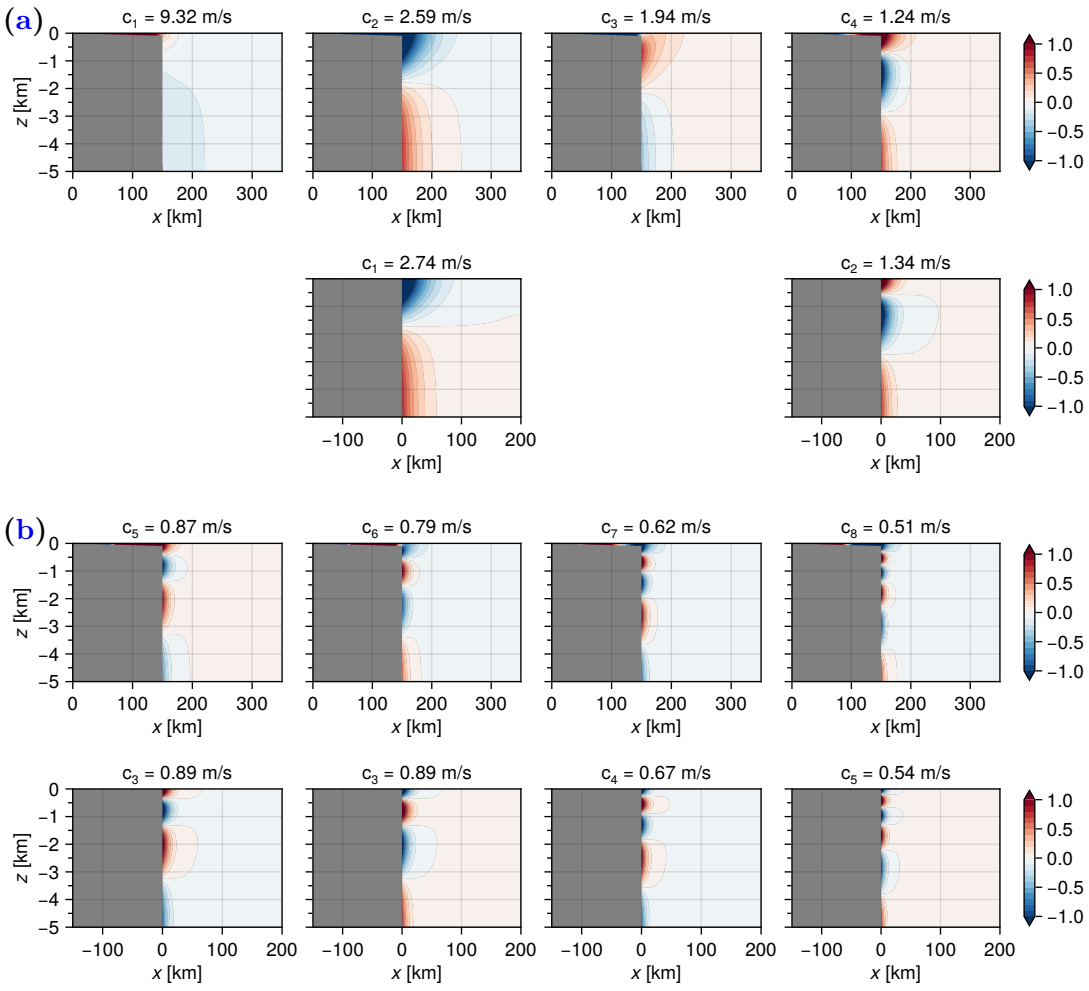

Figure 11: $F^{(n)}(x, z)$: (a) n = 1–4 for Solution ShVW (upper) and n = 1, 2 for Solution VW (lower), and (b) n = 5–8 for Solution ShVW (upper) and n = 3–5 for Solution VW (lower). Note that the $n = 3$ mode is repeated in the last row.

5 Summary and concluding remarks

5.1 Summary and discussion

To numerically solve for coastal trapped wave modes at low frequencies, we have developed a finite-difference scheme and proved that solutions to the set of finite-difference equations exactly satisfy an orthogonality condition and other useful properties which solutions to the original differential equation satisfy. These properties are derived from the symmetry of the bilinear form, $\langle q, \mathcal{L}r \rangle$, associated with the differential operator (section 2), and so the goal of the finite-difference scheme is to enable an analogous symmetric bilinear form. The key idea is to use the "flux form" for the finite difference, which enables "integration by parts" and leads to a symmetric bilinear form (section 3).

A useful result is the exact discrete inner product (11) by which the finite-difference modes are orthogonal to each other (section 3.2). Whatever finite-difference scheme can be used to obtain a set of linearly-independent eigenvectors, but finding the "right" inner product for the discrete system is not trivial (e.g., Appendix B.3 in Furue et al. 1995). Another useful property is that our finite-difference scheme ensures that all eigenvalues are real. This was proven also thanks to the symmetry of the bilinear form (section 3.2). This result is not trivial either. Tanaka (2023) developed the original version of our code that uses the sigma coordinates; the code returns imaginary eigenvalues and eigenvectors.

We next cast the set of finite-difference equations into a generalized matrix eigenvalue problem (section 3.3). If the total number of active grid points is M, the matrices are $M \times M$ and there are M eigenvectors. From the matrix formalism, however, we have proven that there are only exactly as many *physical* eigenvectors as there are grid cells in the vertical and that the remaining solutions are all *unphysical* with $c = 0$. A random $F(x, z)$ field is such an unphysical solution as long as $F = 0$ along the slope/bottom. This makes it trivial to filter out unphysical solutions from the solutions from the matrix eigenvalue solver.

When constructing the matrices, we modified the finite-difference equations in such a way as to make the matrices symmetric. By calculating the bilinear form associated with the main matrix, we proved that the matrix is negative definite under the free-surface condition. These two properties enable us to use a faster eigenvalue-problem solver (section 3.3).

The next section (section 4) showed six examples. The first three used a linear continental slope to discuss practical use of our code. For the first test case, where $N = \text{const.}$, we compared our solutions with BC87's (Brink and Chapman 1987) and found good agreement. The next two solutions indicated how "bad" solutions arise and how to adjust horizontal and vertical resolutions to fix them. The last three cases (section 4.3) demonstrated the usefulness of the z coordinates and the variable (non-uniform) resolution for theoretical consideration when both gentle and steep slopes are present. They also pointed toward a potentially interesting scientific issue about the coupling of deep baroclinic Kelvin waves and shelf waves.

5.2 Concluding remarks

In conclusion, we have developed a program to solve for all the CTW eigenmodes at once as easily as for the ordinary vertical modes. We have made our code public at https://github.com/ryofurue/ctwmodes (DOI:10.5281/zenodo.17507173).

Main advantages of our code are that it gives all the modes at once and allows for variable horizontal and vertical resolutions. Our code, however, by no means supersedes BC87's. The latter is much more versatile: it can handle high frequencies and non-monotonic $h(x)$ and can include a cross-shore variation in f and bottom friction; it can output the mode functions for u, v, and ρ. We will extend our code as needs arise. For high frequencies, however, the x-z differential equation involves both ω and ω^2, where ω is the eigenvalue (Wang and Mooers 1976), and simple discretized forms do not take a form of $A\vec{F} = \lambda B\vec{F}$; a different approach like BC87's is required.

Acknowledgements

We thank Lei Han and Jay McCreary for helpful discussion. We used the Makie package (Danisch and Krumbiegel 2021; https://docs.makie.org/stable/) for the Julia programming language to produce all graphics in this paper.

References

Anderson, E, Bai, Z, Bischof, C, Blackford, S, Demmel, J, Dongarra, J, Du Croz, J, et al. 1999. *LAPACK users' guide.* 3rd ed. The library source code is available from http://www.netlib.org/lapack. Philadelphia, PA: Society for Industrial and Applied Mathematics. https://www.netlib.org/lapack/lug/.

Brink, KH. 1989. "Energy conservation in coastal-trapped wave calculations" [in EN]. *J. Phys. Oceanogr.* 19, no. 7 (July 1, 1989): 1011–1016. https://doi.org/10.1175/1520-0485(1989)019<1011:ECICTW>2.0.CO;2.

———. 1991. "Coastal-trapped waves and wind-driven currents over the continental shelf." *Ann. Rev. Fluid Mech.* 23:389–412. https://doi.org/10.1146/annurev.fl.23.010191.002133.

Brink, KH and Chapman, DC. 1987. *Programs for computing properties of coastal-trapped waves and wind-driven motions over the continental shelf and slope, 2nd ed.* Technical Report WHOI-87-24. [The programs are available from, and updates to them are documented in, https://www.whoi.edu/cms/files/Fortran_30425.htm (2007).] Woods Hole Oceanographic Institution, June. https://www.whoi.edu/cms/files/WHOI-87-24-Programs_for_Computing_text_25484.pdf.

Buchwald, VT and Adams, JK. 1997. "The propagation of continental shelf waves." *Proceedings Of Royal Society Of London Series A Mathematical Physical Sciences* 305, no. 1481 (January): 235–250. https://doi.org/10.1098/rspa.1968.0115.

Church, JA, Freeland, HJ, and Smith, RL. 1986. "Coastal-trapped waves on the East Australian continental shelf part I: Propagation of modes." *J. Phys. Oceanogr.* 16 (11): 1929–1943. https://doi.org/10.1175/1520-0485(1986)016<1929:CTWOTE>2.0.CO;2.

Clarke, AJ. 1977. "Observational and numerical evidence for wind-forced coastal trapped long waves" [in EN]. *J. Phys. Oceanogr.* 7, no. 2 (March 1, 1977): 231–247. https://doi.org/10.1175/1520-0485(1977)007<0231:OANEFW>2.0.CO;2.

Courant, R and Hilbert, D. 1989. *Methods of mathematical physics, volume I.* John Wiley & Sons, Ltd. https://doi.org/10.1002/9783527617210.

Danisch, S and Krumbiegel, J. 2021. "Makie.jl: Flexible high-performance data visualization for Julia" [in en]. *Journal of Open Source Software* 6, no. 65 (September 1, 2021): 3349. https://doi.org/10.21105/joss.03349.

Early, JJ, Lelong, MP, and Smith, KS. 2020. "Fast and accurate computation of vertical modes" [in en]. *J. Adv. Model. Earth Syst.* 12 (2): e2019MS001939. https://doi.org/10.1029/2019MS001939.

Furue, R. 2022. "A seasonal undercurrent along the northwest coast of Australia." *Front. Mar. Sci.* 8. https://doi.org/10.3389/fmars.2021.806659.

Furue, R, Fukao, Y, and Sugioka, H. 2024. "Linear response of deep ocean to a moving tropical cyclone" [in en]. *PLOS Climate* 3, no. 12 (December 17, 2024): e0000376. https://doi.org/10.1371/journal.pclm.0000376.

Furue, R, Nakajima, K, and Ishikawa, I. 1995. "Modal decomposition of deep ocean circulation models: Comparison with reduced-gravity models" [in en]. *J. Geophys. Res. Oceans* 100 (C6): 10567–10588. https://doi.org/10.1029/95JC00750.

Garcia, HE, Boyer, TP, Baranova, OK, Locarnini, RA, Mishonov, AV, Grodsky, A ea, Paver, CR, et al. 2019. *World Ocean Atlas 2018: Product documentation.* https://doi.org/10.25923/tzyw-rp36.

Hughes, CW, Fukumori, I, Griffies, SM, Huthnance, JM, Minobe, S, Spence, P, Thompson, KR, and Wise, A. 2019. "Sea level and the role of coastal trapped waves in mediating the influence of the open ocean on the coast" [in en]. *Surveys in Geophysics* 40, no. 6 (November 1, 2019): 1467–1492. https://doi.org/10.1007/s10712-019-09535-x.

Iga, K. 1995. "Transition modes of rotating shallow water waves in a channel" [in en]. *J. Fluid Mech.* 294 (July): 367–390. https://doi.org/10.1017/S002211209500293X.

McCreary, JP. 1981. "A linear stratified ocean model of the coastal undercurrent." *Philosophical Transactions Of Royal Society Of London Series A Mathematical Physical Sciences* 302, no. 1469 (September 24, 1981): 385–413. https://doi.org/10.1098/rsta.1981.0176.

Miyama, T, McCreary, JP, Sengupta, D, and Senan, R. 2006. "Dynamics of biweekly oscillations in the equatorial Indian Ocean." *J. Phys. Oceanogr.* 36:827–846. https://doi.org/10.1175/JPO2897.1.

Mysak, LA. 1980. "Recent advances in shelf wave dynamics" [in en]. *Reviews of Geophysics* 18 (1): 211–241. https://doi.org/10.1029/RG018i001p00211.

Robinson, AR. 1964. "Continental shelf waves and the response of sea level to weather systems" [in en]. *Journal Of Geophysical Research 1896-1977* 69 (2): 367–368. https://doi.org/10.1029/JZ069i002p00367.

Song, Q, Aiki, H, and Tang, Y. 2023. "The Role of Equatorially Forced Waves in Triggering Benguela Niño/Niña as Investigated by an Energy Flux Diagnosis" [in en]. *J. Geophys. Res. Oceans* 128 (4): e2022JC019272. https://doi.org/10.1029/2022JC019272.

Tanaka, Y. 2023. "Energy conversion rate from subinertial surface tides to internal tides" [in EN]. *J. Phys. Oceanogr.* 53, no. 5 (May 1, 2023): 1355–1374. https://doi.org/10.1175/JPO-D-22-0201.1.

Wang, DP and Mooers, CNK. 1976. “Coastal-trapped waves in a continuously stratified ocean” [in EN]. *J. Phys. Oceanogr.* 6, no. 6 (November 1, 1976): 853–863. https://doi.org/10.1175/1520-0485(1976)006<0853:CTWIAC>2.0.CO;2.

Supplementary Material

Supplementary Text S1 “Coastal trapped wave modes”: discusses the differential equation of the coastal trapped wave modes in detail.

Supplementary Text S2 “Discretized CTW eigenvalue problem”: develops a finite-difference method for the CTW equation and derives exact properties of the numerical solutions.

S1 Coastal trapped wave modes

This appendix collects mathematical discussion relevant to the present study from past studies (e.g., Brink 1991, and references therein) and derives important properties of coastal-trapped wave (CTW) modes in the long-wave limit ($\omega \ll |f|$). Its main purpose is to serve as a reference from the main text and from Section S2. This appendix is designed to be as much self-contained as possible, in order to allow the interested reader to skip Section 3 of the main text and read this instead. To avoid frequently referring to the main text, this appendix contains overlaps with the main text. For such an overlap, the version of the discussion in the main text is much condensed and the version here is extended fully.

Section S1.1 summarizes the well-known CTW eigenvalue problem in the long-wave limit, and Section S1.2 derives the orthogonality of the CTW modes and other properties using bilinear forms. Section S1.3 proves that the so-called "vertical modes" are CTW modes when the "slope" is a purely vertical wall followed by a flat bottom.

S1.1 CTW formulation

We consider CTWs along a north-south coast on an f-plane, assuming that the bottom topography $z = -h(x)$ is monotonic in x and uniform in the meridional (y) direction and that the background stratification $N(z)$ is horizontally uniform. For simplicity, we consider a western boundary so that $x > 0$ and $h_x \geq 0$. The primitive equations linearized around a background state of rest are

$$u_t - fv = -\pi_x, \tag{S1.1a}$$
$$v_t + fu = -\pi_y, \tag{S1.1b}$$
$$0 = -\pi_z + b, \tag{S1.1c}$$
$$-b_t = N^2 w, \tag{S1.1d}$$
$$u_x + v_y + w_z = 0, \tag{S1.1e}$$

where $\pi \equiv p/\rho_\mathrm{o}$, $b \equiv -g\rho'/\rho_\mathrm{o}$, and the other symbols are standard. If we assume that $|u_t| \ll |fv|$ ("longshore geostrophy"), the pressure anomaly of free CTWs can then be written as

$$\rho_\mathrm{o}\pi(x,y,z,t) = \sum_{n=0}^{\infty} F^{(n)}(x,z)\,\phi^{(n)}(y,t), \tag{S1.2}$$

where $\phi^{(n)}$ obeys the simple monodirectional wave equation

$$\phi^{(n)}_t + c_n \phi^{(n)}_y = 0 \tag{S1.3}$$

(e.g., Wang and Mooers 1976; Clarke 1977; Brink 1991). The CTW modes, $F^{(n)}$ and $c^{(n)}$, are solutions to the eigenvalue problem

$$F_{xx} + \left(\frac{F_z}{\tilde{N}^2}\right)_z = 0 \qquad \text{in the interior } (0 < x \text{ and } -h(x) < z < 0), \tag{S1.4a}$$

$$\frac{F_z}{\tilde{N}^2} = -\frac{f^2}{g}F \qquad \text{on } z = 0, \tag{S1.4b}$$

$$F_x \to 0 \qquad \text{as } x \to \infty, \tag{S1.4c}$$

$$F_x + \frac{1}{h_x}\frac{F_z}{\tilde{N}^2} = \frac{f}{c}F \qquad \text{on } z = -h(x), \tag{S1.4d}$$

where $\tilde{N} \equiv N(z)/f$. We are looking for solutions that decay offshore ($x \to \infty$). Note that (S1.4d) includes as special cases

$$F_x = \frac{f}{c}F \qquad \text{(along a vertical wall: } h_x \to \infty), \tag{S1.5a}$$

$$F_z = 0 \qquad \text{(along a flat part of the bottom: } h_x = 0), \tag{S1.5b}$$

which past studies showed as separate boundary conditions. We use (S1.4d) instead for simplicity, keeping in mind that h_x can be zero or infinity.

Equation (S1.4b) is the free-surface boundary condition. We can invoke the usual rigid-lid approximation by setting $g \to \infty$. The rigid-lid approximation hardly affects the solutions (not shown), except obviously for the phase speed $c^{(0)}$ of the barotropic mode. [It is straightforward to verify that under the rigid-lid approximation ($g \to \infty$), $(F, c) = (\text{const.}, \pm\infty)$ is a solution to the set (S1.4). This is obviously the barotropic mode.] We nevertheless retain the free-surface condition because it makes theoretical discussion cleaner (Sections S1.2.3 and S2.4.7) and the numerical calculation faster (Section S2.4).

Past studies have found (e.g., Clarke and Van Gorder 1986) that it is sometimes convenient to use the vector notation

$$\boldsymbol{B} \equiv (F_x, F_z/\tilde{N}). \tag{S1.6}$$

With this, the eigenvalue problem (S1.4) can be written as

$$\boldsymbol{\nabla} \cdot \boldsymbol{B} = 0 \qquad (x, z) \in \Omega \tag{S1.7a}$$

$$\hat{\boldsymbol{n}} \cdot \boldsymbol{B} = \frac{f}{c}\hat{\boldsymbol{n}} \cdot (F, 0) \qquad (x, y) \in \partial\Omega_\mathrm{b} \tag{S1.7b}$$

$$\hat{\boldsymbol{n}} \cdot \boldsymbol{B} = -\frac{f^2}{g}F \qquad (x, y) \in \partial\Omega_\mathrm{s} \tag{S1.7c}$$

$$F_x \to 0 \qquad \text{as } x \to \infty, \tag{S1.4c}$$

where $\hat{\boldsymbol{n}}$ is the unit vector perpendicular to the boundary and pointing outward of the domain, Ω is the domain, and $\partial\Omega_\mathrm{b}$ and $\partial\Omega_\mathrm{s}$ are the bottom/slope part and the surface part of the boundary of the domain.

S1.2 Orthogonality and other properties of the solutions

S1.2.1 Bilinear form

As in the past studies, the eigenmodes can be shown to be orthogonal to each other. Let

$$\mathcal{L}\bullet \equiv \partial_{xx}(\bullet) + \partial_z \frac{\partial_z(\bullet)}{\tilde{N}^2},$$

which is the operator on the left-hand side of (S1.7a), and let

$$\langle q, r\rangle \equiv \iint_\Omega \mathrm{d}x\,\mathrm{d}z\, q(x,z)\, r(x,z),$$

which is an "inner product". Multiplying q on the left-hand side of (S1.7a), integrating them over the domain, and carrying out integration by parts gives

$$\begin{aligned}
\langle q, \mathcal{L}F\rangle &= \iint_\Omega \mathrm{d}x\,\mathrm{d}z\, q\boldsymbol{\nabla}\cdot\boldsymbol{B} \\
&= \oint_{\partial\Omega} \mathrm{d}s\, \hat{\boldsymbol{n}}\cdot(q\boldsymbol{B}) - \iint_\Omega \mathrm{d}x\,\mathrm{d}z\, (\boldsymbol{\nabla}q)\cdot\boldsymbol{B} \\
&= -\int_0^\infty \mathrm{d}x\, h_x\, q\left(F_x + \frac{F_z}{h_x\tilde{N}}\right)\bigg|_{z=-h(x)} - \int_0^\infty \mathrm{d}x\ \frac{f^2}{g} qF\bigg|_{z=0} \\
&\quad - \iint_\Omega \mathrm{d}x\,\mathrm{d}z\left(q_x F_x + \frac{q_z F_z}{\tilde{N}^2}\right),
\end{aligned} \tag{S1.8}$$

where the sea-surface portion of the boundary integral was calculated as

$$\begin{aligned}
\int_{\partial\Omega_\mathrm{s}} \mathrm{d}s\, q\,\hat{\boldsymbol{n}}\cdot\boldsymbol{B} &= \int_\infty^0 (-\mathrm{d}x)\ q\,\frac{F_z}{\tilde{N}^2}\bigg|_{z=0} \\
&= -\int_0^\infty q\,\frac{f^2}{g}F\bigg|_{z=0}
\end{aligned}$$

from (S1.7c). The $x\to\infty$ part of the boundary integral vanished because we can first set the boundary at $x=a$ and then move it to infinity:

$$\begin{aligned}
\int_{x\to\infty} \mathrm{d}s\,\hat{\boldsymbol{n}}\cdot(q\,\boldsymbol{B}) &= \lim_{a\to\infty}\int \mathrm{d}z\,\hat{\boldsymbol{i}}\cdot q\boldsymbol{B}|_{x=a} \\
&= \lim_{a\to\infty}\int \mathrm{d}z\ qF_x|_{x=a} \\
&= 0
\end{aligned}$$

from (S1.4c). The $z = -h(x)$ part of the boundary integral in (S1.8) was calculated as

$$\begin{aligned}
&\int \mathrm{d}s\, \hat{\boldsymbol{n}} \cdot (q\boldsymbol{B}) \\
&= \int_0^\infty \mathrm{d}x\, \sqrt{1+h_x^2}\, q \left(F_x \frac{-h_x}{\sqrt{1+h_x^2}} + \frac{F_z}{\tilde{N}} \frac{-1}{\sqrt{1+h_x^2}} \right) \Bigg|_{z=-h(x)} \\
&= -\int_0^\infty \mathrm{d}x\, q \left(h_x F_x + \frac{F_z}{\tilde{N}} \right) \Bigg|_{z=-h(x)},
\end{aligned} \tag{S1.9}$$

because

$$\mathrm{d}s = \mathrm{d}x\, \sqrt{1+h_x^2}, \quad \hat{\boldsymbol{n}} = \left(\frac{-h_x}{\sqrt{1+h_x^2}}, \frac{-1}{\sqrt{1+h_x^2}} \right).$$

Note that the result of this calculation is still valid even when the bottom boundary $z = -h(x)$ includes "vertical walls", where $h_x = \infty$. Suppose, for example, that there is a downward step from $z = z_1$ to $z = z_2$, where $z_1 > z_2$, at $x = x_1$. Along this vertical wall, $\hat{\boldsymbol{n}} = (-1, 0)$ and the boundary differential is $\mathrm{d}s = -\mathrm{d}z$. Therefore,

$$\int_{\text{wall}} \mathrm{d}s\, \hat{\boldsymbol{n}} \cdot (q\,\boldsymbol{B}) = -\int_{z_1}^{z_2} \mathrm{d}z\ q(-F_x)|_{x=x_1} = -\int_{z_2}^{z_1} \mathrm{d}z\ qF_x|_{x=x_1}\,.$$

The wall part of eq. (S1.9), on the other hand, can be rewritten as

$$\begin{aligned}
-\int_{x_1-0}^{x_1+0} \mathrm{d}x\, h_x\, q \left(F_x + \frac{F_z}{h_x \tilde{N}} \right) \Bigg|_{z=-h(x)} &= -\int_{x_1-0}^{x_1+0} \mathrm{d}x\, h_x\ qF_x|_{z=-h(x)} \quad (\because h_x = \infty) \\
&= -\int_{z_1}^{z_2} (-\mathrm{d}z)\ qF_x|_{x=x_1}
\end{aligned}$$

because $\mathrm{d}z = \mathrm{d}(-h) = -(\mathrm{d}h/\mathrm{d}x)\mathrm{d}x$ along the wall. (This is an informal derivation using the idea of Stieltjes integral.) This (informally) proves that although the derivation uses h_x and $\sqrt{1+h_x^2}$ in the intermediate steps, the result is still valid even when $h_x = \infty$.

Plugging (S1.4d) into (S1.8) yields

$$\begin{aligned}
\langle q, \mathcal{L}F \rangle &= -\iint \mathrm{d}x\, \mathrm{d}z \left(q_x F_x + \frac{q_z F_z}{\tilde{N}^2} \right) - \frac{f^2}{g} \int_0^\infty \mathrm{d}x\ qF|_{z=0} \\
&\quad - \frac{f}{c} \int_0^\infty \mathrm{d}x\, h_x\ qF|_{z=-h(x)} \qquad \text{(S1.10a)} \\
&\equiv A(q,F) - \frac{f}{c} \langle q, F \rangle_{\mathrm{b}}, \qquad \text{(S1.10b)}
\end{aligned}$$

where

$$\begin{aligned}
A(q,r) &\equiv -\iint_\Omega \mathrm{d}x\, \mathrm{d}z \left(q_x r_x + \frac{q_z r_z}{\tilde{N}^2} \right) - \frac{f^2}{g} \int_0^\infty \mathrm{d}x\ qr|_{z=0} \\
\langle q, r \rangle_{\mathrm{b}} &\equiv \int_0^\infty \mathrm{d}x\, h_x\, qr|_{z=-h(x)}\,,
\end{aligned} \tag{S1.11}$$

for arbitrary functions $q(x,z)$ and $r(x,z)$. Note that all these "bilinear" forms are symmetric, in that $\langle q, r \rangle = \langle r, q \rangle$, $A(q,r) = A(r,q)$, etc.

Finally, since $\mathcal{L}F = 0$ for a solution ((S1.4a)), (S1.10a) implies

$$A(q,F) = \frac{f}{c} \langle q, F \rangle_{\mathrm{b}}. \tag{S1.12}$$

S1.2.2 Orthogonality, amplitude, and spectrum

The bilinear form $A(,)$ is negative definite: if $r \not\equiv 0$, $A(r,r) < 0$. Setting $q = F$ in (S1.12) and multiplying it by c gives

$$cA(F,F) = f\langle F,F\rangle_{\mathrm{b}},$$

which suggests that there may be strange solutions such that

$$F|_{z=-h} = 0, \quad c = 0.$$

Although we do not know how to prove the existence of such solutions for the continuous problem we are dealing with now, we report that we prove the existence of such solutions for our discrete version of the eigenvalue problem (Section S2.4.7). In the following discussion, we exclude such solutions.

Plugging $q = F^{(l)}$ and $F = F^{(n)}$ into (S1.12) gives one equation and swapping l and n gives another. By subtracting the former from the latter yields

$$\left(\frac{f}{c^{(l)}} - \frac{f}{c^{(n)}}\right)\langle F^{(l)}, F^{(n)}\rangle_{\mathrm{b}} = 0, \tag{S1.13a}$$

or

$$\langle F^{(l)}, F^{(n)}\rangle_{\mathrm{b}} = 0 \quad \text{if } c^{(l)} \neq c^{(n)}, \tag{S1.13b}$$

because $A(,)$ and $\langle,\rangle_{\mathrm{b}}$ are both symmetric. This is the orthogonality relation between the CTW modes (e.g., Wang and Mooers 1976).

Since F's are real-valued functions (see below), $\langle F,F\rangle_{\mathrm{b}} \geq 0$, with the equality holding only if $F \equiv 0$. For this reason, $\sqrt{\langle F,F\rangle_{\mathrm{b}}}$ can be and is used to measure the amplitude of F. A common practice is to scale the amplitude of the function so that $\langle F,F\rangle_{\mathrm{b}} = 1$ (nondimensional). Brink (1989), on the other hand, found that when f slowly changes in y, $\langle F^{(n)}, F^{(n)}\rangle_{\mathrm{b}}$ has to be proportional to f^{-1} to conserve energy flux in y. This is how BC87 scales the numerical solutions in their code. In this study, however, we sometimes normalize F's in such a way that $\langle F,F\rangle_{\mathrm{b}} = D$. This choice is convenient because with it, F is dimensionless and also $F = \mathcal{O}(1)$.

Moreover, suppose that some function $q(x,z)$ is expanded into the modes:

$$q = \sum_n \alpha_n F^{(n)}(x,z).$$

Orthogonality makes it easy to calculate α:

$$\alpha_n = \frac{1}{D}\langle F^{(n)}, q\rangle_{\mathrm{b}}.$$

Also,

$$\frac{1}{D}\langle q,q\rangle_{\mathrm{b}} = \sum_n \alpha_n^2 \frac{1}{D}\langle F^{(n)}, F^{(n)}\rangle_{\mathrm{b}} = \sum_n \alpha_n^2;$$

The variance of the original function is equal to the sum of the variances of the modes. That is, $\{\alpha_0^2, \alpha_1^2, \ldots\}$ is the power spectrum of q. The above relation is commonly known as Parseval's theorem.

S1.2.3 Properties of eigenvalues

If a solution $(F(x,z), c)$ takes complex values, it is clear from the form of the eigenvalue problem (S1.4) that its complex conjugate $(F^*(x,z), c^*)$ is also a solution. Substituting $F^{(l)} = F^*$, $F^{(n)} = F$, $c^{(l)} = c^*$, and $c^{(n)} = c$ into (S1.13a), then, yields

$$\left(\frac{f}{c^*} - \frac{f}{c}\right) \int_0^\infty \mathrm{d}x\, h_x\, |F|^2\big|_{z=-h(x)} = 0. \tag{S1.14}$$

Since the integral is nonzero, all eigenvalues are real.

If F is imaginary (i.e., $\Im[F] \neq 0$), the eigenvalue c is degenerate, having (at least) two independent eigenfunctions F and F^*. In this case, however, any linear combination of F and F^* is also an eigenfunction associated with the same c, and using this property, we can transform the complex-conjugate pair into a pair of independent real functions via $F_R \equiv (F + F^*)/2 = \Re[F]$ and $F_I \equiv (F - F^*)/(2i) = \Im[F]$. That is, if an imaginary eigenfunction is obtained, its complex conjugate is also an eigenfunction associated with the same c and the pair can always be transformed into a pair of independent real eigenfunctions. We can therefore completely ignore imaginary eigenfunctions and assume that all eigenfunctions are real without loss of generality.

Moreover, substituting $F = F^{(l)} = F^{(n)}$ into (S1.12) gives

$$A(F,F) - \frac{f}{c}\langle F, F\rangle_\mathrm{b} = 0.$$

For the barotropic mode under the rigid-lid approximation ($g \to \infty$, $F(x,z)$ is uniform), $A(F,F) = 0$ and $c = \infty$, which satisfy the above relation. Except for this case, $A(F,F) < 0$; and since $\langle F, F\rangle_\mathrm{b} > 0$,

$$f/c < 0. \tag{S1.15}$$

This is a mathematical expression of that in the northern hemisphere ($f > 0$), the phase speed of CTW is southward ($c < 0$) along the western boundary.

S1.2.4 Boundary integral

As we have seen, the boundary integral $\int \mathrm{d}x\, h_x \bullet$ is central as a "measure". This boundary integral can be viewed as a "vertical" integral in that

$$\int_0^\infty \mathrm{d}x\, h_x\, q|_{z=-h(x)} = -\int_0^\infty \mathrm{d}x\, Z_x\, q|_{z=-h(x)} = \int_{-D}^0 \mathrm{d}Z(x)\, q|_{z=-h(x)}\,, \tag{S1.16}$$

where $Z(x) \equiv -h(x)$ and the last form is a Stieltjes integral. Note that the above integral is well defined even if $h(x)$ includes steps (where $h_x = \infty$). In particular, if $h(x)$ consists of a series of steps Δz_i at $x = x_i$ interspersed by flat regions ($h_x = 0$),

$$\int_0^\infty \mathrm{d}x\, h_x\, q|_{z=-h(x)} = \sum_{k=M_\mathrm{v}}^{1} \int_{z_k}^{z_{k-1}} \mathrm{d}z\, q(x_k, z), \tag{S1.17}$$

if there are M_v steps in total, where $[z_k, z_{k-1}]$ is the vertical range of the step at $x = x_k$ with $z_{M_\mathrm{v}} = -D$ and $z_0 = 0$. The general form (S1.16) can be viewed as a limit of the sum of infinitely many vertical integrals like this.

S1.3 Vertical wall and vertical modes

In this subsection, we derive how long-wave CTW modes are related to the so-called vertical modes. Consider a case where $x = 0$ is a vertical wall ($h_x = \infty$ there) followed by a flat bottom ($h_x = 0$ there). The boundary conditions along these boundaries are (S1.5). In this case, the solutions take a separable form $F(x, z) = X(x)\psi(z)$. Plugging this expression into (S1.4a) gives

$$\frac{1}{X}\frac{X_{xx}}{f^2} + \frac{1}{\psi}\left(\frac{\psi_z}{N^2}\right)_z = 0,$$

where $\tilde{N}^2 = N^2/f^2$ has been substituted. The following relation must hold

$$\frac{1}{\psi}\left(\frac{\psi_z}{N^2}\right)_z = -C = -\frac{1}{X}\frac{X_{xx}}{f^2}, \tag{S1.18}$$

with a constant of separation C. From the boundary condition (S1.5a), then,

$$X(x) = \exp\left(-\frac{x}{|c/f|}\right) \tag{S1.19}$$

and $C = 1/c^2$; here, we have chosen one of the two roots so that $X(x) \to 0$ as $x \to \infty$. The other equation is

$$\left(\frac{\psi_z}{\tilde{N}^2}\right)_z = -\frac{1}{c^2}\psi, \tag{S1.20a}$$

and the boundary conditions for ψ are

$$\psi_z = -\frac{N^2}{g}\psi \quad \text{at } z = 0 \tag{S1.20b}$$

$$\psi_z = 0 \quad \text{at } z = -D \tag{S1.20c}$$

from (S1.4b) and (S1.5b). Equations (S1.20) form the standard eigenvalue problem of vertical modes (e.g., McCreary 1981).

The solutions to the CTW eigenvalue problem (S1.4) are, therefore,

$$F^{(n)}(x, z) = \exp\left(-\frac{x}{|c^{(n)}/f|}\right)\psi^{(n)}(z), \tag{S1.21}$$

where $\psi^{(n)}$ and $c^{(n)}$ are solutions to the eigenvalue problem (S1.20). Each "vertical-wall CTW mode" (S1.21) is a product of a vertical mode and an associated exponential decay with a decay scale of the deformation radius $|c^{(n)}/f|$. This is the x-z structure of the standard coastal Kelvin wave (KW). For the barotropic mode under the rigid-lid approximation ($g \to \infty$), this solution reduces to $F^{(0)} = \text{const.}$ and $c^{(0)} = \infty$ as expected.

For KWs, the orthogonality condition reduces to that of the vertical modes: Since the bottom topography $h(x)$ consists of just one vertical wall at $x = 0$ followed by a flat

bottom, the orthogonality condition (S1.13b) reduces to

$$0 = \langle F^{(l)}, F^{(n)} \rangle_{\mathrm{b}} = \int_{-D}^{0} \mathrm{d}z\, F^{(l)}(0,z)\, F^{(n)}(0,z) = \int_{-D}^{0} \mathrm{d}z\, \psi^{(l)}(z)\, \psi^{(n)}(z),$$

which can also be derived directly from (S1.20) (e.g., McCreary 1981).

S1.4 Self-adjointness

For Sturm-Liouville equations like (S1.20), it is standard to prove the reality of the eigenvalues and the orthogonality of the eigenfunctions in the following way. First we prove that the operator on the left-hand side, $\mathcal{L}'\bullet \equiv [(\bullet)_z/N^2]_z$, is self-adjoint under the given boundary condtions:

$$\begin{aligned}
\langle \psi^{(l)}, \mathcal{L}'\psi^{(n)} \rangle_{\mathrm{b}} &= \left[\frac{\psi^{(l)}\psi_z^{(l)}}{N^2} \right]_{z=-D}^{z=0} - \int_{-D}^{0} \mathrm{d}z\, \frac{\psi_z^{(l)}\psi_z^{(n)}}{N^2} && \text{(S1.22a)} \\
&= -\left. \frac{\psi^{(l)}\psi^{(l)}}{g} \right|_{z=0} - \int_{-D}^{0} \mathrm{d}z\, \frac{\psi_z^{(l)}\psi_z^{(n)}}{N^2} && \text{(S1.22b)} \\
&= \langle \mathcal{L}'\psi^{(l)}, \psi^{(n)} \rangle_{\mathrm{b}}
\end{aligned}$$

Once it is proven, then from

$$\begin{aligned}
\langle \psi^{(l)}, \mathcal{L}'\psi^{(n)} \rangle_{\mathrm{b}} &= -\frac{1}{{c^{(n)}}^2} \langle \psi^{(l)}, \psi^{(n)} \rangle_{\mathrm{b}} \\
\langle \mathcal{L}'\psi^{(l)}, \psi^{(n)} \rangle_{\mathrm{b}} &= -\frac{1}{{c^{(l)}}^2} \langle \psi^{(l)}, \psi^{(n)} \rangle_{\mathrm{b}}
\end{aligned}$$

we get

$$-\left[\frac{1}{{c^{(n)}}^2} - \frac{1}{{c^{(l)}}^2} \right] \langle \psi^{(l)}, \psi^{(n)} \rangle_{\mathrm{b}} = 0,$$

proving the orthogonality that

$$\langle \psi^{(l)}, \psi^{(n)} \rangle_{\mathrm{b}} = 0 \quad \text{if } {c^{(n)}}^2 \neq {c^{(l)}}^2.$$

The reality of the eigenvalues is also be derived likewise.

But, the self-adjointness of $\mathcal{L}'$ is not essential. From the eigenvalue problem (S1.20),

$$0 = \langle \psi^{(l)}, \mathcal{L}'\psi^{(n)} + \frac{1}{{c^{(n)}}^2}\psi^{(n)} \rangle_{\mathrm{b}} = A'(\psi^{(l)}, \psi^{(l)}) + \frac{1}{{c^{(n)}}^2} \langle \psi^{(l)}, \psi^{(l)} \rangle_{\mathrm{b}}, \tag{S1.23}$$

where

$$A'(\psi^{(l)}, \psi^{(l)}) \equiv -\left. \frac{\psi^{(l)}\psi^{(l)}}{g} \right|_{z=0} - \int_{-D}^{0} \mathrm{d}z\, \frac{\psi_z^{(l)}\psi_z^{(n)}}{N^2}.$$

This integral equation has the same form as the corresponding integral equation for CTW modes (S1.10b). Using only the symmetry of $A'(q,r)$ and $\langle q, r \rangle_{\mathrm{b}}$, therefore, we can derive the reality of eigenvalues and the orthogonality of eigenfunctions. Moreover, since $A'(r,r) < 0$ for any nonzero $r(z)$, it is easy to see from (S1.23) that $c^2 > 0$. This argument is the same as when we derived $f/c < 0$ for CTW modes (Section S1.2.3).

The operator on the left-hand side of the CTW interior equation (S1.4a) is not self-adjoint: (S1.10b) indicates that

$$\langle F^{(l)}, \mathcal{L}F^{(n)} \rangle \neq \langle \mathcal{L}F^{(l)}, F^{(n)} \rangle.$$

Even though $\mathcal{L}$ of the CTW problem is not self-adjoint, the orthogonality is proven in a very similar manner.

What the two problems share is the symmetry of the domain integrals like (S1.22) and (S1.10). The self-adjointness of $\mathcal{L}'$ followed from the symmetry of $A'(,)$. In this view, the self-adjointness of the operator $\mathcal{L}'$ is not essential; the symmetry of $A'(q,r)$ and $\langle q, r \rangle_\mathrm{b}$ is.

Indeed, we can formulate the same eigenvalue problem as follows: Find a pair (ψ, c^2) that satisfies

$$A'(q,\psi) + \frac{1}{c^2}\langle q, \psi \rangle_\mathrm{b} = 0$$

for an arbitrary function $q(z)$. Taking a variation on q, one can prove (not shown) that the above problem is equivalent to the origianl eigenvalue problem (S1.20). Likewise, the CTW eigenvalue problem (S1.4) is equivalent to: Find a pair (F, c) that satisfies

$$A(q,F) - \frac{f}{c}\langle q, F \rangle_\mathrm{b} = 0$$

for an arbitrary function $q(z)$.

Finally and conversely, we can define operators $\mathcal{A}$ and $\mathcal{B}$ such that

$$\langle q, \mathcal{A}r \rangle = A(q,r), \quad \langle q, \mathcal{B}r \rangle = \langle q, r \rangle_\mathrm{b}$$

for arbitrary functions $q(x,z)$ and $r(x,z)$. Since $\langle,\rangle$, $\langle,\rangle_\mathrm{b}$, and $A(,)$ are all bilinear, it is easy to demonstrate that $\mathcal{A}$ and $\mathcal{B}$ are linear operators, and since $\langle,\rangle$, $\langle,\rangle_\mathrm{b}$, and $A(,)$ are all symmetric, it is easy to demonstrate that $\mathcal{A}$ and $\mathcal{B}$ are self-adjoint. Using these definitions, the CTW eigenvalue problem can be formulated as: Find a pair (F, c) that satisfies

$$\langle q, \mathcal{A}F \rangle - \frac{f}{c}\langle q, \mathcal{B}F \rangle = 0$$

for an arbitrary function $q(z)$ or equivalently,

$$\mathcal{A}F - \frac{f}{c}\mathcal{B}F = 0.$$

In Section S2.4, we find that a finite-difference form of (S1.20) takes the form of

$$A\vec{F} - \frac{f}{c}B\vec{F} = 0$$

with symmetric matrices A and B, that the reality of the eigenvalues and the orthogonality of the eivenvectors follow from the symmetry of A and B, and that the result $f/c < 0$ follows from the negative-definiteness of A and the positive-definiteness of B. (Strictly speaking, B is positive definite only for physically valid eigenvectors. See Section S2.4.)

This is the underlying connection between the matrix formalism of the finite-difference scheme (Section S2.4) and the continuous eigenvalue problem (S1.4).

References

Brink, KH. 1989. "Energy conservation in coastal-trapped wave calculations" [in EN]. *J. Phys. Oceanogr.* 19, no. 7 (July 1, 1989): 1011–1016. https://doi.org/10.1175/1520-0485(1989)019<1011:ECICTW>2.0.CO;2.

———. 1991. "Coastal-trapped waves and wind-driven currents over the continental shelf." *Ann. Rev. Fluid Mech.* 23:389–412. https://doi.org/10.1146/annurev.fl.23.010191.002133.

Brink, KH and Chapman, DC. 1987. *Programs for computing properties of coastal-trapped waves and wind-driven motions over the continental shelf and slope, 2nd ed.* Technical Report WHOI-87-24. [The programs are available from, and updates to them are documented in, https://www.whoi.edu/cms/files/Fortran_30425.htm (2007).] Woods Hole Oceanographic Institution, June. https://www.whoi.edu/cms/files/WHOI-87-24-Programs_for_Computing_text_25484.pdf.

Clarke, AJ. 1977. "Observational and numerical evidence for wind-forced coastal trapped long waves" [in EN]. *J. Phys. Oceanogr.* 7, no. 2 (March 1, 1977): 231–247. https://doi.org/10.1175/1520-0485(1977)007<0231:OANEFW>2.0.CO;2.

Clarke, AJ and Van Gorder, S. 1986. "A method for estimating wind-driven frictional, time-dependent, stratified shelf and slope water flow." *J. Phys. Oceanogr.* 16 (6): 1013–1028. https://doi.org/10.1175/1520-0485(1986)016<1013:AMFEWD>2.0.CO;2.

McCreary, JP. 1981. "A linear stratified ocean model of the equatorial undercurrent." *Phil. Trans. Roy. Soc. Lond. A* 298 (January 21, 1981): 603–635. https://doi.org/10.1098/rsta.1981.0002.

Wang, DP and Mooers, CNK. 1976. "Coastal-trapped waves in a continuously stratified ocean" [in EN]. *J. Phys. Oceanogr.* 6, no. 6 (November 1, 1976): 853–863. https://doi.org/10.1175/1520-0485(1976)006<0853:CTWIAC>2.0.CO;2.

S2 Discretized CTW eigenvalue problem

This appendix derives a finite-difference scheme to solve the coastal trapped wave (CTW) eigenvalue problem (1) and derives its properties. To explain ideas and techniques used to construct and manipulate the finite-difference equations, we first explain them for the "vertical-mode" eigenvalue problem (Section S2.1) before applying them to the CTW problem to construct the finite-difference equations (Section S2.2) and to derive their properties (Section S2.3). We then cast the set of the finite-difference equations to a matrix form (Section S2.4) to further derive important properties of the solutions (Section S2.5). Finally, Section S2.6 shows that the finite-difference CTW equations become separable in x and z to yield a finite-difference version of the standard vertical-mode eigenvalue problem and a finite-difference version of the $X_{xx}+(c/f)^2X=0$, which determines the offshore structure of the mode.

This appendix together with Section S1 is designed to be as much self-contained as possible, in order to allow the interested reader to skip Section 3 of the main text and read the appendices instead. To avoid frequently referring to the main text, the two appendices contain overlaps with the main text. For such an overlap, the version of the discussion in the main text is much condensed and the version here is extended fully.

S2.1 1-d finite difference

We reproduce the vertical-mode eigenvalue problem (eq. (7)):

$$\begin{aligned} &\mathcal{L}'F + c^{-2}F = 0, \\ &\qquad F_z/N^2 = -F/g \quad \text{at } z=0, \\ &\qquad F_z/N^2 = 0 \qquad\quad \text{at } z=-D, \end{aligned}$$

where $\mathcal{L}'r \equiv (r_z/N^2)_z$. We use a standard grid configuration and a standard finite-difference scheme for this 1-d problem:

$$\mathcal{L}'\psi|_k = \frac{1}{\Delta z_k}\left(\frac{\psi_{k-1}-\psi_k}{N^2_{k-1}\Delta\bar{z}_{k-1}} - \frac{\psi_k-\psi_{k+1}}{N^2_k\Delta\bar{z}_k}\right), \tag{S2.1}$$

where

$$\Delta\bar{z}_k \equiv \frac{\Delta z_k + \Delta z_{k+1}}{2}, \tag{S2.2}$$

$\psi_k \equiv \psi(z_k)$ is defined at cell centers, and the function $N(z)$ is defined at cell edges. The above finite difference is "conservative" because the domain "integral"

$$\begin{aligned} \sum_{k=1}^{M}\Delta z_k\mathcal{L}'\psi|_k &= \sum_{k=1}^{M}\left(\frac{\psi_{k-1}-\psi_k}{N^2_{k-1}\Delta\bar{z}_{k-1}} - \frac{\psi_k-\psi_{k+1}}{N^2_k\Delta\bar{z}_k}\right) \\ &= \sum_{k=0}^{M-1}\frac{\psi_k-\psi_{k+1}}{N^2_k\Delta\bar{z}_k} - \sum_{k=1}^{M}\frac{\psi_k-\psi_{k+1}}{N^2_k\Delta\bar{z}_k} \\ &= \frac{\psi_0-\psi_1}{N^2_0\Delta\bar{z}_0} - \frac{\psi_M-\psi_{M+1}}{N^2_M\Delta\bar{z}_M} \end{aligned} \tag{S2.3}$$

includes only "fluxes" across the surface and bottom boundaries. Imagine that ψ obeys the fictitious "diffusion" equation: $\psi_t = \mathcal{L}'\psi$. Then, the "total amount of ψ" is conserved:

$$\partial_t \sum_k \Delta z_k \psi_k = \frac{\psi_0 - \psi_1}{N_0^2 \Delta \bar{z}_0} - \frac{\psi_M - \psi_{M+1}}{N_M^2 \Delta \bar{z}_M}.$$

This "conservation" holds because the same "flux" ψ_z/N^2 that leaves one grid cell enters the next grid cell; there is no sink or source in the interior, leaving only the boundary fluxes as potential source or sink.

The corresponding bilinear form, analogous to (S1.22a), is

$$\begin{aligned}
\langle q, \mathcal{L}'\psi\rangle_{\mathrm{b}} &= \sum_{k=1}^{M} \Delta z_k q_k \frac{1}{\Delta z_k}\left(\frac{\psi_{k-1}-\psi_k}{N_{k-1}^2\Delta\bar{z}_{k-1}} - \frac{\psi_k - \psi_{k+1}}{N_k^2 \Delta \bar{z}_k}\right) \\
&= \sum_{k=1}^{M} q_k \frac{\psi_{k-1}-\psi_k}{N_{k-1}^2\Delta\bar{z}_{k-1}} - \sum_{k=1}^{M} q_k \frac{\psi_k - \psi_{k+1}}{N_k^2 \Delta \bar{z}_k} \\
&= \sum_{k=0}^{M-1} q_{k+1} \frac{\psi_k - \psi_{k+1}}{N_k^2 \Delta \bar{z}_k} - \sum_{k=1}^{M} q_k \frac{\psi_k - \psi_{k+1}}{N_k^2 \Delta \bar{z}_k} \qquad \text{(S2.4a)} \\
&= q_1 \frac{\psi_0 - \psi_1}{N_0^2 \Delta \bar{z}_0} - q_M \frac{\psi_M - \psi_{M+1}}{N_M^2 \Delta \bar{z}_M} \\
&\quad - \sum_{k=1}^{M-1} \Delta \bar{z}_k \frac{q_k - q_{k+1}}{\Delta \bar{z}_k} \frac{1}{N_k^2} \frac{\psi_k - \psi_{k+1}}{\Delta \bar{z}_k}. \qquad \text{(S2.4b)}
\end{aligned}$$

In the transformation that led to (S2.4a), we transformed $k \to k+1$ only for the first summation and found that the "flux" $(\psi_k - \psi_{k+1})/(N_k^2 \Delta \bar{z}_k)$ was exactly the same between the two summations whereas the factor on the flux was q_{k+1} in the first summation and q_k in the second. The summations were then combined to form the last line of (S2.4b) except for the $k = 0$ term of the first summation and the $k = M$ term of the second. These two terms are the surface and bottom "energy" fluxes on the last-but-one line. This "integration by parts" was possible only because the finite difference is written in a "conservative" form (S2.1).

We next use the free-surface boundary condition (S1.20b) and the standard bottom boundary condition (S1.20c), which are naturally implemented as

$$\frac{\psi_0 - \psi_1}{N_0^2 \Delta \bar{z}_0} = -\frac{1}{g}\bar{\psi}_0, \quad \frac{\psi_M - \psi_{M+1}}{N_0^2 \Delta \bar{z}_M} = 0,$$

where $\bar{\psi}_0 \equiv (\psi_0 + \psi_1)/2$ is the surface value. From the bottom boundary condition, the bottom flux in (S2.4b) vanishes. To bring (S2.4b) to a symmetric form, we add a new term that is identically zero and we "split" the original term into two halves:

$$\begin{aligned}
& q_1 \frac{\psi_0 - \psi_1}{N_0^2 \Delta \bar{z}_0} && + 0 \\
=& q_1 \left(\frac{1}{2}\frac{\psi_0 - \psi_1}{N_0^2 \Delta \bar{z}_0} + \frac{1}{2}\frac{\psi_0 - \psi_1}{N_0^2 \Delta \bar{z}_0}\right) && + \frac{q_0}{2}\left(-\frac{1}{g}\bar{\psi}_0 + \frac{1}{g}\bar{\psi}_0\right) \\
=& q_1 \left(\frac{1}{2}\frac{\psi_0 - \psi_1}{N_0^2 \Delta \bar{z}_0} - \frac{1}{2}\frac{\bar{\psi}_0}{g}\right) && + \frac{q_0}{2}\left(-\frac{1}{g}\bar{\psi}_0 - \frac{\psi_0 - \psi_1}{N_0^2 \Delta \bar{z}_0}\right)
\end{aligned}$$

$$
\begin{aligned}
&= -\frac{q_1+q_0}{2}\frac{\bar{\psi}_0}{g} - \frac{q_0-q_1}{2}\frac{\psi_0-\psi_1}{N_0^2\Delta\bar{z}_0} \\
&= -\frac{\overline{q}_0\bar{\psi}_0}{g} \qquad - \frac{\Delta\bar{z}_0}{2}\frac{q_0-q_1}{\Delta\bar{z}_0}\frac{1}{N_0^2}\frac{\psi_0-\psi_1}{\Delta\bar{z}_0}.
\end{aligned} \tag{S2.5}
$$

In the above derivation, we have used the surface boundary condition twice to switch between $(\psi_0-\psi_1)/(N_0^2\Delta\bar{z}_0)$ and $-\bar{\psi}_0/g$. After this transformation, we find that (S2.4b) is symmetric in q and ψ:

$$
\begin{aligned}
\langle q, \mathcal{L}'\psi\rangle_\mathrm{b} = &-\frac{\overline{q}_0\bar{\psi}_0}{g} \\
&- \frac{\Delta\bar{z}_0}{2}\frac{q_0-q_1}{\Delta\bar{z}_0}\frac{1}{N_0^2}\frac{\psi_0-\psi_1}{\Delta\bar{z}_0} - \sum_{k=1}^{M-1}\Delta\bar{z}_k\frac{q_k-q_{k+1}}{\Delta\bar{z}_k}\frac{1}{N_k^2}\frac{\psi_k-\psi_{k+1}}{\Delta\bar{z}_k}.
\end{aligned} \tag{S2.6}
$$

This is the analog of (S1.22b). The second line can be interpreted as the vertical integral

$$
\int_{-D}^{0} \mathrm{d}z\, \frac{q_z\psi_z}{N^2}
$$

evaluated with the trapezoidal rule, where the integrand is defined at the edges of the cells. The contribution from the bottom edge, e.g., $k=M$ of the summation, is missing because of the bottom boundary condition.

Since $\langle\psi^{(l)}, \mathcal{L}'\psi^{(n)}\rangle_\mathrm{b}$ is symmetric, the solutions to the eigenvalue problem $\mathcal{L}'F = \lambda F$ satisfy the orthogonality relation

$$
\langle\psi^{(l)}, \psi^{(n)}\rangle_\mathrm{b} = \sum_{k=1}^{M}\Delta z_k\psi_k^{(l)}\psi_k^{(n)} = 0 \quad \text{if } \lambda^{(l)} \neq \lambda^{(n)}
$$

and the eigenvalues are real. Moreover, since $\langle\psi^{(l)}, \mathcal{L}'\psi^{(n)}\rangle_\mathrm{b}$ is negative and $\langle\psi^{(l)}, \psi^{(n)}\rangle_\mathrm{b}$ is positive, $\lambda < 0$. This is the same argument we developed for the continuous system in Section S1.4.

Under the rigid-lid approximation ($g \to \infty$), $\psi^{(0)} = (b, b, \ldots, b)$ with an arbitrary $b \neq 0$ is a solution to the original eigenvalue problem with $\lambda^{(0)} = 0$. This is the barotropic mode. In this case, $\langle\psi^{(0)}, \mathcal{L}'\psi^{(0)}\rangle_\mathrm{b} = 0$; this integral is only negative semi-definite. As we shall see, definiteness of the corresponding integral affects the choice of the matrix solver for numerical solutions to the CTW eigenvalue problem (Section S2.4).

These results are not trivial. The finite-difference scheme (S2.1) is just one of many potential ones and not all schemes lead to these useful properties that mirror those of the original continuous system. The success is due to the successful "integration by parts" (S2.4), which in turn is due to the conservative nature of the finite-difference

scheme (S2.1). In the next subsection, we extend this method to the CTW eigenvalue problem.

S2.2 Finite difference form of the CTW eigenvalue problem

The CTW differential operator is

$$\mathcal{L}F \equiv \boldsymbol{\nabla}\cdot\boldsymbol{B} = F_{xx} + \left(\frac{F_z}{\tilde{N}^2}\right)_z.$$

We use the same inner product

$$\langle q, r\rangle \equiv \iint_\Omega \mathrm{d}x\,\mathrm{d}z\, q(x,z)\, r(x,z)$$

as defined in (S1.11). Under the CTW boundary conditions (S1.4d), (S1.4b) and (S1.4c), the eigenfunctions satisfy the orthogonal relation (S1.13) and other useful properties (Section S1.2.3). In this section, we extend the methods in Section S2.1 and develop a finite-different scheme that has the same useful properties as derived for the continuous system (Section S1.2.3). These properties turn out to be more useful for the CTW problem because they are useful to quickly distinguish unphysical solutions (Section S2.4).

We use the z coordinates. The simplest scheme is to treat the bottom slope, not as an approximation but *really* as a series of steps, which greatly simplifies the mathematical handling of the finite-difference equations as well as coding the scheme. This nice finite-difference scheme, however, resulted in significant error in the eigenvalues (c's) (not shown). For this reason, we use a somewhat more sophisticated bottom-slope boundary condition, which has, unfortunately, greatly complicated the calculations below.

Figure 1 is a schematic diagram showing the grid configuration. The computational domain $(x,z) \in (0, L_\mathrm{x}) \times (-D, 0)$ is divided into rectangle cells (i,k) with $i = 1,\ldots,M_\mathrm{h}$ and $k = 1,\ldots,M_\mathrm{v}$. Some of the cells outside this domain (Fig. 1) are used to handle boundary conditions (see below). The grid cell at (i,k) has a width and height of Δx_i and Δz_k; the distances between cell centers are

$$\Delta\bar{x}_i \equiv \frac{1}{2}(\Delta x_{i+1} + \Delta x_i) \qquad (i = 0,\ldots,M_\mathrm{h}) \tag{S2.7a}$$

$$\Delta\bar{z}_k \equiv \frac{1}{2}(\Delta z_{k+1} + \Delta z_k) \qquad (k = 0,\ldots,M_\mathrm{v}), \tag{S2.7b}$$

which are defined on cell edges. Note the index scheme here: the right edge of cell i is edge i and the bottom edge of cell k is edge k. Purely for mathematics, we should be using a notation like $i + \frac{1}{2}$ to indicate the edge between cells i and $i+1$, but our indices are designed to mirror those in our computer program.

The mode function value F "stored" in cell (i,k) is denoted by $F_{i,k}$ or $F(i,k)$, whichever is convenient depending on the context. Further, we sometimes write F_i or F_k to mean $F_{i,k}$ when the omission is obvious from the context. In the "interior", the value $F(i,k)$ is "defined" at the center of cell (i,k). The handling of boundary values is discussed below. The normalized Brunt-Väisaälä frequency, $\tilde{N}_k$, is defined at the lower edge of the grid cell (i,k); this arrangement is necessary for "conservation" (Section S2.1). We denote the left-most ocean point at each depth k by $i = i_\mathrm{s}[k]$ and the deepest ocean point for

each position i by $k = k_{\rm s}[i]$. The "ocean domain" can then be spanned either by

$$k = 1, \ldots, k_{\rm s}[i] \quad \text{scanning downward at each } i = 1, \ldots, M_{\rm h} \tag{S2.8a}$$

or by

$$i = i_{\rm s}[k], \ldots, M_{\rm h} \quad \text{scanning rightward at each } k = 1, \ldots, M_{\rm v}. \tag{S2.8b}$$

For simplicity, we sometimes use the notation "$(i,k) \in \Omega_+$" when the point is in the ocean.

The "corner cell" is a special case. Figure 1 shows cells with diagonal thick lines cutting through them; they are the corner cells. The corner cell is the deepest for its position i and the left-most for its depth k: that is, $(i,k) = (i_{\rm s}[k], k) = (i, k_{\rm s}[i])$ for it. In our terminology, it is an "ocean cell" belonging to Ω_+ and its center is a "boundary point". We call the part of the ocean domain that excludes the corner cells "the interior" and denote it by Ω.

The number of the grid cells which are not ocean in the $1 \le i \le M_{\rm h}$ and $1 \le k \le M_{\rm v}$ range is

$$M_{\rm land} = \textstyle\sum_{k=1}^{M_{\rm v}} \left(\sum_{1 \le i < i_{\rm s}[k]} \right)$$

and then the total number of the ocean grid cells is $M_{\rm h} M_{\rm v} - M_{\rm land}$.

The "boundary values", denoted by $\overline{F}$, are located and *defined* on the boundaries (Fig. 1). Along the sea surface and the right edge ($x = L_{\rm x}$), the symbol $\overline{F}$ is used as a short hand for the average

$$\overline{F}_{i,0} \equiv \frac{F_{i,0} + F_{i,1}}{2}, \qquad i = 1, \ldots, M_{\rm h}, \tag{S2.9}$$

$$\overline{F}_{M_{\rm h},k} \equiv \frac{F_{M_{\rm h},k} + F_{M_{\rm h}+1,k}}{2}, \quad k = 1, \ldots, M_{\rm v}, \tag{S2.10}$$

where $F_{i,0}$ is defined at the center of "ghost cell" $(i,0)$ above the sea surface and $F_{M_{\rm v}+1,k}$ is defined at the center of ghost cell $(M_{\rm v}+1, k)$ to the right of the right edge (Figure 1). We call these regions that consist of ghost cells above the sea-surface or to the right of the right edge, "lobes".

In contrast, on the "slope/bottom surface", depicted by the thick black line in Fig. 1, the boundary values themselves are used in the equations (below). Along a vertical wall, the closest ocean point is $(i_{\rm s}[k], k)$ and the boundary value is denoted by $\overline{F}(i_{\rm s}[k]-1, k)$, which we "store" in the $(i_{\rm s}[k]-1, k)$ cell; that is, in the mathematical derivation below, we write $F(i_{\rm s}[k]-1, k)$ to mean $\overline{F}(i_{\rm s}[k]-1, k)$ whenever it is convenient to do so. Likewise, along the flat part(s) of the slope or of the flat bottom ($z = -D$), $(i, k_{\rm s}[i])$ is the closet ocean point and $F(i, k_{\rm s}[i]+1) = \overline{F}(i, k_{\rm s}[i])$ is defined at the bottom boundary but stored below the bottom. At a diagonal portion of the slope, the center of the corner cell is the boundary point and therefore simply $F(i,k) = \overline{F}(i,k)$. No extra grid cell is used for this value.

There is one potential problem: If there is a vertical "cliff" at the right edge of a flat region in the slope/bottom topography, the ghost cell (i,k) to the lower-left of the cliff edge would have to store both the value below the flat bottom, $F(i, k_{\rm s}[i]+1)$, and the value to the left of the cliff, $F(i_{\rm s}[k]-1, k)$. To avoid this situation, we always shave off the cliff edge and make (i,k) a corner cell. The treatment also contributes to smooth the

given topography. Our program includes a subroutine to modify the slope topography this way if necessary, with a warning message.

To summarize our terminology, the ocean cells include interior cells and corner cells. On the boundaries are the boundary points; along the sea surface and right edge, the $\overline{F}$ values at the boundary points are represented by averages between the neighboring interior values and ghost-point values; on the diagonals of corner cells, the $\overline{F}$ values are defined at the cell centers; on vertical-wall or flat-bottom boundaries, $\overline{F}$ values are defined on the boundaries and "stored" in the neighboring ghost cells (Figure 1). We these preparations, we now define the finite-difference equations.

S2.2.1 Surface and right-edge boundary conditions

We start with the simplest of the equations, which are the surface and right-edge boundary conditions. The surface boundary condition (S1.4b) is discretized as

$$\frac{F_{i,0}-F_{i,1}}{\tilde{N}_0^2\Delta\bar{z}_0}+\frac{f^2}{g}\frac{F_{i,0}+F_{i,1}}{2}=0,\quad i=1,\ldots,M_\mathrm{h}, \tag{S2.11a}$$

where $F_{i,0}$ is defined in the surface lobe (Fig. 1) and $\Delta\bar{z}_0=(\Delta z_0+\Delta z_1)/2=\Delta z_1$ because we always set $\Delta z_0=\Delta z_1$. The above boundary condition can then be rewritten as

$$\frac{\overline{F}_{i,0}-F_{i,1}}{\tilde{N}_0^2\Delta z_1/2}+\frac{f^2}{g}\overline{F}_{i,0}=0, \tag{S2.11b}$$

where the surface value is defined as $\overline{F}_{i,0}=(F_{i,0}+F_{i,1})/2$. For consistency with the handling of the slope-bottom boundary to be explained below, we could use the form (S2.11b) and *store* $\overline{F}_{i,0}$ in the surface lobe, but that would further increase complexity of coding in the handling of $\Delta\bar{z}_k$ without any practical advantage. For this reason, we stick to the form (S2.11a). Likewise, the x-boundary condition at $x=L_\mathrm{x}$ is

$$\frac{F_{M_\mathrm{h}+1,k}-F_{M_\mathrm{h},k}}{\Delta\bar{x}_{M_\mathrm{h}}}=0,\quad k=1,\ldots,M_\mathrm{v}, \tag{S2.12}$$

where $F_{M_\mathrm{h}+1,k}$ is defined in the right lobe (Fig. 1). We also ensure that $\Delta x_{M_\mathrm{h}+1}=\Delta z_{M_\mathrm{h}}$.

S2.2.2 Diagonal-slope boundary condition

To derive a discrete version of the slope boundary condition (S1.4d), we integrate the interior equation (S1.7a) over the upper triangle of the corner cell and apply Gauss's theorem to get

$$\Delta z_k F_x(i,k)+\Delta x_i\frac{F_z(i,k-1)}{\tilde{N}(k-1)}+\hat{\boldsymbol{n}}\cdot\boldsymbol{B}(i,k)\sqrt{\Delta x_i^2+\Delta z_k^2}=0, \tag{S2.13}$$

where the functions symbolically represent their values on the three edges of the triangle. The derivatives $F_x(i,k)$ and $F_z(i,k-1)$ on the right and upper edges of the triangle are naturally discretized as

$$F_x(i,k)=\frac{F_{i+1}-F_i}{\Delta\bar{x}_i},\quad F_z(i,k-1)=\frac{F_{k-1}-F_k}{\Delta\bar{z}_{k-1}}. \tag{S2.14}$$

Noting that

$$\hat{\boldsymbol{n}} = \left(-\frac{\Delta z}{\sqrt{\Delta x^2 + \Delta z^2}}, -\frac{\Delta x}{\sqrt{\Delta x^2 + \Delta z^2}} \right)$$

on the diagonal and using the boundary condition (S1.7b), we find that

$$\begin{aligned} \hat{\boldsymbol{n}} \cdot \boldsymbol{B}(i,k) \sqrt{\Delta x_i^2 + \Delta z_k^2} &= \frac{f}{c} \hat{\boldsymbol{n}} \cdot (F(i,k), 0) \sqrt{\Delta x_i^2 + \Delta z_k^2} \\ &= -\frac{f}{c} \Delta z_k F(i,k). \end{aligned} \tag{S2.15}$$

Plugging (S2.14) and (S2.15) into (S2.13) gives

$$\frac{F_{i+1,k} - F_{i,k}}{\Delta \bar{x}_i} + \frac{\Delta x_i}{\Delta z_k} \frac{F_{i,k-1} - F_{i,k}}{\Delta \bar{z}_{k-1} \tilde{N}_{k-1}} = \frac{f}{c} F_{i,k}, \quad (i,k) \in \text{Corner Cells}. \tag{S2.16}$$

In this equation, $F_{i,k}$ is at the central gridpoint of the corner cell and located on the diagonal (cyan cross in Fig. 1). Recognizing that $h_x(i,k) = \Delta z_k / \Delta x_i$ for the grid cell, we note that the above equality is a natural, single-sided finite differencing of the slope boundary condition (S1.4d).

Even though (S2.16) can be used as is to obtain solutions, the matrix of the eigenvalue problem would not be symmetric, which is inconvenient for solving the problem (see below). Here we transform (S2.16) for at $k = 1$, combining it with the surface boundary condition (S2.11a). That is, applying the technique we showed for the 1-d problem (Section S2.1), we "split" $F_z / \tilde{N}^2 \big|_{z=0}$ as

$$\begin{aligned} \frac{F_{i,0} - F_{i,1}}{\tilde{N}_0^2 \Delta \bar{z}_0} &= \frac{1}{2} \frac{F_{i,0} - F_{i,1}}{\tilde{N}_0^2 \Delta \bar{z}_0} + \frac{1}{2} \frac{F_{i,0} - F_{i,1}}{\tilde{N}_0^2 \Delta \bar{z}_0} \\ &= \frac{1}{2} \frac{F_{i,0} - F_{i,1}}{\tilde{N}_0^2 \Delta \bar{z}_0} - \frac{1}{2} \frac{f^2}{g} \frac{F_{i,0} + F_{i,1}}{2}. \end{aligned} \tag{S2.17}$$

This expression can be incorporated into (S2.16) to yield

$$\begin{aligned} &\frac{F_{i+1,k} - F_{i,k}}{\Delta \bar{x}_i} + \frac{\Delta x_i}{\Delta z_k} \left(\gamma_k \frac{F_{i,k-1} - F_{i,k}}{\Delta \bar{z}_{k-1} \tilde{N}_{k-1}} - \varsigma_k \frac{f^2}{g} \frac{F_{i,k-1} + F_{i,k}}{2} \right) = \frac{f}{c} F_{i,k}, \\ &(i,k) \in \text{Corner Cells} \end{aligned} \tag{S2.18}$$

where

$$(\gamma_k, \varsigma_k) \equiv \begin{cases} (\frac{1}{2}, \frac{1}{2}) & k = 1, \\ (1, 0) & \text{otherwise}. \end{cases}$$

These factors affect the equation only at $k = 1$ and are introduced for later convenience when manipulating the equations (Section S2.4). This modification appears artificial but is crucial in transforming the operator into a symmetric form.

S2.2.3 Vertical wall and flat bottom

We also place boundary points right on the boundary as indicated by circles in Fig. 1 and we accordingly halve Δx_i and Δz_k for the finite differences of F_x and F_z here. The x-boundary condition (S1.5a) at a vertical segment of the slope is therefore

$$\frac{F(i_s[k], k) - \overline{F}(i_s[k] - 1, k)}{\Delta x_{i_s[k]} / 2} = \frac{f}{c} \overline{F}(i_s[k] - 1, k), \tag{S2.19}$$

where $\overline{F}$ is the value on the vertical segment (circles in Fig. 1 on vertical slope segments); and the z-boundary condition at a flat segment of the slope or the bottom (S1.5b) is

$$\frac{F(i,k_\mathrm{s}[i]) - \overline{F}(i,k_\mathrm{s}[i]+1)}{\Delta z_{k_\mathrm{s}[i]}/2} = 0, \tag{S2.20}$$

where again $\overline{F}$ is the value on the flat segment.

Below, we modify the definitions of $\Delta\bar{x}$ and $\Delta\bar{z}$ at the vertical-wall and flat-bottom boundaries for notational convenience:

$$\Delta\bar{x}_{i-1} = \begin{cases} (\Delta x_i + \Delta x_{i-1})/2 & i > i_\mathrm{s}[k] \\ \Delta x_i/2 & i = i_\mathrm{s}[k] \end{cases}$$

for each k and

$$\Delta\bar{z}_k = \begin{cases} (\Delta z_k + \Delta x_{k+1})/2 & k < k_\mathrm{s}[i] \\ \Delta z_k/2 & k = k_\mathrm{s}[i] \end{cases}$$

for each i. Even though the modified $\Delta\bar{x}_i$ depends on k and the modified $\Delta\bar{z}_k$ depends on i next to the respective boundaries, we omit these extra indices because the omission is always obvious.

S2.2.4 Interior equation

The most straightforward "conservative" finite difference scheme for the interior equation (S1.4a) is

$$\begin{aligned} 0 &= \mathcal{L}F|_{i,k} \\ &= \frac{1}{\Delta x_i}\left(\frac{F_{i+1,k}-F_{i,k}}{\Delta\bar{x}_i} - \frac{F_{i,k}-F_{i-1,k}}{\Delta\bar{x}_{i-1}}\right) \\ &\quad + \frac{1}{\Delta z_k}\left(\frac{F_{i,k-1}-F_{i,k}}{\tilde{N}^2_{k-1}\Delta\bar{z}_{k-1}} - \frac{F_{i,k}-F_{i,k+1}}{\tilde{N}^2_k\Delta\bar{z}_k}\right) \quad \text{for } (i,k)\in\Omega. \end{aligned} \tag{S2.21}$$

It is possible that $i = i_\mathrm{s}[k]$ when cell (i,k) is next to a vertical segment of the slope (Fig. 1). In that case, the cell to the left of (i,k) is the ghost cell $(i-1,k)$ and therefore $F_{i-1,k} = \overline{F}_{i_\mathrm{s}[k]-1,k}$, the value on the vertical wall. Likewise, it is possible that $k = k_\mathrm{s}[i]$ and there $F_{i,k_\mathrm{s}[k]+1} = \overline{F}_{i,k_\mathrm{s}[k]}$ is stored in the ghost cell below the bottom. Similarly, just below the surface or just to the left of the $x = L_\mathrm{x}$ boundary, the above equation includes grid cells that are just outside the ocean; as discussed earlier, the F values above the sea surface, $F_{i,0}$, are stored in the top lobe (Fig. 1) and those to the right of $x = L_\mathrm{x}$, $F_{M_\mathrm{h}+1,k}$, are stored in the right lobe.

For the same reason as for (S2.18), (S2.17) can be incorporated into (S2.21) to yield

$$\begin{aligned} 0 &= \Delta z_k\left(\frac{F_{i+1,k}-F_{i,k}}{\Delta\bar{x}_i} - \frac{F_{i,k}-F_{i-1,k}}{\Delta\bar{x}_{i-1}}\right) \\ &\quad + \Delta x_i\left(\gamma_k\frac{F_{i,k-1}-F_{i,k}}{\tilde{N}^2_{k-1}\Delta\bar{z}_{k-1}} - \varsigma_k\frac{f^2}{g}\frac{F_{i,k-1}+F_{i,k}}{2} - \frac{F_{i,k}-F_{i,k+1}}{\tilde{N}^2_k\Delta\bar{z}_k}\right) \\ &\quad \text{for } (i,j)\in\Omega, \end{aligned} \tag{S2.22}$$

S2.3 Bilinear form for the discretized system

With these preparations, we calculate the bilinear form $\langle q, \mathcal{L}F\rangle$. For the continuous system it is an area integral over the ocean domain (eq. (S1.11)). For the finite-differenced system, the most natural definition would be

$$\langle q, r\rangle = \sum_{(i,k)\in\Omega} \Delta x_i\, \Delta z_k\, q_{i,k}\, r_{i,k}.$$

(Recall that the corner cells and boundary points (Fig. 1) are excluded from this interior "integral".) We demonstrate that this is the "right one".

In the following, we calculate $\langle q, \mathcal{L}F\rangle$ for our finite-difference form shown above, using the techniques, developed for the 1-d problem (Section S2.1), of "integrating by parts" and adding and subtracting boundary terms to bring the integral to a symmetric form. Here, we focus on bringing it to a symmetric form and showing that it is negative definite. We will not attempt to bring the result as close to the continuous form (S1.10a) as possible: the form we obtain below is complicated enough and further manipulation is not worth. Since the derivation is complicated, we calculate components of the sum piece by piece and add them together at the end.

S2.3.1 $\int \mathrm{d}x\, q\, F_{xx}$

At depth k where $i = i_\mathrm{s}[k]$ is *not* a corner cell, we calculate the zonal integral

$$\begin{aligned}
&\int \mathrm{d}x\, q\, F_{xx} \\
&= \sum_{i=i_\mathrm{s}}^{i=M_\mathrm{h}} \Delta x_i\, q_i \frac{1}{\Delta x_i}\left(\frac{F_{i+1}-F_i}{\Delta\bar{x}_i} - \frac{F_i - F_{i-1}}{\Delta\bar{x}_{i-1}}\right) \\
&= \sum_{i=i_\mathrm{s}}^{i=M_\mathrm{h}} q_i \frac{F_{i+1}-F_i}{\Delta\bar{x}_i} - \sum_{i=i_\mathrm{s}-1}^{i=M_\mathrm{h}-1} q_{i+1}\frac{F_{i+1}-F_i}{\Delta\bar{x}_i} \\
&= -\sum_{i=i_\mathrm{s}}^{i=M_\mathrm{h}-1} (q_{i+1}-q_i)\frac{F_{i+1}-F_i}{\Delta\bar{x}_i} + q_{M_\mathrm{h}}\frac{F_{M_\mathrm{h}+1}-F_{M_\mathrm{h}}}{\Delta\bar{x}_{M_\mathrm{h}}} - q_{i_\mathrm{s}}\frac{F_{i_\mathrm{s}}-\overline{F}_{i_\mathrm{s}-1}}{\Delta\bar{x}_{i_\mathrm{s}-1}} \\
&= -\sum_{i=i_\mathrm{s}}^{i=M_\mathrm{h}-1} (q_{i+1}-q_i)\frac{F_{i+1}-F_i}{\Delta\bar{x}_i} - q_{i_\mathrm{s}}\frac{F_{i_\mathrm{s}}-\overline{F}_{i_\mathrm{s}-1}}{\Delta\bar{x}_{i_\mathrm{s}-1}},
\end{aligned}$$

where we have used the $x = L_\mathrm{x}$ boundary condition (S2.12) and substituted $F_{i_\mathrm{s}-1} = \overline{F}_{i_\mathrm{s}-1}$. In the 1-d problem (Section S2.1), we added and subtracted a term to bring in a boundary term. Similarly, we add a term which is identically zero from the boundary condition (S2.19) and get

$$\begin{aligned}
&\int \mathrm{d}x\, q\, F_{xx} + \overline{q}_{i_\mathrm{s}-1}\left(\frac{F_{i_\mathrm{s}}-\overline{F}_{i_\mathrm{s}-1}}{\Delta\bar{x}_{i_\mathrm{s}-1}} - \frac{f}{c}\overline{F}_{i_\mathrm{s}-1}\right) \\
&= -\sum_{i=i_\mathrm{s}}^{i=M_\mathrm{h}-1} (q_{i+1}-q_i)\frac{F_{i+1}-F_i}{\Delta\bar{x}_i} \\
&\quad - (q_{i_\mathrm{s}} - \overline{q}_{i_\mathrm{s}-1})\frac{F_{i_\mathrm{s}}-\overline{F}_{i_\mathrm{s}-1}}{\Delta\bar{x}_{i_\mathrm{s}-1}} - \overline{q}_{i_\mathrm{s}-1}\frac{f}{c}\overline{F}_{i_\mathrm{s}-1}.
\end{aligned} \tag{S2.23a}$$

At depth k where $i = i_\mathrm{s}[k]$ *is* a corner cell, that cell is excluded from the "interior" integral:

$$\begin{aligned}
&\int \mathrm{d}x\, q\, F_{xx} \\
&= \sum_{i=i_\mathrm{s}+1}^{i=M_\mathrm{h}} \Delta x_i\, q_i \frac{1}{\Delta x_i}\left(\frac{F_{i+1}-F_i}{\Delta\bar{x}_i} - \frac{F_i - F_{i-1}}{\Delta\bar{x}_{i-1}}\right) \\
&= -\sum_{i=i_\mathrm{s}+1}^{i=M_\mathrm{h}-1} (q_{i+1}-q_i)\frac{F_{i+1}-F_i}{\Delta\bar{x}_i} - q_{i_\mathrm{s}+1}\frac{F_{i_\mathrm{s}+1}-F_{i_\mathrm{s}}}{\Delta\bar{x}_{i_\mathrm{s}}}
\end{aligned} \tag{S2.23b}$$

S2.3.2 $\int \mathrm{d}z\, q(F_z/\tilde{N})_z$

Likewise, at position i where $k = k_\mathrm{s}[i]$ is *not* a corner cell,

$$\begin{aligned}
&\int \mathrm{d}z\, q\left(\frac{F_z}{\tilde{N}^2}\right)_z \\
&= \sum_{k=1}^{k=k_\mathrm{s}} \Delta z_k q_k \frac{1}{\Delta z_k}\left(\frac{F_{k-1}-F_k}{\tilde{N}^2_{k-1}\Delta\bar{z}_{k-1}} - \frac{F_k - F_{k+1}}{\tilde{N}^2_k \Delta\bar{z}_k}\right) \\
&= \sum_{k=1}^{k=k_\mathrm{s}} q_k \frac{F_{k-1}-F_k}{\tilde{N}^2_{k-1}\Delta\bar{z}_{k-1}} - \sum_{k=2}^{k=k_\mathrm{s}+1} q_{k-1}\frac{F_{k-1}-F_k}{\tilde{N}^2_{k-1}\Delta\bar{z}_{k-1}} \\
&= -\sum_{k=2}^{k=k_\mathrm{s}} (q_{k-1}-q_k)\frac{F_{k-1}-F_k}{\tilde{N}^2_{k-1}\Delta\bar{z}_{k-1}} + q_1\frac{F_0-F_1}{\tilde{N}^2_0\Delta\bar{z}_0} - q_{k_\mathrm{s}}\frac{F_{k_\mathrm{s}}-F_{k_\mathrm{s}+1}}{\tilde{N}^2_{k_\mathrm{s}}\Delta\bar{z}_{k_\mathrm{s}}} \\
&= -\sum_{k=2}^{k=k_\mathrm{s}} (q_{k-1}-q_k)\frac{F_{k-1}-F_k}{\tilde{N}^2_{k-1}\Delta\bar{z}_{k-1}} + q_1\frac{F_0-F_1}{\tilde{N}^2_0\Delta\bar{z}_0}
\end{aligned}$$

where we have used the surface boundary condition. We "split" the surface F_z term with formula (S2.17) and again add a boundary term that is identically zero (eq. (S2.11a)):

$$\begin{aligned}
&= -\sum_{k=2}^{k=k_\mathrm{s}} (q_{k-1}-q_k)\frac{F_{k-1}-F_k}{\tilde{N}^2_{k-1}\Delta\bar{z}_{k-1}} + q_1\left(\frac{1}{2}\frac{F_0-F_1}{\tilde{N}^2_0\Delta\bar{z}_0} - \frac{1}{2}\frac{f^2}{g}\frac{F_0+F_1}{2}\right) \\
&\quad - q_0\frac{1}{2}\left(\frac{F_0-F_1}{\tilde{N}^2_0\Delta\bar{z}_0} + \frac{f^2}{g}\frac{F_0+F_1}{2}\right) \\
&= -\sum_{k=2}^{k=k_\mathrm{s}} (q_{k-1}-q_k)\frac{F_{k-1}-F_k}{\tilde{N}^2_{k-1}\Delta\bar{z}_{k-1}} - \frac{q_0-q_1}{2}\frac{F_0-F_1}{\tilde{N}^2_0\Delta\bar{z}_0} - \frac{f^2}{g}\frac{q_0+q_1}{2}\frac{F_0+F_1}{2}
\end{aligned} \tag{S2.23c}$$

Likewise, at position i where $k = k_\mathrm{s}[i]$ *is* a corner cell,

$$\begin{aligned}
&\int \mathrm{d}z\, q \left(\frac{F_z}{\tilde{N}^2}\right)_z \\
&= \sum_{k=1}^{k=k_\mathrm{s}-1} \Delta z_k q_k \frac{1}{\Delta z_k}\left(\frac{F_{k-1}-F_k}{\tilde{N}^2_{k-1}\Delta\bar{z}_{k-1}} - \frac{F_k - F_{k+1}}{\tilde{N}^2_k \Delta\bar{z}_k}\right) \\
&= -\sum_{k=2}^{k=k_\mathrm{s}-1} (q_{k-1}-q_k)\frac{F_{k-1}-F_k}{\tilde{N}^2_{k-1}\Delta\bar{z}_{k-1}} - q_{k_\mathrm{s}-1}\frac{F_{k_\mathrm{s}-1}-F_{k_\mathrm{s}}}{\tilde{N}^2_{k_\mathrm{s}-1}\Delta\bar{z}_{k_\mathrm{s}-1}} \\
&- \frac{q_0-q_1}{2}\frac{F_0-F_1}{\tilde{N}^2_0\Delta\bar{z}_0} - \frac{f^2}{g}\frac{q_0+q_1}{2}\frac{F_0+F_1}{2}
\end{aligned} \tag{S2.23d}$$

S2.3.3 Lines intersecting corner points

We first combine one horizontal integral and one vertical integral which intersect with a single corner cell (i', k'). With that definition, $i' = i_\mathrm{s}[k']$ and $k' = k_\mathrm{s}[i']$. We also add a term that is identically zero from the slope boundary condition (S2.16):

$$\begin{aligned}
&\Delta z_{k'}\text{(S2.23b)} + \Delta x_{i'}\text{(S2.23d)} \\
&\quad + q_{i',k'}\Delta z_{k'}\left(\frac{F_{i'+1,k'}-F_{i',k'}}{\Delta\bar{x}_{i'}} + \frac{\Delta x_{i'}}{\Delta z_{k'}}\frac{F_{i',k'-1}-F_{i',k'}}{\Delta\bar{z}_{k'-1}\tilde{N}_{k'-1}} - \frac{f}{c}F_{i',k'}\right) \\
&= -\Delta z_{k'}\sum_{i=i_\mathrm{s}+1}^{i=M_\mathrm{h}-1}(q_{i+1,k'}-q_{i,k'})\frac{F_{i+1,k'}-F_{i,k'}}{\Delta\bar{x}_i} - \Delta z_{k'}q_{i_\mathrm{s}+1,k'}\frac{F_{i_\mathrm{s}+1,k'}-F_{i_\mathrm{s},k'}}{\Delta\bar{x}_{i_\mathrm{s}}} \\
&\quad - \Delta x_{i'}\sum_{k=2}^{k=k_\mathrm{s}-1}(q_{i',k-1}-q_{i',k})\frac{F_{i',k-1}-F_{i',k}}{\tilde{N}^2_{k-1}\Delta\bar{z}_{k-1}} - \Delta x_{i'}q_{i',k_\mathrm{s}-1}\frac{F_{i',k_\mathrm{s}-1}-F_{i',k_\mathrm{s}}}{\tilde{N}^2_{k_\mathrm{s}-1}\Delta\bar{z}_{k_\mathrm{s}-1}} \\
&\quad - \Delta x_{i'}\frac{q_0-q_1}{2}\frac{F_0-F_1}{\tilde{N}^2_0\Delta\bar{z}_0} - \Delta x_{i'}\frac{f^2}{g}\frac{q_0+q_1}{2}\frac{F_0+F_1}{2} \\
&\quad + q_{i',k'}\Delta z_{k'}\frac{F_{i'+1,k'}-F_{i',k'}}{\Delta\bar{x}_{i'}} + q_{i',k'}\Delta x_{i'}\frac{F_{i',k'-1}-F_{i',k'}}{\Delta\bar{z}_{k'-1}\tilde{N}_{k'-1}} - \frac{f}{c}q_{i',k'}\Delta z_{k'}F_{i',k'} \\
&= -\Delta z_{k'}\sum_{i=i_\mathrm{s}}^{i=M_\mathrm{h}-1}(q_{i+1,k'}-q_{i,k'})\frac{F_{i+1,k'}-F_{i,k'}}{\Delta\bar{x}_i} \\
&\quad - \Delta x_{i'}\sum_{k=2}^{k=k_\mathrm{s}}(q_{i',k-1}-q_{i',k})\frac{F_{i',k-1}-F_{i',k}}{\tilde{N}^2_{k-1}\Delta\bar{z}_{k-1}} - \frac{f}{c}q_{i',k'}\Delta z_{k'}F_{i',k'} \\
&\quad - \Delta x_{i'}\frac{q_0-q_1}{2}\frac{F_0-F_1}{\tilde{N}^2_0\Delta\bar{z}_0} - \Delta x_{i'}\frac{f^2}{g}\frac{q_0+q_1}{2}\frac{F_0+F_1}{2}
\end{aligned} \tag{S2.24}$$

S2.3.4 Adding the rest

Summing 1) this expression over all corner cells (i', k'), 2) $\Delta z_k \times$(S2.23a) over k except for k's that include corner cells, and 3) $\Delta x_i \times$(S2.23c) over i except for i's that include corner cells completes the domain integral $\langle q, \mathcal{L}F\rangle$. Recall that we have added terms that are identically zero along the slope/bottom boundary. The sum of those terms corresponds

to the line integral, along the slope, of the slope boundary condition. Symbolically, then,

$$
\begin{aligned}
0 &= \langle q, \mathcal{L}F\rangle + \int_{\partial\Omega'} \mathrm{d}s\, q(F_x + h_x^{-1} q_z/\tilde{N}^2 - f/cF) \\
&= \sum_{k\in[k|(i_\mathrm{s}[k],k)\neq\text{corner cell}]} \Delta z_k \text{(S2.23a)} \quad + \sum_{i\in\{i|(i,k_\mathrm{s}[i])\neq\text{corner cell}\}} \Delta x_i \text{(S2.23c)} \quad + \sum_{(i',k')\in\{\text{corner cells}\}} \text{(S2.24)} \\
&= -\sum_k \Delta z_k \sum_{i=i_\mathrm{s}}^{i=M_\mathrm{h}-1} (q_{i+1,k} - q_{i,k}) \frac{F_{i+1,k} - F_{i,k}}{\Delta\bar{x}_i} \\
&\quad - \sum_k \Delta z_k (q_{i_\mathrm{s},k} - \overline{q}_{i_\mathrm{s}-1,k}) \frac{F_{i_\mathrm{s},k} - \overline{F}_{i_\mathrm{s}-1,k}}{\Delta\bar{x}_{i_\mathrm{s}-1,k}} \\
&\quad - \sum_i \Delta x_i \left[\sum_{k=2}^{k=k_\mathrm{s}} (q_{i,k-1} - q_{i,k}) \frac{F_{i,k-1} - F_{i,k}}{\tilde{N}^2_{k-1}\Delta\bar{z}_{k-1}} + \frac{q_{i,0} - q_{i,1}}{2} \frac{F_{i,0} - F_{i,1}}{\tilde{N}_0^2 \Delta\bar{z}_0} \right] \\
&\quad - \sum_i \Delta x_i \frac{f^2}{g} \frac{q_{i,0} + q_{i,1}}{2} \frac{F_{i,0} + F_{i,1}}{2} - \sum_{(i,k)\in(\text{slope/wall})} \frac{f}{c} \overline{q}_{(i,k)} \Delta z_k \overline{F}_{(i,k)} \\
&= -\sum_k \Delta z_k \left[(q_{i_\mathrm{s},k} - \overline{q}_{i_\mathrm{s}-1,k}) \frac{F_{i_\mathrm{s},k} - \overline{F}_{i_\mathrm{s}-1,k}}{\Delta\bar{x}_{i_\mathrm{s}-1,k}} + \sum_{i=i_\mathrm{s}+1}^{i=M_\mathrm{h}} (q_{i,k} - q_{i-1,k}) \frac{F_{i,k} - F_{i-1,k}}{\Delta\bar{x}_{i-1}} \right] \\
&\quad - \sum_i \Delta x_i \left[(\overline{q}_{i,0} - q_{i,1}) \frac{\overline{F}_{i,0} - F_{i,1}}{\tilde{N}_0^2 \Delta\bar{z}_0/2} + \sum_{k=2}^{k=k_\mathrm{s}} (q_{i,k-1} - q_{i,k}) \frac{F_{i,k-1} - F_{i,k}}{\tilde{N}^2_{k-1}\Delta\bar{z}_{k-1}} \right] \\
&\quad - \frac{f^2}{g} \sum_i \Delta x_i \overline{q}_{i,0} \overline{F}_{i,0} - \frac{f}{c} \sum_k \Delta z_k \overline{q}_k \overline{F}_k. \qquad \text{(S2.25)}
\end{aligned}
$$

In the final summation, "$\overline{F}_k$" is a shorthand for the boundary value on along the slope as there is only one slope-boundary point for each k. This is the discrete version of the bilinear form (S1.10a) for our finite-difference scheme. We can also rewrite the above expression as

$$A(\vec{q}, \vec{F}) - \frac{f}{c}\langle \vec{q}, \vec{F}\rangle_\mathrm{b} = 0,$$

which corresponds to (S1.10b). Both $A(,)$ and $\langle,\rangle_\mathrm{b}$ are symmetric.

Then, the same argument as for (S1.10a) proves the orthogonality that

$$\langle \vec{F}^{(l)}, \vec{F}^{(n)}\rangle_\mathrm{b} = \sum_k \Delta z_k \overline{F}_k^{(l)} \overline{F}_k^{(n)} = 0 \quad \text{if } c^{(l)} \neq c^{(n)} \qquad \text{(S2.26)}$$

and the reality of the eigenvalues. This "integral" takes the form of "vertical" (Stieltjes) integral of (S1.16), which is because $\mathrm{d}x\, h_x = \Delta x_i(\Delta z_k/\Delta x_i) = \Delta z_k$ for corner cells. Likewise, all eigenvalues are proven to be real.

Next, consider $A(\vec{r}, \vec{r})$ for an arbitrary nonzero vector $\vec{r} \neq 0$. Then all the terms are sums of squared real numbers, and therefore, $A(\vec{r}, \vec{r}) \leq 0$. Is it possible that $A(\vec{r}, \vec{r}) = 0$? For the first two terms of A to vanish, all the r values involved in (S2.25) must be the same: $\vec{r} = [b, b, \ldots, b] \neq 0$. But, the third term $(-(f^2/g)\sum_i \overline{r}_{0,i}^2)$ is negative because $\vec{r} \neq 0$. This proves that $A(,)$ is negative definite under the free-surface condition. Under the rigid-lid condition ($g \to \infty$), $A(\vec{r}, \vec{r}) = 0$ with this $\vec{r}$. The $A(,)$ is only negative semi-definite under the rigid-lid condition.

If we plug $r = F$, an eigenvector, into the equation $A(\vec{F}, \vec{F}) = (f/c)\langle \vec{F}, \vec{F} \rangle_{\rm b}$, we conclude that the rigid-lid condition allows for a solution such that $F =$ uniform $\neq 0$ with $c = \pm\infty$ (since $\langle \vec{F}, \vec{F} \rangle_{\rm b} > 0$). This is the barotropic mode under the rigid-lid condition.

Is it possible that $\langle \vec{F}, \vec{F} \rangle_{\rm b} = 0$? It is possible only when $\overline{F}_k = 0$ for all k along the slope. Is it possible that $A(\vec{F}, \vec{F}) = 0$ at the same time? That would demand that $F =$ uniform $\neq 0$, contradicting to $\langle \vec{F}, \vec{F} \rangle_{\rm b} = 0$. Therefore $\langle \vec{F}, \vec{F} \rangle_{\rm b} = 0$ requires that $A(\vec{F}, \vec{F}) < 0$. Therefore, $\langle \vec{F}^{(n)}, \vec{F}^{(n)} \rangle_{\rm b} = 0$ implies that $c = 0$. Our numerical solutions do include such unphysical solutions as explained in Section S2.4 below.

For physical modes, $\langle \vec{F}, \vec{F} \rangle_{\rm b} > 0$, and then $A(\vec{F}, \vec{F}) < 0$ proves that $f/c < 0$ except for the barotropic mode under the rigid-lid condition. In this way, all properties of the solutions in the continuous system (Section S1.2.3) hold for our finite-difference system.

S2.4 Matrix formalism

We have pictured the gridpoints as arranged in the 2-d x-z space (Fig. 1) and viewed gridded values of $F(x, z)$ as a 2-d array $[F_{i,k}]_{i,k}$. To cast the set of the finite-difference equations (Section S2.2) into matrix form, we line up all active grid-point values in a 1-d column vector $\vec{F}$. The order of the values is determined as follows.

We assign a serial number to the "active" gridpoints, e.g., gridpoints which appear in the finite differnce equations including the boundary points and those in the lobes (Section S2.2). We then denote the gridpoint number of gridpoint (i, k) by $\nu(i, k)$ and the value of F there by $F[\nu(i, k)]$, that is, $F[\nu(i, k)] \equiv F_{i,k}$. With this notation, $\vec{F} = [F[1], F[2], \ldots, F[M]]^T$, where M is the total number of all the active gridpoints.

There are also M equations, the set of which can be summarized as

$$A\vec{F} = \frac{f}{c} B\vec{F}; \tag{S2.27}$$

that is, equation λ takes the form of

$$\sum_{\nu=1}^{M} A[\lambda, \nu]F[\nu] = \frac{f}{c} \sum_{\nu=1}^{M} B[\lambda, \nu]F[\nu],$$

where λ is a serial number of the finite-difference equation, which is the row number of the matrix equation. In what follows, we determine the coefficients, $A[l, \nu]$'s and $B[l, \nu]$'s. Since the majority of the coefficients are zero, we define only the non-zero components.

To make A and B symmetric, two issues are critical: the ordering of the equations and the addition of boundary terms that are identically zero. For the ordering, the critical observation is that each equation includes just one "unique" gridpoint, which we call the "central" gridpoint of the equation. In the derivation below, we identify the central gridpoints.

To make the bilinear form (S2.25) symmetric, we added some boundary terms that are identically zero. We apply an equivalent treatment to the equations themselves. Even though the addition does not change the values of the left-hand sides of the equations (of course!), the coefficients on the individual gridded values (F's) change, which is critical to make A and B symmetric.

For each k along the slope, the boundary gridpoint is either a vertical-wall point or the center of a corner cell (circles on the slope in Fig. 1). Where the boundary is a vertical wall, the boundary value is $\overline{F}(i_\mathrm{s}[k]-1,k) = F(i_\mathrm{s}[k]-1,k)$ and where it is a corner cell, the boundary value is $F(i_\mathrm{s}[k],k)$. For convenience, we denote these boundary points by $(i_\mathrm{b}[k],k)$.

S2.4.1 Interior equations

First, we write down the interior equations (S2.22). Remember each of these equations is defined for a pair of (i,k), which is an "interior cell", that is, an ocean cells which is not a corner cell. That particular cell is the "center" of the equation, which also uses F values from neighboring cells.

We first line up the interior cells (i,k) and give them numbers $\nu = 1,\ldots,M_\mathrm{int}$, where the order of the cells is arbitrary; but once we have assigned the numbers to the interior cells, we re-order the interior equations in such a way that $\lambda = \nu(i,k)$; that is, *the equation number is set equal to the gridpoint number of the central cell* of the equation.

For each $k = 1,\ldots,M_\mathrm{v}$, interior cells are (i,k) for $i = i_\mathrm{b}[k]+1,\ldots,M_\mathrm{h}$. From the interior equations (S2.22), we find that

$$A[\nu(i,k),\nu(i,k)] = -\frac{\Delta z_k}{\Delta\bar{x}_i} - \frac{\Delta z_k}{\Delta\bar{x}_{i-1}} - \gamma_k\frac{\Delta x_i}{\tilde{N}^2_{k-1}\Delta\bar{z}_{k-1}} - \frac{\Delta x_i}{\tilde{N}^2_k\Delta\bar{z}_k} - \varsigma_k\frac{f^2}{g}\frac{\Delta x_i}{2} \tag{S2.28a}$$

$$A[\nu(i,k),\nu(i+1,k)] = \frac{\Delta z_k}{\Delta\bar{x}_i} \tag{S2.28b}$$

$$A[\nu(i,k),\nu(i-1,k)] = \frac{\Delta z_k}{\Delta\bar{x}_{i-1}} \tag{S2.28c}$$

$$A[\nu(i,k),\nu(i,k-1)] = \gamma_k\frac{\Delta x_i}{\tilde{N}^2_{k-1}\Delta\bar{z}_{k-1}} - \varsigma_k\frac{f^2}{g}\frac{\Delta x_i}{2} \tag{S2.28d}$$

$$A[\nu(i,k),\nu(i,k+1)] = \frac{\Delta x_i}{\tilde{N}^2_k\Delta\bar{z}_k}, \tag{S2.28e}$$

$$k = 1,\ldots,M_\mathrm{v}; i = i_\mathrm{b}[k]+1,\ldots,M_\mathrm{h}.$$

Note that the first index into A is always $\lambda = \nu(i,k)$, referring to the equation number *and* central gridpoint whereas the second indices include off-center gridpoints and even non-interior gridpoints when the center is next to a boundary.

S2.4.2 Sea surface

Next we line up the M_h surface boundary conditions $\lambda = M_\mathrm{int}+1,\ldots,M_\mathrm{int}+M_\mathrm{h}$. Each of these M_h equations introduces a new grid cell, $(i,0)$, in the upper lobe, which is the "central" cell of the equation. Accordingly, we give them the same cell numbers as the equation numbers:

$$\begin{aligned}
\lambda &= M_\mathrm{int}+1 &&= \nu(1,0)\\
\lambda &= M_\mathrm{int}+2 &&= \nu(2,0)\\
&\cdots\\
\lambda &= M_\mathrm{int}+M_\mathrm{h} &&= \nu(M_\mathrm{h},0)
\end{aligned}$$

We multiply each surface boundary condition (S2.11a) by $-\frac{1}{2}\Delta x_i$ and then the coefficients are

$$A[\nu(i,0),\nu(i,0)] = -\gamma_1 \frac{\Delta x_i}{\tilde{N}_0^2 \Delta \bar{z}_0} - \varsigma_1 \frac{f^2}{g}\frac{\Delta x_i}{2}, \tag{S2.29a}$$

$$A[\nu(i,0),\nu(i,1)] = \gamma_1 \frac{\Delta x_i}{\tilde{N}_0^2 \Delta \bar{z}_0} - \varsigma_1 \frac{f^2}{g}\frac{\Delta x_i}{2} \tag{S2.29b}$$

because $\gamma_1 = \varsigma_1 = \frac{1}{2}$. The reason for the factor $-\frac{1}{2}\Delta x_i$ will become clear when we consider the symmetry of matrix A.

S2.4.3 Right-edge boundary condition

Likewise, we line up the $x = L_\mathrm{x}$ boundary conditions; they introduce M_v new grid cells $(M_\mathrm{h}+1, k)$ for $k = 1, \ldots, M_\mathrm{v}$, which we give the same cell numbers as the equation numbers, as

$$\begin{aligned}
\lambda &= M_\mathrm{int} + M_\mathrm{h} + 1 &&= \nu(M_\mathrm{h}+1, 1)\\
\lambda &= M_\mathrm{int} + M_\mathrm{h} + 2 &&= \nu(M_\mathrm{h}+1, 2)\\
&\ldots\\
\lambda &= M_\mathrm{int} + M_\mathrm{h} + M_\mathrm{v} &&= \nu(M_\mathrm{h}+1, M_\mathrm{v}).
\end{aligned}$$

We multiply each of these boundary conditions (S2.12) by $-\Delta z_k$ and then their coefficients are

$$A[\nu(M_\mathrm{h}+1,k),\nu(M_\mathrm{h}+1,k)] = -\frac{\Delta z_k}{\Delta \bar{x}_{M_\mathrm{h}}}, \tag{S2.30a}$$

$$A[\nu(M_\mathrm{h}+1,k),\nu(M_\mathrm{h},k)] = \frac{\Delta z_k}{\Delta \bar{x}_{M_\mathrm{h}}}. \tag{S2.30b}$$

S2.4.4 Flat bottom

Along the slope, there can be flat-bottom regions (Fig. 1). We handle these potential flat-bottom regions and the flat bottom at $z = -D$ after the slope together. Let M_flat be the number of the bottom-boundary grid points in these flat-bottom regions. Since one corner cell takes up one horizontal grid spacing, the number of flat-bottom gridpoints decreases from M_h by the number of corner cells, M_corner. That is, $M_\mathrm{flat} + M_\mathrm{corner} = M_\mathrm{h}$. We denote the i indices of these flat-bottom gridpoints as $i(1), i(2), \ldots, i(M_\mathrm{flat})$. Physically, these bottom-boundary grid points are located right at the bottom, but in the code, we store these values in the cells below the bottom, $(i, k_\mathrm{s}[i]+1)$.

We then give these cells the same cell numbers as the equation numbers:

$$\begin{aligned}
\lambda &= M_\mathrm{int} + M_\mathrm{h} + M_\mathrm{v} + 1 &&= \nu(i(1), M_\mathrm{v}+1)\\
\lambda &= M_\mathrm{int} + M_\mathrm{h} + M_\mathrm{v} + 2 &&= \nu(i(2), M_\mathrm{v}+1)\\
&\ldots\\
\lambda &= M_\mathrm{int} + M_\mathrm{h} + M_\mathrm{v} + M_\mathrm{flat} &&= \nu(i(M_\mathrm{flat}), M_\mathrm{v}+1).
\end{aligned}$$

We multiply each of the bottom boundary conditions by $-\Delta x_i/\tilde{N}^2_{k_\mathrm{s}[i]}$ and then the coefficients of the boundary conditions are

$$A[\nu(i,k_\mathrm{s}[i]+1),\nu(i,k_\mathrm{s}[i]+1)] = -\frac{\Delta x_i}{\tilde{N}^2_{k_\mathrm{s}[i]}\Delta\bar{z}_{k_\mathrm{s}[i]}}, \tag{S2.31a}$$

$$A[\nu(i,k_\mathrm{s}[i]+1),\nu(i,k_\mathrm{s}[i])] = \frac{\Delta x_i}{\tilde{N}^2_{k_\mathrm{s}[i]}\Delta\bar{z}_{k_\mathrm{s}[i]}} \tag{S2.31b}$$

for $i = i(1), i(2), \ldots, i(M_\mathrm{flat})$.

S2.4.5 Vertical-wall grid points and corner cells

So far, only A has given nonzero components, since the remaining M_v equations are the only ones that include f/c and therefore give nonzero values to B. They are the vertical-wall boundary conditions (S2.19) and the corner-cell boundary conditions (S2.18). Since each $k = 1, \ldots, M_\mathrm{v}$ has exactly one of these conditions, we just order the equations from $k = 1$ to $k = M_\mathrm{v}$:

$$\begin{aligned}\lambda &= M_\mathrm{int} + M_\mathrm{h} + M_\mathrm{v} + M_\mathrm{flat} + 1 \quad &&= \nu(i_\mathrm{b}[1], 1)\\ &\ldots\\ \lambda &= M_\mathrm{int} + M_\mathrm{h} + M_\mathrm{v} + M_\mathrm{flat} + M_\mathrm{v} &&= \nu(i_\mathrm{b}[M_\mathrm{v}], M_\mathrm{v}).\end{aligned}$$

and use either the vertical-wall boundary condition (S2.19) or the corner-cell boundary condition (S2.18).

We multiply each of the vertical-wall boundary conditions by Δz_k and then the coefficients are

$$A[\nu(i_\mathrm{b}[k],k),\nu(i_\mathrm{b}[k],k)] = -\frac{\Delta z_k}{\Delta x_{i_\mathrm{s}[k]}/2}, \tag{S2.32a}$$

$$A[\nu(i_\mathrm{b}[k],k),\nu(i_\mathrm{b}[k]+1,k)] = \frac{\Delta z_k}{\Delta x_{i_\mathrm{s}[k]}/2}, \tag{S2.32b}$$

$$B[\nu(i_\mathrm{b}[k],k),\nu(i_\mathrm{b}[k],k)]. = \Delta z_k. \tag{S2.32c}$$

Recall that $i_\mathrm{b}[k] = i_\mathrm{s}[k] - 1$ for these points. We multiply the corner-cell boundary conditions (S2.18) by Δz_k and the coefficients are

$$A[\nu(i_\mathrm{b}[k],k),\nu(i_\mathrm{b}[k],k)] = -\frac{\Delta z_k}{\Delta\bar{x}_i} - \gamma_k\frac{\Delta x_i}{\tilde{N}^2_{k-1}\Delta\bar{z}_{k-1}} - \varsigma_k\frac{f^2}{g}\frac{\Delta x_i}{2}, \tag{S2.33a}$$

$$A[\nu(i_\mathrm{b}[k],k),\nu(i_\mathrm{b}[k]+1,k)] = \frac{\Delta z_k}{\Delta\bar{x}_i}, \tag{S2.33b}$$

$$A[\nu(i_\mathrm{b}[k],k),\nu(i_\mathrm{b}[k],k-1)] = \gamma_k\frac{\Delta x_i}{\tilde{N}^2_{k-1}\Delta\bar{z}_{k-1}} - \varsigma_k\frac{f^2}{g}\frac{\Delta x_i}{2}, \tag{S2.33c}$$

$$B[\nu(i_\mathrm{b}[k],k),\nu(i_\mathrm{b}[k],k)] = \Delta z_k, \tag{S2.33d}$$

where we have used $i = i_\mathrm{b}[k] = i_\mathrm{s}[k]$ as a short hand. Either (S2.32) or (S2.33) applies to each k. Note that the only nonzero components of B are the M_v diagonal components $B(\nu_k, \nu_k) = \Delta z_k$, where $\nu_k \equiv \nu(i_\mathrm{b}[k], k)$.

S2.4.6 Symmetry

Symmetry in i. Replacing $i \to i-1$ in (S2.28b) gives

$$A[\nu(i-1,k), \nu(i,k)] = \frac{\Delta z_k}{\Delta \bar{x}_{i-1}}, \quad i = i_\mathrm{b}[k]+2, \ldots, M_\mathrm{h}+1.$$

Comparing this with (S2.28c), we see that

$$A[\nu(i-1,k), \nu(i,k)] = A[\nu(i,k), \nu(i-1,k)], \quad i = i_\mathrm{b}[k]+2, \ldots, M_\mathrm{h}. \tag{S2.34}$$

Next, setting $i = i_\mathrm{b}[k]+1$ in (S2.28c) gives

$$A[\nu(i_\mathrm{b}[k]+1,k), \nu(i_\mathrm{b}[k],k)] = \frac{\Delta z_k}{\Delta \bar{x}_{i_\mathrm{b}[k]}}.$$

If the gridpoint $(i_\mathrm{b}[k], k)$ is a corner-cell point, $i_\mathrm{b}[k] = i_\mathrm{s}[k]$ and therefore comparison with (S2.33b) indicates that

$$A[\nu(i_\mathrm{b}[k]+1,k), \nu(i_\mathrm{b}[k],k)] = A[\nu(i_\mathrm{b}[k],k), \nu(i_\mathrm{b}[k]+1,k)]. \tag{S2.35}$$

If the gridpoint $(i_\mathrm{b}[k], k)$ is a vertical-wall point, $i_\mathrm{b}[k] = i_\mathrm{s}[k]-1$ and $\Delta \bar{x}_{i_\mathrm{b}[k]} = \Delta x_{i_\mathrm{s}[k]}/2$ and therefore comparison with (S2.32b) indicates (S2.35) again. Equation (S2.35) is an extension of (S2.34) to $i = i_\mathrm{b}[k]+1$.

Setting $i = M_\mathrm{h}$ in (S2.28b) and comparing the result with (S2.30b) gives

$$A[\nu(M_\mathrm{h}+1,k), \nu(M_\mathrm{h},k)] = A[\nu(M_\mathrm{h},k), \nu(M_\mathrm{h}+1,k)].$$

This is an extension of (S2.34) to $i = M_\mathrm{h}+1$. To summarize, then,

$$A[\nu(i-1,k), \nu(i,k)] = A[\nu(i,k), \nu(i-1,k)], \quad i = i_\mathrm{b}[k]+1, \ldots, M_\mathrm{h}+1 \tag{S2.36}$$

for $k = 1, \ldots, M_\mathrm{v}$. The gridpoints involved, $(i-1,k)$ and (i,k), cover all the gridpoints in the $1 \le k \le M_\mathrm{v}$ range.

Symmetry in k. For each i, we define $k = k_\mathrm{b}[i]$ to be k of the bottom-boundary point; at a flat-bottom point, $k_\mathrm{b}[i] = k_\mathrm{s}[i]+1$, and at a corner cell, $k_\mathrm{b}[i] = k_\mathrm{s}[i]$. The interior equations (S2.28) hold only for $k = 1, \ldots, k_\mathrm{b}[i]-1$ for each i.

When $k_\mathrm{b}[i] > 1$, replacing $k \to k+1$ in (S2.28d) gives

$$A[\nu(i,1), \nu(i,0)] = \frac{1}{2}\frac{\Delta x_i}{\tilde{N}_0^2 \Delta \bar{z}_0} - \frac{1}{2}\frac{f^2}{g}\frac{\Delta x_i}{2} \tag{S2.37a}$$

$$A[\nu(i,k+1), \nu(i,k)] = \frac{\Delta x_i}{\tilde{N}_k^2 \Delta \bar{z}_k} \tag{S2.37b}$$

for $k = 1, \ldots, k_\mathrm{b}[i]-2$ for each of $i = 1, \ldots, M_\mathrm{h}$ such that $k_\mathrm{b}[i] > 1$. For positions i where the deepest grid point is on a flat bottom, the bottom boundary condition (S2.31b) extends (S2.37) to $k = k_\mathrm{s}[i] = k_\mathrm{b}[i]-1$. For positions i where the deepest grid point is

in a corner cell, the corner boundary equation (S2.33c) implies

$$A[\nu(i,k_\mathrm{b}[i]),\nu(i,k_\mathrm{b}[i]-1)] = \frac{\Delta x_i}{\tilde{N}^2_{k_\mathrm{b}[i]-1}\Delta\bar{z}_{k_\mathrm{b}[i]-1}}$$

because $k = k_\mathrm{b}[i] > 1$ for the corner cell. The expression also extends (S2.37) to $k = k_\mathrm{s}[i] = k_\mathrm{b}[i] - 1$.

When $k_\mathrm{b}[i] = 1$ for some i, the interior equations (S2.28d) cannot be used; and the entire water column is a single corner cell and the corner boundary equation (S2.33c) implies

$$A[\nu(i,1),\nu(i,0)] = \frac{1}{2}\frac{\Delta x_i}{\tilde{N}^2_0\Delta\bar{z}_0} - \frac{1}{2}\frac{f^2}{g}\frac{\Delta x_i}{2}$$

because $k_\mathrm{b}[i] = k_\mathrm{s}[i] = 1$ for such corner cells. Therefore, (S2.37) holds whether $k_\mathrm{b}[i] > 1$ or $k_\mathrm{b}[i] = 1$.

Comparison of (S2.37) with (S2.29b) and (S2.28e) indicates that

$$A[\nu(i,k+1),\nu(i,k)] = A[\nu(i,k),\nu(i,k+1)], \quad k = 0,\ldots,k_\mathrm{b}[i]-1 \tag{S2.38}$$

for each $i = 1,\ldots,M_\mathrm{h}$. These grid points, $(i,k+1)$ and (i,k), cover all gridpoints in the range $i = 1,\ldots,M_\mathrm{h}$.

Finally, eqs. (S2.36) and (S2.38) include all off-diagonal components of matrix A, proving that A is symmetric. Matrix B is obviously symmetric as only its last M_v rows include non-zero values (Δz_k) only on its diagonal.

S2.4.7 Properties of the solutions

Except for the negative definiteness of A, all properties we derived for the eigenvalue problem can be more easily derived in the matrix formalism; not only that, but also one more important property is derived from it. The matrix formalism is also necessary to utilize existing eigenvalue-problem solvers.

First, we consider this bilinear form:

$$\vec{q}^T A\vec{r} = (\vec{q}^T A\vec{r})^T = \vec{r}^T A^T\vec{q} = \vec{r}^T A\vec{q}.$$

That is, the bilinear form is symmetric because A is symmetric. The binary form associated with B is also symmetric. Following the same argument as in Section S2.3, we arrive at the orthogonality condition

$$\left(\frac{1}{c^{(l)}} - \frac{1}{c^{(n)}}\right)(\vec{F}^{(l)})^T B\vec{F}^{(n)} = 0;$$

that is, the eigenvectors are "B-orthogonal". This result is exactly the same as (S2.26), because, from the definition of B as shown in eqs. (S2.32c) and (S2.33d),

$$(\vec{F}^{(l)})^T B\vec{F}^{(n)} = \sum_k \Delta z_k \overline{F}^{(l)}_k \overline{F}^{(n)},$$

where $\overline{F}_k = F(i_\mathrm{b}[k],k)$ by definition. Using the above bilinear form, it is also straightforward to prove that c's are real.

As stated above, B is diagonal and only its last M_v diagonals are nonzero. Therefore, there are $M - M_\mathrm{v}$ linearly independent vectors that satisfy $B\vec{F} = 0$. Such a vector must satisfy

$$\Delta z_k \overline{F}_k = 0$$

for each $k = 1, \ldots, M_\mathrm{v}$. Since $\Delta z_k > 0$ for all k, it is concluded that $\overline{F}_k = 0$ for all k for such a vector. Conversely, if $\overline{F}_k = 0$ for all k, $B\vec{F} = 0$ regardless of the other components of $\vec{F}$.

Any vector such that $B\vec{F} = 0$ is a solution to the eigenvalue problem

$$B\vec{F} = \frac{c}{f} A\vec{F} \tag{S2.39}$$

with $c = 0$, regardless of the values of $A\vec{F}$.

Is it possible that $A\vec{F} = B\vec{F} = 0$ for $\vec{F} \neq 0$? Using the same argument as before, only under the rigid-lid approximation is $A\vec{F} = 0$ possible but that would result in $B\vec{F} \neq 0$ because $\vec{F} =$ uniform $\neq 0$ in that case. Therefore, it is impossible that $A\vec{F} = B\vec{F} = 0$ as long as $\vec{F} \neq 0$. For this reason, $B\vec{F} = 0$ implies $c = 0$ and vice versa.

To conclude, there are $M - M_\mathrm{v}$ linearly independent eigenvectors all with $c = 0$ and $\overline{F}_k = 0$, and conversely, any vector with $\overline{F}_k = 0$ is an eigenvector with $c = 0$. These are clearly *unphysical* solutions. For the other solutions, $B\vec{F} \neq 0$.

S2.4.8 Consequences from the negative definiteness of A

Further, the next section (Section S2.5) actually calculates $\vec{q}^T A\vec{r}$ and shows that $\vec{r}^T A\vec{r} \leq 0$ and that only under the rigid-lid condition is it possible that $\vec{r}^T A\vec{r} = 0$. The same argument as in Section S2.3 therefore proves that $f/c < 0$ under the free-surface condition.

An equivalent eigenvalue problem $(-B)\vec{F} = (c/f)(-A)\vec{F}$ can then be transformed into the form $B'\vec{F}' = (c/f)\vec{F}'$ with a symmetric B'.

Proof: Since $(-A)$ is positive definite and symmetric, all its eigenvalues are positive and its eigenvectors are orthogonal, allowing for the diagonalization:

$$P^T(-A)P = \mathrm{diag}(a_1^2, \ldots, a_M^2),$$

where $a_j^2 > 0$ are the eigenvalues and P is an orthonormal matrix ($P^T P = I$) constructed from the eigenvectors. Further,

$$Q^T(-A)Q = \mathrm{diag}(1, \ldots, 1) = I,$$

where $Q \equiv P\,\mathrm{diag}(a_1^{-1}, \ldots, a_M^{-1})$. Note that $Q^{-1} = \mathrm{diag}(a_1, \ldots, a_M)P^T$. Then, the eigenvalue problem can be transformed into

$$Q^T(-B)QQ^{-1}\vec{F} = Q^T(c/f)(-A)QQ^{-1}\vec{F}$$

$\Rightarrow$

$$B'\vec{F}' = (c/f)\vec{F}',$$

where $B' \equiv Q^T(-B)Q$, $A' \equiv Q^T(-A)Q$, and $\vec{F}' \equiv Q^{-1}\vec{F}$. The matrix B' is obviously symmetric. Since B' is symmetric, there are M independent eigenvectors, which can be

transformed back with $\vec{F} = Q\vec{F}'$. Since Q is invertible, the set of the M independent eigenvectors are transformed to a set of M linearly independent vectors, which are the eigenvectors of the original problem. □

This argument proves that there are exactly M_v *physical* solutions with $c \neq 0$. In practice, this property makes it straightforward to filter out the unphysical modes. Under the rigid-lid condition, we do not know whether there should always be exactly M_v physical solutions. (In the above proof we used the property that A is negative definite.) We suspect that there is a proof even when A is negative semi-definite (when there is a vector $\vec{r} \neq 0$ such that $\vec{r}^T A\vec{r} = 0$). Our experience with our numerical solutions is that there are exactly M_v physical solutions even under the rigid-lid condition.

Finally, there are two subroutines in LAPACK to solve the type of generalized eigenvalue problem we are dealing with (Section 4). One is the most general one, which are able to solve non-symmetric eigenvalue problems with complex eigenvalues. The other works only when A and B are symmetric and one of them is positive definite. Even though both are symmetric for our case, B is hardly definite as there are vectors such that $B\vec{F} = 0$. Also, $A\vec{F}^{(0)} = 0$ for the barotropic mode under the rigid-lid approximation. On the other hand A is negative definite under the free-surface boundary condition.

For this reason, we use the free-surface boundary condition by default and transform the eigenvalue problem into the form

$$(-B)\vec{F} = \frac{c}{f}(-A)\vec{F}. \tag{S2.40}$$

The LAPACK routine fails with an error message if some of the prerequisites on $-B$ or $-A$ are not satisfied.

If, for any reason, we need to use the rigid-lid boundary condition, we use the general eigenvalue-problem solver. The only practical difference is that the general solver is much slower, uses more memory, and returns complex eigenvalues, because of which we have to check whether the imaginary parts are really zero as they should.

S2.5 Bilinear form using the matrices

We calculate

$$\vec{q}^T A\vec{r} = \sum_\lambda q[\lambda] \sum_\nu A[\lambda, \nu] r[\nu]$$

without assuming that either q or r is a solution to the eigenvalue problem. We use the definition $r[\nu(i,k)] = r_{i,k}$.

First, we calculate the "interior" section (Section S2.4.1) of the summation $\sum_\lambda$:

$$
\begin{aligned}
&\sum_{\lambda=1}^{M_{\mathrm{int}}} q[\lambda] \sum_{\nu} A[\lambda,\nu] r[\nu] \\
&= \sum_{(i,k)\in\Omega} q_{i,k} \Bigg[\Bigg(-\frac{\Delta z_k}{\Delta \bar{x}_i} - \frac{\Delta z_k}{\Delta \bar{x}_{i-1}} - \gamma_k \frac{\Delta x_i}{\tilde{N}_{k-1}^2 \Delta \bar{z}_{k-1}} - \varsigma_k \frac{f^2}{g} \frac{\Delta x_i}{2} - \frac{\Delta x_i}{\tilde{N}_k^2 \Delta \bar{z}_k} \Bigg) r_{i,k} \\
&\qquad\qquad + \frac{\Delta z_k}{\Delta \bar{x}_i} r_{i+1,k} + \frac{\Delta z_k}{\Delta \bar{x}_{i-1}} r_{i-1,k} \\
&\qquad\qquad + \Bigg(\gamma_k \frac{\Delta x_i}{\tilde{N}_{k-1}^2 \Delta \bar{z}_{k-1}} - \varsigma_k \frac{f^2}{g} \frac{\Delta x_i}{2} \Bigg) r_{i,k-1} + \frac{\Delta x_i}{\tilde{N}_k^2 \Delta \bar{z}_k} r_{i,k+1} \Bigg] \\
&= \sum_{(i,k)\in\Omega} q_{i,k} \Bigg[\Delta z_k \Bigg(\frac{r_{i+1,k} - r_{i,k}}{\Delta \bar{x}_i} - \frac{r_{i,k} - r_{i-1,k}}{\Delta \bar{x}_{i-1}} \Bigg) \\
&\qquad\qquad + \Delta x_i \Bigg(\gamma_k \frac{r_{i,k-1} - r_{i,k}}{\tilde{N}_{k-1}^2 \Delta \bar{z}_{k-1}} - \varsigma_k \frac{f^2}{g} \frac{r_{i,k-1} + r_{i,k}}{2} - \frac{r_{i,k} - r_{i,k+1}}{\tilde{N}_k^2 \Delta \bar{z}_k} \Bigg) \Bigg]
\end{aligned}
\tag{S2.41}
$$

Next, the sea-surface section (Section S2.4.2) is

$$
\begin{aligned}
&\sum_{\lambda=M_{\mathrm{int}}+1}^{M_{\mathrm{int}}+M_{\mathrm{h}}} q[\lambda] \sum_{\nu} A[\lambda,\nu] r[\nu] \\
&= \sum_{i=1}^{M_{\mathrm{h}}} q_{i,0} \Bigg[\Bigg(-\gamma_1 \frac{\Delta x_i}{\tilde{N}_0^2 \Delta \bar{z}_0} - \varsigma_1 \frac{f^2}{g} \frac{\Delta x_i}{2} \Bigg) r_{i,0} + \Bigg(\gamma_1 \frac{\Delta x_i}{\tilde{N}_0^2 \Delta \bar{z}_0} - \varsigma_1 \frac{f^2}{g} \frac{\Delta x_i}{2} \Bigg) r_{i,1} \Bigg] \\
&= \sum_{i=1}^{M_{\mathrm{h}}} q_{i,0} \Delta x_i \Bigg(-\gamma_1 \frac{r_{i,0} - r_{i,1}}{\tilde{N}_0^2 \Delta \bar{z}_0} - \varsigma_1 \frac{f^2}{g} \frac{r_{i,0} + r_{i,1}}{2} \Bigg)
\end{aligned}
\tag{S2.42}
$$

Recall, in what follows, that $i_{\mathrm{b}}[k] = i_{\mathrm{s}}[k] - 1$ when $(i_{\mathrm{s}}[k], k)$ is next to a vertical wall whereas $i_{\mathrm{b}}[k] = i_{\mathrm{s}}[k]$ when $(i_{\mathrm{s}}[k], k)$ is a corner point. With this notation, $i = i_{\mathrm{b}}[k] + 1, \ldots, M_{\mathrm{h}}$ denote the interior. In particular, $i_{\mathrm{b}}[1] = 0$ if $(1,1)$ is a vertical wall boundary point and the boundary value is stored in the $(0,1)$ cell. Likewise, $k_{\mathrm{b}}[i] = k_{\mathrm{s}}[i] + 1$ when $(i, k_{\mathrm{s}}[i])$ is above a flat bottom or a flat part of the slope and $k_{\mathrm{b}}[i] = k_{\mathrm{s}}[i]$ when $(i, k_{\mathrm{s}}[i])$ is a corner point.

Combining the partial sums (S2.41) and (S2.42) gives

$$
\begin{aligned}
&\sum_{\lambda=1}^{M_{\mathrm{int}}+M_{\mathrm{h}}} q[\lambda] \sum_{\nu} A[\lambda,\nu] r[\nu] \\
&= \sum_{(i,k)\in\Omega} q_{i,k}\Delta z_k \left(\frac{r_{i+1,k}-r_{i,k}}{\Delta\bar{x}_i} - \frac{r_{i,k}-r_{i-1,k}}{\Delta\bar{x}_{i-1}} \right) \\
&\quad + \sum_{i=i_{\mathrm{b}}[1]+1}^{M_{\mathrm{h}}} \sum_{k=2}^{k_{\mathrm{b}}[i]-1} q_{i,k}\Delta x_i \left(\frac{r_{i,k-1}-r_{i,k}}{\tilde{N}_{k-1}^2\Delta\bar{z}_{k-1}} - \frac{r_{i,k}-r_{i,k+1}}{\tilde{N}_k^2\Delta\bar{z}_k} \right) \\
&\quad + \sum_{i=i_{\mathrm{b}}[1]+1}^{M_{\mathrm{h}}} q_{i,1}\Delta x_i \left(\gamma_1 \frac{r_{i,0}-r_{i,1}}{\tilde{N}_0^2\Delta\bar{z}_0} - \varsigma_1 \frac{f^2}{g}\frac{r_{i,0}+r_{i,1}}{2} - \frac{r_{i,1}-r_{i,2}}{\tilde{N}_1^2\Delta\bar{z}_1} \right) \\
&\quad + \sum_{i=1}^{M_{\mathrm{h}}} q_{i,0}\Delta x_i \left(-\gamma_1 \frac{r_{i,0}-r_{i,1}}{\tilde{N}_0^2\Delta\bar{z}_0} - \varsigma_1 \frac{f^2}{g}\frac{r_{i,0}+r_{i,1}}{2} \right) \\
&= \sum_{k} \sum_{i=i_{\mathrm{b}}[k]+1}^{M_{\mathrm{h}}} q_{i,k}\Delta z_k \frac{r_{i+1,k}-r_{i,k}}{\Delta\bar{x}_i} - \sum_{k} \sum_{i=i_{\mathrm{b}}[k]}^{M_{\mathrm{h}}-1} q_{i+1,k}\Delta z_k \frac{r_{i+1,k}-r_{i,k}}{\Delta\bar{x}_i} \\
&\quad + \sum_{i=i_{\mathrm{b}}[1]+1}^{M_{\mathrm{h}}} \sum_{k=1}^{k_{\mathrm{b}}[i]-2} q_{i,k+1}\Delta x_i \frac{r_{i,k}-r_{i,k+1}}{\tilde{N}_k^2\Delta\bar{z}_k} - \sum_{i=i_{\mathrm{b}}[1]+1}^{M_{\mathrm{h}}} \sum_{k=2}^{k_{\mathrm{b}}[i]-1} q_{i,k}\Delta x_i \frac{r_{i,k}-r_{i,k+1}}{\tilde{N}_k^2\Delta\bar{z}_k} \\
&\quad - \sum_{i=i_{\mathrm{b}}[1]+1}^{M_{\mathrm{h}}} q_{i,1}\Delta x_i \frac{r_{i,1}-r_{i,2}}{\tilde{N}_1^2\Delta\bar{z}_1} \\
&\quad + \sum_{i=i_{\mathrm{b}}[1]+1}^{M_{\mathrm{h}}} q_{i,1}\Delta x_i \left(-\gamma_1(q_{i,0}-q_{i,1}) \frac{r_{i,0}-r_{i,1}}{\tilde{N}_0^2\Delta\bar{z}_0} - \varsigma_1(q_{i,0}+q_{i,1}) \frac{f^2}{g}\frac{r_{i,0}+r_{i,1}}{2} \right) \\
&\quad + \varpi(i_{\mathrm{b}}[1]>0)\Delta x_1 q_{1,0} \left(-\gamma_1 \frac{r_{1,0}-r_{1,1}}{\tilde{N}_0^2\Delta\bar{z}_0} - \varsigma_1 \frac{f^2}{g}\frac{r_{1,0}+r_{1,1}}{2} \right)
\end{aligned}
\tag{S2.43}
$$

For the first two lines, we are in the process of applying the "integration-by-parts" trick. For the second line, we have written $i = i_{\mathrm{b}}[1]+1$ as the lower bound of the summation to exclude the potential corner cell at $i = 1$. The last line is a potential leftover which exists if the $(1,1)$ is a corner point because in that case, $(1,1)$ is not included in the summation starting from $i = i_{\mathrm{b}}[1]+1$; ϖ is an ad-hoc notation such that

$$
\varpi(i_{\mathrm{b}}[1]>0) = \begin{cases} 0 & \text{if } i_{\mathrm{b}}[1]=0, \\ 1 & \text{if } i_{\mathrm{b}}[1]>0 \end{cases}
$$

to include or exclude the term from the potential corner cell.

To continue the calculation,

$$
\begin{aligned}
&\sum_{\lambda=1}^{M_{\mathrm{int}}+M_{\mathrm{h}}} q[\lambda] \sum_{\nu} A[\lambda,\nu] r[\nu] \\
&= -\sum_{k} \sum_{i=i_{\mathrm{b}}[k]+1}^{M_{\mathrm{h}}-1} (q_{i+1,k} - q_{i,k}) \Delta z_k \frac{r_{i+1,k} - r_{i,k}}{\Delta \bar{x}_i} \\
&\quad + \sum_{k} q_{M_{\mathrm{h}},k}\, \Delta z_k \frac{r_{M_{\mathrm{h}}+1,k} - r_{M_{\mathrm{h}},k}}{\Delta \bar{x}_{M_{\mathrm{h}}}} - \sum_{k} q_{i_{\mathrm{b}}[k]+1,k} \Delta z_k \frac{r_{i_{\mathrm{b}}[k]+1,k} - r_{i_{\mathrm{b}}[k],k}}{\Delta \bar{x}_{i_{\mathrm{b}}[k]}} \\
&\quad - \sum_{i=i_{\mathrm{b}}[1]+1}^{M_{\mathrm{h}}} \sum_{k=2}^{k_{\mathrm{b}}[i]-2} (q_{i,k} - q_{i,k+1}) \Delta x_i \frac{r_{i,k} - r_{i,k+1}}{\tilde{N}_k^2 \Delta \bar{z}_k} \\
&\quad + \sum_{i=i_{\mathrm{b}}[1]+1}^{M_{\mathrm{h}}} q_{i,2} \Delta x_i \frac{r_{i,1} - r_{i,2}}{\tilde{N}_1^2 \Delta \bar{z}_1} - \sum_{i=i_{\mathrm{b}}[1]+1}^{M_{\mathrm{h}}} q_{i,k_{\mathrm{b}}[i]-1} \Delta x_i \frac{r_{i,k_{\mathrm{b}}[i]-1} - r_{i,k_{\mathrm{b}}[i]}}{\tilde{N}_{k_{\mathrm{b}}[i]-1}^2 \Delta \bar{z}_{k_{\mathrm{b}}[i]-1}} \\
&\quad - \sum_{i=i_{\mathrm{b}}[1]+1}^{M_{\mathrm{h}}} q_{i,1} \Delta x_i \frac{r_{i,1} - r_{i,2}}{\tilde{N}_1^2 \Delta \bar{z}_1} \\
&\quad + \sum_{i=i_{\mathrm{b}}[1]+1}^{M_{\mathrm{h}}} q_{i,1} \Delta x_i \left(-\gamma_1 (q_{i,0} - q_{i,1}) \frac{r_{i,0} - r_{i,1}}{\tilde{N}_0^2 \Delta \bar{z}_0} - \varsigma_1 (q_{i,0} + q_{i,1}) \frac{f^2}{g} \frac{r_{i,0} + r_{i,1}}{2} \right) \\
&\quad + \varpi(i_{\mathrm{b}}[1] > 0) \Delta x_1 q_{1,0} \left(-\gamma_1 \frac{r_{1,0} - r_{1,1}}{\tilde{N}_0^2 \Delta \bar{z}_0} - \varsigma_1 \frac{f^2}{g} \frac{r_{1,0} + r_{1,1}}{2} \right) \\
&= -\sum_{k} \sum_{i=i_{\mathrm{b}}[k]+1}^{M_{\mathrm{h}}-1} (q_{i+1,k} - q_{i,k}) \Delta z_k \frac{r_{i+1,k} - r_{i,k}}{\Delta \bar{x}_i} \\
&\quad + \sum_{k} q_{M_{\mathrm{h}},k}\, \Delta z_k \frac{r_{M_{\mathrm{h}}+1,k} - r_{M_{\mathrm{h}},k}}{\Delta \bar{x}_{M_{\mathrm{h}}}} - \sum_{k} q_{i_{\mathrm{b}}[k]+1,k} \Delta z_k \frac{r_{i_{\mathrm{b}}[k]+1,k} - r_{i_{\mathrm{b}}[k],k}}{\Delta \bar{x}_{i_{\mathrm{b}}[k]}} \\
&\quad - \sum_{i=i_{\mathrm{b}}[1]+1}^{M_{\mathrm{h}}} \sum_{k=1}^{k_{\mathrm{b}}[i]-2} (q_{i,k} - q_{i,k+1}) \Delta x_i \frac{r_{i,k} - r_{i,k+1}}{\tilde{N}_k^2 \Delta \bar{z}_k} \\
&\quad - \sum_{i=i_{\mathrm{b}}[1]+1}^{M_{\mathrm{h}}} q_{i,k_{\mathrm{b}}[i]-1} \Delta x_i \frac{r_{i,k_{\mathrm{b}}[i]-1} - r_{i,k_{\mathrm{b}}[i]}}{\tilde{N}_{k_{\mathrm{b}}[i]-1}^2 \Delta \bar{z}_{k_{\mathrm{b}}[i]-1}} \\
&\quad + \sum_{i=i_{\mathrm{b}}[1]+1}^{M_{\mathrm{h}}} q_{i,1} \Delta x_i \left(-\gamma_1 (q_{i,0} - q_{i,1}) \frac{r_{i,0} - r_{i,1}}{\tilde{N}_0^2 \Delta \bar{z}_0} - \varsigma_1 (q_{i,0} + q_{i,1}) \frac{f^2}{g} \frac{r_{i,0} + r_{i,1}}{2} \right) \\
&\quad + \varpi(i_{\mathrm{b}}[1] > 0) \Delta x_1 q_{1,0} \left(-\gamma_1 \frac{r_{1,0} - r_{1,1}}{\tilde{N}_0^2 \Delta \bar{z}_0} - \varsigma_1 \frac{f^2}{g} \frac{r_{1,0} + r_{1,1}}{2} \right).
\end{aligned}
\tag{S2.44}
$$

The section of the summation from the right-edge boundary equations (Section S2.4.3) is

$$
\begin{aligned}
\sum_{\lambda=M_{\mathrm{int}}+M_{\mathrm{h}}+1}^{M_{\mathrm{int}}+M_{\mathrm{h}}+M_{\mathrm{v}}} q[\lambda] \sum_{\nu} A[\lambda,\nu] r[\nu] &= \sum_{k} q_{M_{\mathrm{h}}+1,k} \left(\frac{\Delta z_k}{\Delta \bar{x}_{M_{\mathrm{h}}}} r_{M_{\mathrm{h}},k} - \frac{\Delta z_k}{\Delta \bar{x}_{M_{\mathrm{h}}}} r_{M_{\mathrm{h}}+1,k} \right) \\
&= -\sum_{k} q_{M_{\mathrm{h}}+1,k} \Delta z_k \frac{r_{M_{\mathrm{h}}+1,k} - r_{M_{\mathrm{h}},k}}{\Delta \bar{x}_{M_{\mathrm{h}}}},
\end{aligned}
$$

which we add to (S2.44) to obtain

$$
\begin{aligned}
&\sum_{\lambda=1}^{M_{\mathrm{int}}+M_{\mathrm{h}}+M_{\mathrm{v}}} q[\lambda] \sum_{\nu} A[\lambda,\nu] r[\nu] \\
&= -\sum_{k} \sum_{i=i_{\mathrm{b}}[k]+1}^{M_{\mathrm{h}}-1} (q_{i+1,k} - q_{i,k}) \Delta z_k \frac{r_{i+1,k} - r_{i,k}}{\Delta \bar{x}_i} \\
&\quad - \sum_{k} (q_{M_{\mathrm{h}}+1,k} - q_{M_{\mathrm{h}},k})\, \Delta z_k \frac{r_{M_{\mathrm{h}}+1,k} - r_{M_{\mathrm{h}},k}}{\Delta \bar{x}_{M_{\mathrm{h}}}} - \sum_{k} q_{i_{\mathrm{b}}[k]+1,k} \Delta z_k \frac{r_{i_{\mathrm{b}}[k]+1,k} - r_{i_{\mathrm{b}}[k],k}}{\Delta \bar{x}_{i_{\mathrm{b}}[k]}} \\
&\quad - \sum_{i=i_{\mathrm{b}}[1]+1}^{M_{\mathrm{h}}} \sum_{k=1}^{k_{\mathrm{b}}[i]-2} (q_{i,k} - q_{i,k+1}) \Delta x_i \frac{r_{i,k} - r_{i,k+1}}{\tilde{N}_k^2 \Delta \bar{z}_k} \\
&\quad - \sum_{i=i_{\mathrm{b}}[1]+1}^{M_{\mathrm{h}}} q_{i,k_{\mathrm{b}}[i]-1} \Delta x_i \frac{r_{i,k_{\mathrm{b}}[i]-1} - r_{i,k_{\mathrm{b}}[i]}}{\tilde{N}_{k_{\mathrm{b}}[i]-1}^2 \Delta \bar{z}_{k_{\mathrm{b}}[i]-1}} \\
&\quad + \sum_{i=i_{\mathrm{b}}[1]+1}^{M_{\mathrm{h}}} \Delta x_i \left[-\gamma_1 (q_{i,0} - q_{i,1}) \frac{r_{i,0} - r_{i,1}}{\tilde{N}_0^2 \Delta \bar{z}_0} - \varsigma_1 (q_{i,0} + q_{i,1}) \frac{f^2}{g} \frac{r_{i,0} + r_{i,1}}{2} \right] \\
&\quad + \varpi(i_{\mathrm{b}}[1] > 0) \Delta x_1 q_{1,0} \left(-\gamma_1 \frac{r_{1,0} - r_{1,1}}{\tilde{N}_0^2 \Delta \bar{z}_0} - \varsigma_1 \frac{f^2}{g} \frac{r_{1,0} + r_{1,1}}{2} \right).
\end{aligned}
\tag{S2.45}
$$

The flat-bottom piece (Section S2.4.4) is

$$
\begin{aligned}
&\sum_{\lambda=M_{\mathrm{int}}+M_{\mathrm{h}}+M_{\mathrm{v}}}^{M_{\mathrm{int}}+M_{\mathrm{h}}+M_{\mathrm{v}}+M_{\mathrm{flat}}} q[\lambda] \sum_{\nu} A[\lambda,\nu] r[\nu] \\
&= \sum_{i \in \{\text{flat bottom}\}} q_{i,k_{\mathrm{b}}[i]} \left(-\frac{\Delta x_i}{\tilde{N}_{k_{\mathrm{s}}[i]}^2 \Delta \bar{z}_{k_{\mathrm{s}}[i]}} r_{i,k_{\mathrm{b}}[i]} + \frac{\Delta x_i}{\tilde{N}_{k_{\mathrm{s}}[i]}^2 \Delta \bar{z}_{k_{\mathrm{s}}[i]}} r_{i,k_{\mathrm{b}}[i]-1} \right) \\
&= \sum_{i \in \{\text{flat bottom}\}} q_{i,k_{\mathrm{b}}[i]} \Delta x_i \frac{r_{i,k_{\mathrm{b}}[i]-1} - r_{i,k_{\mathrm{b}}[i]}}{\tilde{N}_{k_{\mathrm{b}}[i]-1}^2 \Delta \bar{z}_{k_{\mathrm{b}}[i]-1}}.
\end{aligned}
\tag{S2.46}
$$

Note that $k_{\mathrm{s}}[i] = k_{\mathrm{b}}[i] - 1$ for a flat bottom. Likewise, the vertical-wall piece (Section S2.4.5) is

$$
\begin{aligned}
&\sum_{\lambda \in \text{vert.wall}} q[\lambda] \sum_{\nu} A[\lambda,\nu] r[\nu] \\
&= \sum_{k \in \{\text{vert.wall}\}} q_{i_{\mathrm{b}}[k],k} \left(-\frac{\Delta z_k}{\Delta x_{i_{\mathrm{s}}[k]}/2} r_{i_{\mathrm{b}}[k],k} + \frac{\Delta z_k}{\Delta x_{i_{\mathrm{s}}[k]}/2} r_{i_{\mathrm{b}}[k]+1,k} \right) \\
&= \sum_{k \in \{\text{vert.wall}\}} q_{i_{\mathrm{b}}[k],k} \Delta z_k \frac{r_{i_{\mathrm{b}}[k]+1,k} - r_{i_{\mathrm{b}}[k],k}}{\Delta \bar{x}_{i_{\mathrm{b}}[k]}}.
\end{aligned}
\tag{S2.47}
$$

Note that $\Delta \bar{x}_{i_{\mathrm{b}}[k]} = \Delta x_{i_{\mathrm{s}}[k]}/2$ for vertical-wall boundaries.

The corner-cell piece (Section S2.4.5) is

$$\begin{aligned}
&\sum_{\lambda\in\text{corner}} q[\lambda]\sum_{\nu} A[\lambda,\nu]r[\nu] \\
&= \sum_{(i,k)\in\text{corner}} q_{i,j}\Bigg[\left(-\frac{\Delta z_k}{\Delta\bar{x}_i} - \gamma_k\frac{\Delta x_i}{\tilde{N}_{k-1}^2\Delta\bar{z}_{k-1}} - \varsigma_k\frac{f^2}{g}\frac{\Delta x_i}{2}\right)r_{i,k} \\
&\qquad\qquad + \frac{\Delta z_k}{\Delta\bar{x}_i}r_{i+1,k} + \left(\gamma_k\frac{\Delta x_i}{\tilde{N}_{k-1}^2\Delta\bar{z}_{k-1}} - \varsigma_k\frac{f^2}{g}\frac{\Delta x_i}{2}\right)r_{i,k-1}\Bigg] \\
&= \sum_{(i,k)\in\text{corner}} q_{i,k}\left(\Delta z_k\frac{r_{i+1,k}-r_{i,k}}{\Delta\bar{x}_i} + \gamma_k\Delta x_i\frac{r_{i,k-1}-r_{i,k}}{\tilde{N}_{k-1}^2\Delta\bar{z}_{k-1}} - \varsigma_k\Delta x_i\frac{f^2}{g}\frac{r_{i,k}+r_{i,k-1}}{2}\right).
\end{aligned} \tag{S2.48}$$

Then, we combine these three partial sums for the slope-bottom boundary to get

$$\begin{aligned}
&\sum_{\lambda\in\text{slope/bottom}} q[\lambda]\sum_{\nu} A[\lambda,\nu]r[\nu] \\
&= \sum_{k=1}^{M_\text{v}} q_{i_\text{b}[k],k}\Delta z_k\frac{r_{i_\text{b}[k]+1,k}-r_{i_\text{b}[k],k}}{\Delta\bar{x}_i} \\
&\quad + \varpi(i_\text{b}[1]>0)q_{1,1}\left(\gamma_1\Delta x_1\frac{r_{1,0}-r_{1,1}}{\tilde{N}_0^2\Delta\bar{z}_0} - \varsigma_1\Delta x_1\frac{f^2}{g}\frac{r_{1,1}+r_{1,0}}{2}\right) \\
&\quad + \sum_{i=i_\text{b}[1]+1}^{M_\text{h}} q_{i,k_\text{b}[i]}\Delta x_i\frac{r_{i,k_\text{b}[i]-1}-r_{i,k_\text{b}[i]}}{\tilde{N}_{k_\text{b}[i]-1}^2\Delta\bar{z}_{k_\text{b}[i]-1}}
\end{aligned} \tag{S2.49}$$

If $(1,1)$ is a corner cell, $\varpi=1$ and the last i summation starts from 2 to exclude the corner cell; if $(1,1)$ is not a corner cell, the ϖ vanishes and the last i summation starts from 1.

Finally, adding this contribution from the slope-bottom boundary to (S2.45), we obtain

$$
\begin{aligned}
&\vec{q}^T A\vec{r} \\
&= \sum_\lambda q[\lambda] \sum_\nu A[\lambda,\nu] r[\nu] \\
&= -\sum_k \sum_{i=i_\mathrm{b}[k]+1}^{M_\mathrm{h}-1} (q_{i+1,k} - q_{i,k}) \Delta z_k \frac{r_{i+1,k} - r_{i,k}}{\Delta \bar{x}_i} \\
&\quad - \sum_k (q_{M_\mathrm{h}+1,k} - q_{M_\mathrm{h},k})\, \Delta z_k \frac{r_{M_\mathrm{h}+1,k} - r_{M_\mathrm{h},k}}{\Delta \bar{x}_{M_\mathrm{h}}} \\
&\quad - \sum_k (q_{i_\mathrm{b}[k]+1,k} - q_{i_\mathrm{b}[k]}) \Delta z_k \frac{r_{i_\mathrm{b}[k]+1,k} - r_{i_\mathrm{b}[k],k}}{\Delta \bar{x}_{i_\mathrm{b}[k]}} \\
&\quad - \sum_{i=i_\mathrm{b}[1]+1}^{M_\mathrm{h}} \sum_{k=1}^{k_\mathrm{b}[i]-2} (q_{i,k} - q_{i,k+1}) \Delta x_i \frac{r_{i,k} - r_{i,k+1}}{\tilde{N}_k^2 \Delta \bar{z}_k} \\
&\quad - \sum_{i=i_\mathrm{b}[1]+1}^{M_\mathrm{h}} (q_{i,k_\mathrm{b}[i]-1} - q_{i,k_\mathrm{b}[i]}) \Delta x_i \frac{r_{i,k_\mathrm{b}[i]-1} - r_{i,k_\mathrm{b}[i]}}{\tilde{N}_{k_\mathrm{b}[i]-1}^2 \Delta \bar{z}_{k_\mathrm{b}[i]-1}} \\
&\quad + \sum_{i=i_\mathrm{b}[1]+1}^{M_\mathrm{h}} \Delta x_i \left[-\gamma_1 (q_{i,0} - q_{i,1}) \frac{r_{i,0} - r_{i,1}}{\tilde{N}_0^2 \Delta \bar{z}_0} - \varsigma_1 (q_{i,0} + q_{i,1}) \frac{f^2}{g} \frac{r_{i,0} + r_{i,1}}{2} \right] \\
&\quad + \varpi(i_\mathrm{b}[1] > 0) \Delta x_1 \left[-\gamma_1 (q_{1,0} - q_{1,1}) \frac{r_{1,0} - r_{1,1}}{\tilde{N}_0^2 \Delta \bar{z}_0} - \varsigma_1 (q_{1,0} + q_{1,1}) \frac{f^2}{g} \frac{r_{1,0} + r_{1,1}}{2} \right] \\
&= -\sum_k \sum_{i=i_\mathrm{b}[k]}^{M_\mathrm{h}} (q_{i+1,k} - q_{i,k}) \Delta z_k \frac{r_{i+1,k} - r_{i,k}}{\Delta \bar{x}_i} \\
&\quad - \sum_{i=i_\mathrm{b}[1]+1}^{M_\mathrm{h}} \sum_{k=1}^{k_\mathrm{b}[i]-1} (q_{i,k} - q_{i,k+1}) \Delta x_i \frac{r_{i,k} - r_{i,k+1}}{\tilde{N}_k^2 \Delta \bar{z}_k} \\
&\quad + \sum_{i=1}^{M_\mathrm{h}} \Delta x_i \left[-\gamma_1 (q_{i,0} - q_{i,1}) \frac{r_{i,0} - r_{i,1}}{\tilde{N}_0^2 \Delta \bar{z}_0} - \varsigma_1 (q_{i,0} + q_{i,1}) \frac{f^2}{g} \frac{r_{i,0} + r_{i,1}}{2} \right] \\
&= -\sum_k \sum_{i=i_\mathrm{b}[k]}^{M_\mathrm{h}} \Delta z_k (q_{i+1,k} - q_{i,k}) \frac{r_{i+1,k} - r_{i,k}}{\Delta \bar{x}_i} \\
&\quad - \sum_{i=1}^{M_\mathrm{h}} \Delta x_i \left[(q_{i,0} - q_{i,1}) \frac{r_{i,0} - r_{i,1}}{\tilde{N}_0^2 \Delta \bar{z}_0 / 2} + \sum_{k=1}^{k_\mathrm{b}[i]-1} (q_{i,k} - q_{i,k+1}) \frac{r_{i,k} - r_{i,k+1}}{\tilde{N}_k^2 \Delta \bar{z}_k} \right] \\
&\quad - \frac{f^2}{g} \sum_{i=1}^{M_\mathrm{h}} \Delta x_i \frac{q_{i,0} + q_{i,1}}{2} \frac{r_{i,0} + r_{i,1}}{2}.
\end{aligned}
\tag{S2.50}
$$

For the second line, the lower bound has been switched from $i = i_\mathrm{b}[1] + 1$ to $i = 1$. If $(1,1)$ is a corner cell, $i_\mathrm{b}[1] = 1$ and $k_\mathrm{b}[1] = 1$ so that the k-summation from $k = 1$ to $k = k_\mathrm{b}[1] - 1 = 0$ vanishes and whether starting from $i = 1$ or $i = 2$ does not change the sum. If $(1,1)$ is a vertical-wall cell, $i_\mathrm{b}[1] = 0$ and the summation starts from $i = i_\mathrm{b}[1] + 1 = 1$. The i-summation can therefore starts from $i = 1$ in either case. The merger of the ϖ term was possible for the same reason.

The above form is identical to (S2.25) minus the f/cB term, except that (S2.25) lacks the $(F_{k_s[i]} - F_{k_s[i]+1})/(\tilde{N}^2 \Delta\bar{z})$ terms for the flat-bottom parts. They are absent in (S2.25) because they are zero according to the flat-bottom boundary condition.

Equation (S2.25) started as an interior integral $\langle q, \mathcal{L}F \rangle$ and the boundary conditions enter it through the assumption that F is a solution to the eigenvalue problem. In contrast, the matrix A includes the boundary conditions and the calculation of $\vec{q}^T A \vec{r}$ without assuming anything led to (S2.50).

The symmetry of $\vec{q}^T A \vec{r}$ in q and r comes from the symmetry of A without the explicit calculation above.

Using the same argument as in Section S2.3, we prove that A is negative definite. With $q = r$, all the terms are the negative of squared real numbers. Most of the terms are proportional to $(r[\nu] - r[\nu'])^2$ and for these terms to vanish, $\vec{r}$ has to be constant, that is, $\vec{r} = [b, b, b, \ldots, b]$, as all components of the vector appear in one of those terms and all $r[\nu]$'s are connected. If $\vec{r} = [b, b, b, \ldots, b]$ with $b \neq 0$,

$$\vec{r}^T A \vec{r} = -\frac{f^2}{g} \sum_i \Delta x_i b^2 < 0.$$

This also proves that under the rigid-lid condition ($g \to \infty$), $\vec{r}^T A \vec{r} = 0$ with this uniform vector and A is not negative definite.

S2.6 Vertical modes from CTW equations

The original continuous CTW problem becomes separable when the "slope" is a purely-vertical wall and yields Kelvin wave modes of the form $\exp(-x/|c/f|)\psi(z)$, where $\psi(z)$ is a vertical mode (Section S1.3). This subsection shows that the finite-difference version of the CTW problem (Section S2.2) has exactly the same property. Moreover, the separation of variables yields the same finite-difference scheme for the vertical modes as the scheme (S2.1) we showed for the vertical-mode problem (Section S2.1); and a finite difference equation in x that approximately gives $\exp(-x/|c/f|)$.

We consider a case with a vertical wall at $x = 0$ followed by a flat bottom. Following the previous derivation (Section S1.3), we try to find solutions in the form $F_{i,k} = X_i \psi_k$. The equations are eqs. (S2.11a), (S2.12) and (S2.19) to (S2.21) without the boundary condition of corner cells, where $i_s[k] = 1$ for all k and $k_s[i] = M_v$ for all i. The wall-boundary values are all defined at $x = 0$ as $\overline{F}_{0,k}$ and the bottom values at $z = -D$ as $\overline{F}_{i,M_v}$.

The z-boundary conditions (eqs. (S2.11a) and (S2.20)) can be simplified to

$$\frac{\psi_0 - \psi_1}{\tilde{N}_0^2 \Delta\bar{z}_0} + \frac{f^2}{g}\frac{\psi_0 + \psi_1}{2} = 0, \quad \frac{\psi_{M_v} - \bar{\psi}_{M_v+1}}{\Delta z_{M_v}/2} = 0, \tag{S2.51}$$

for $i = 1, \ldots, M_h$; X_i has been factored out from both because the vertical positions of the boundaries do not depend on i. These boundary conditions are exactly the same as the finite-difference versions of the boundary condtions we considered in Section S2.1. Likewise, the x-boundary conditions (eqs. (S2.12) and (S2.19)) are

$$\frac{X_1 - \bar{X}_0}{\Delta x_1/2} = \frac{f}{c}\bar{X}_0, \quad \frac{X_{M_h+1} - X_{M_h}}{\Delta\bar{x}_{M_h}} = 0, \tag{S2.52}$$

for $k = 1, \ldots, M_\mathrm{v}$. The interior equation (S2.21) gives

$$0 = \frac{1}{X_i}\frac{1}{\Delta x_i f^2}\left(\frac{X_{i+1} - X_i}{\Delta \bar{x}_i} - \frac{X_i - X_{i-1}}{\Delta \bar{x}_{i-1}}\right) + \frac{1}{\psi_k}\frac{1}{\Delta z_k}\left(\frac{\psi_{k-1} - \psi_k}{N_{k-1}^2 \Delta \bar{z}_{k-1}} - \frac{\psi_k - \psi_{k+1}}{N_k^2 \Delta \bar{z}_k}\right) \tag{S2.53}$$

$i = 1, \ldots, M_\mathrm{h}$ and $k = 1, \ldots, M_\mathrm{v}$, except that we utilize the convention for the slope-boundary points (Section S2.2): $X_{i-1} = \bar{X}_{i-1}$ and $\Delta \bar{x}_{i-1} = \Delta x_i/2$ when $i = 1$, and $\psi_{k+1} = \bar{\psi}_{M_\mathrm{v}}$ and $\Delta \bar{z}_k = \Delta z_k/2$ when $k = M_\mathrm{v}$.

The separation of variables implies

$$\frac{1}{\psi_k}\frac{1}{\Delta z_k}\left(\frac{\psi_{k-1} - \psi_k}{N_{k-1}^2 \Delta \bar{z}_{k-1}} - \frac{\psi_k - \psi_{k+1}}{N_k^2 \Delta \bar{z}_k}\right) = -C = -\frac{1}{X_i}\frac{1}{\Delta x_i f^2}\left(\frac{X_{i+1} - X_i}{\Delta \bar{x}_i} - \frac{X_i - X_{i-1}}{\Delta \bar{x}_{i-1}}\right) \tag{S2.54}$$

with some constant C. From this, we conclude that $\{X_i\}$ is a solution to

$$\frac{1}{\Delta x_i}\left(\frac{X_{i+1} - X_i}{\Delta \bar{x}_i} - \frac{X_i - X_{i-1}}{\Delta \bar{x}_{i-1}}\right) = f^2 C X_i \tag{S2.55}$$

under the boundary conditions (S2.52) and that $\{\psi_k\}$ is a solution to

$$\frac{1}{\Delta z_k}\left(\frac{\psi_{k-1} - \psi_k}{N_{k-1}^2 \Delta \bar{z}_{k-1}} - \frac{\psi_k - \psi_{k+1}}{N_k^2 \Delta \bar{z}_k}\right) = -C\psi_k$$

under boundary conditions (S2.51). The latter is exactly the same as the finite-difference version of the vertical-mode operator $\mathcal{L}'$ we considered in Section S2.1 and its solutions are the vertical modes $\psi_k^{(n)}$ with eigenvalues $c^{(n)} = C^{-1/2}$. This fixes the value of C. The next step should therefore be to determine the combination of $\{X_i\}$ and c that satisfy the x boundary condition (S2.52) and the X equation (S2.55) with the given $C = 1/(c^{(n)})^2$.

Equation (S2.55) is obviously a finite-difference analogue of (S1.18) and the solution X should be an approximation to the exponential decay at a scale of the deformation radius $|f/c^{(n)}|$ as (S1.19). To demonstrate that, we consider a simple case where Δx_i is constant and $x = L_\mathrm{x}$ is far enough so that we can throw away solutions that grow in the $+x$ direction. In this case, we can assume that $X_j = \bar{X}_0\, \mu^{j-1/2}$ for $j = 1, \ldots, M_\mathrm{h}$ with $0 < \mu < 1$, where the exponent is half integers because the gridpoints are located at $x_j = (j - 1/2)\Delta x$, and then (S2.55) gives

$$\frac{1}{\Delta x}\left(\frac{\mu^2 - \mu}{\Delta x} - \frac{\mu - 1}{\Delta x}\right) = \frac{f^2}{(c^{(n)})^2}\mu \quad \Rightarrow \quad \mu^2 - (2 + a)\mu + 1 = 0,$$

where $a \equiv \Delta x^2 f^2/(c^{(n)})^2$. The solution to the quadratic equation is

$$\mu = \frac{2 + a}{2} - \frac{1}{2}\sqrt{(2 + a)^2 - 4},$$

where we have retained only the solution such that $\mu < 1$. For accurate solutions, we must ensure that $a \ll 1$ (the deformation radius being adequately resolved) and in that case,

$$\mu \approx \frac{2}{2} - \frac{1}{2}\sqrt{4a} = 1 - \sqrt{a},$$

which determines μ. The solution is

$$\begin{aligned} X_j^{(n)} &= \bar{X}_0 \mu^{j-1/2} \approx \bar{X}_0 (1-\sqrt{a})^{j-1/2} \\ &\approx \bar{X}_0 \exp[-\sqrt{a}\,(j-1/2)] \\ &= \bar{X}_0 \exp\left(-\frac{x_j}{\Delta x/\sqrt{a}}\right) \end{aligned}$$

where $x_j \equiv (j-1/2)\Delta x$ and we have used the formula $(1+\epsilon)^p \approx e^{\epsilon p}$ if $|\epsilon| \ll 1$ and $|p\epsilon^2| \ll 1$.

Assuming that the solution decays fast enough, we consider the offshore boundary condition of (S2.52) as already satisfied. The $x = 0$ boundary condition of (S2.52) then becomes

$$\frac{\mu - \mu^{1/2}}{\Delta x/2} = \frac{f}{c}\mu^{1/2} \quad \Rightarrow \quad \frac{f}{c} = \frac{\mu^{1/2}-1}{\Delta x/2},$$

which determines c. An approximate value is

$$\frac{f}{c} \approx \frac{(1-\sqrt{a}/2)-1}{\Delta x/2} = -\frac{\sqrt{a}}{\Delta x} = -\left|\frac{f}{c^{(n)}}\right|.$$

The eigenvalue, f/c, of the original problem is negative as it should (Section S2.3) and $|c|$ is approximately equal to $c^{(n)}$, the latter from the vertical-mode eigenvalue problem. The solution is

$$X_j^{(n)} \approx \bar{X}_0 \exp\left(-\frac{x_j}{|c^{(n)}/f|}\right).$$